8-9-2014

Investigation of Thermal Performance of Nanoparticle Enhanced Ionic Liquids (NEILs) for Solar Collector Applications

Titan Chandra Paul
University of South Carolina - Columbia

INVESTIGATION OF THERMAL PERFORMANCE OF NANOPARTICLE ENHANCED IONIC LIQUIDS (NEILs) FOR SOLAR COLLECTOR APPLICATIONS

By

Titan Chandra Paul

Bachelor of Science
Bangladesh University of Engineering and Technology, 2005

Master of Science
Tuskegee University, 2009

Submitted in Partial Fulfillment of the Requirements

For the Degree of Doctor of Philosophy in

Mechanical Engineering

College of Engineering and Computing

University of South Carolina

2014

Accepted by:

Jamil A. Khan, Major Professor

Jeff Morehouse, Committee Member

Curtis Rhodes, Committee Member

Jasim Imran, Committee Member

Lacy Ford, Vice Provost and Dean of Graduate Studies

DEDICATION

To my parents and wife

ACKNOWLEDGEMENTS

The author would like to express his sincere thanks and deepest gratitude to his advisor, Prof. Jamil Khan, for his continuous support, encouragement, motivation and guidance throughout all phases of his Ph.D. study. It has been a great privilege and honor for the author to work with him.

The author would like to thank his PhD committee members, Prof. Jeff Morehouse, Prof. Curtis Rhodes and Prof. Jasim Imran, for their comments, suggestions and time for reviewing this work.

Special thanks to Enhanced Heat Transfer research group: Dr. Ruixian Fang, Dr. Dale Allen Mccants, Mr. Muhammad Yakut Ali, Dr. A.K.M. Monjur Morshed, Mr. Umair Najeeb and Mr. Eshwarprashad Trinuvakarussu for their invaluable suggestions, comments, and friendship. Special thanks to Mr. Reza-E-Rabby and Dr. Jahid Ferdous for his invaluable help in this research.

The author would like to acknowledge the financial support from the Department ofEnergy (DOE) Solar Energy Technology Program through Savannah River National Laboratory. The author would like to thank Dr. Elise B. Fox,team leader of the project.

Finally, the author would like to express special thanks to his family and friends for their support, constant encouragement and unconditional love.

ABSTRACT

Concentrated Solar Power (CSP) is a prominent alternative energy technology, where mirrors or lenses are used to concentrate sunlight from a large area and stored in a collector filled with heat transfer fluid (HTF). The energy from this HTF is used to produce steam for power generation. CSP system requires high heat storage capacity and thermally stable HTF to reduce its operating cost. Having suitable thermophysical properties, ionic liquids (ILs) is considered as a potential HTF for the CSP applications; however thermophysical properties of ILs can be further enhanced by dispersing small volume percentages of nanoparticles. This liquid is called Nanoparticle Enhanced Ionic Liquids (NEILs). The present research focuses on the experimental and numerical evaluation of the NEILs as a potential working fluid for the CSP applications.

The experimental assessment includes thermophysical property measurements, and convective heat transfer (forced and natural convection) performance evaluation. For this research, four representative ILs ($[C_4mpyrr][NTf_2]$, $[C_4mim][NTf_2]$. $[C_4mmim][NTf_2]$, $[N_{4111}][NTf_2]$) are selected. The thermophysical properties of Al_2O_3 NEILs demonstrate enhanced density, thermal conductivity, viscosity, and heat capacity compared to the base ILs. Plausible reasons of enhanced properties are discussed and compared with the existing model.

To evaluate the forced convection performance of ILs and NEILs experiments are conducted in a circular tube with constant heat flux condition. The experimental results obtained for ILs correlate well with the Shah's equation in laminar flow condition and Gnielinski's equation for turbulent flow condition. Whereas, results obtained for NEILs show higher forced convection heat transfer coefficient than the base ILs. This is due to enhanced thermal conductivity and particle migration behavior in the boundary layer. The numerical simulation by FLUENT also shows the enhancement of heat transfer coefficient of NEILs compared to base ILs.

Natural convection experiments were performed in rectangular cavity with different aspect ratios (1 and 1.5) heated from below. New correlations for Nusselt Number as a function of Rayleigh number is proposed for ILs. It is noted that the natural convection behavior of NEILs demonstrates much lower heat transfer coefficient compared to the base ILs. The relative change of effective thermophysical properties are not fully responsible for the degradation of the natural convection of NEILs which also confirms the numerical simulation of natural convection of ILs and NEILs. In addition to thermophysical properties, particle-fluid interaction and clustering of nanoparticles also plays a role in degrading the natural convection heat transfer.

TABLE OF CONTENTS

LIST OF TABLES

LIST OF FIGURES

LIST OF SYMBOLS

T	Temperature
V	Voltage
I	Current
A	Surface area
$q^{"}$	Heat flux
$q^{"}_{corr}$	Corrected heat flux
T_{hf}	Hot surface temperature
T_{cf}	Cold surface temperature
k	Thermal conductivity
x	Thickness of copper plate
h	Heat transfer coefficient
Q	Power
D_o	Outer diameter of tube
L	Heating length of tube
$h(x)$	Local heat transfer coefficient
$T'_w(x)$	Inner surface wall local temperature
$T_f(x)$	Local bulk fluid temperature
r	Radius of tube
$T_w(x)$	Outer surface wall local temperature
T_{fi}	Fluid inlet temperature

x_1	Axial distance
C_p	Heat capacity
V'	Volumetric flow rate
W_p	Total uncertainty
w'	Uncertainty of the independent variables
p'	Variables of functional dependence
a'	Variables of functional dependence
a, b, A, B, C	Constant
ϕ_m	Maximum particle packing fraction
ϕ_a	Effective volume fraction of aggregates
D'	Fractal index
t	Interfacial layer thickness
Nu	Nusselt number
H	Height of the test enclosure
Pr	Prandtl number
Gr	Grashof number
g	Gravitational acceleration
ΔT	Temperature difference
Ra	Rayleigh number
Re	Reynolds number
f'	Friction factor
u	Velocity
x_t	Thermal entry length
x_h	Hydrodynamic entry length
$\vec{V}$	Velocity vector

Nu_{av}	Average Nusselt number
h_{av}	Average heat transfer coefficient

Greek Symbols:

β	Volumetric thermal expansion coefficient
ρ	Density
μ	Dynamic viscosity
ϕ	Nanoparticle volume fraction
γ	Constant
γ_1	Constant
ν_f	Kinematic viscosity
α	Thermal diffusivity
δ_t	Boundary layer thickness

Subscripts:

p	Pressure
hf	Hot surface
cf	Cold surface
c	Copper
i	Inner
o	Outer
w	Wall
s	Stainless steel
av	Average
in	Inlet

out	Outlet
f	Fluid
$NEIL$	Nanoparticle enhanced ionic liquid
BL	Base liquid
n	Nanoparticles
a	Aggregate
lr	Interfacial layer

CHAPTER 1

INTRODUCTION

1.1 Motivation for the Study

The energy crisis is one of the most important issues in the recent global world. Based on International Energy Outlook 2013 (Briefing 2013) report, there will be a 56% increase in energy demand between 2010-2040. Currently the 80.6% energy sources are from conventional fossil fuel (Rogner 2012). The environmental community and energy researchers are concerned about the global warming and the emission of CO_2 from the burning of fossil fuel in energy production (Khoo and Tan 2006). Environmental concerns, quick depletion, and soaring prices of conventional carbon based fuel push energy researchers to find reliable and economically viable alternate source of energy (Nakata 2004; Mason 2007). Renewable energy is the potential solution in terms of sustainability, cost effective, environmental friendly and abundant sources. The options of renewable energy sources are wind, hydro, solar, biomass, biofuel, and geothermal. From the many options of renewable energy, solar energy is one of the most abundant alternate sources of energy in the world and has already been proven to be a reliable and economically viable alternative source of energy (Herzog 2001).

Solar energy can be harvested either by direct conversion of solar energy into electric energy by photo voltaic solar cells or can be collected and transferred by means of a fluid known as solar thermal collector (Chu 2011). While solar cells have

low efficiency and high cost effective ratio, solar thermal collectors possess superior performance over the solar cell (Kalogirou 2004). In solar thermal collector, where the solar energy is collected directly from the sun and the collector field with the working fluid then that heat is transferred to produce steam for generating power. The main advantage of the solar thermal energy system is that the energy can be stored in other forms and can be used when the sun is not visible. There are different types of solar thermal collectors depending on the design and uses such as: low temperature collector for space heating and cooling, medium temperature collector for cooking, and high temperature collector for power generation. The high temperature solar power is the Concentrated Solar Power (CSP) system where mirrors or lenses are used to concentrate sunlight from a large area and stored in collector filled with heat transfer fluid (HTF). The CSP system has different designs such as parabolic trough, power tower, and dish. CSP system is the growing technology for electricity generation. On commercial level application 14MW Solar Energy Generating System or SEGS plant was built first in California, US in 1980 and now worldwide in 2012 it's become 2553 MW. Also 2000 MW plants are in under construction all over the world (Coggin 2013).

The energy efficiency of the CSP system is mostly dependent on the operating temperature and thermal stability of the HTF. Currently used commercially available HTFs are Therminol VP-1 (eutectic mixture of biphenyl and diphenyl oxide), molten salt, and mineral oil. Therminol VP-1 has high vapor pressure at higher operating temperature which is harmful for the storage tank (Solutia 2014); molten salts has higher operating temperature over 500^{o}C but also has higher melting temperature which helps to freeze up the liquid during the winter season (Kearney, Herrmann et al. 2003); and mineral oil has

lower decomposition temperature (Moens and Blake 2010). The above mentioned properties of currently used HTFs are affecting the energy storage capacity and reducing the overall system efficiency, which increases the operating cost. Therefore, there is an acute need for new energy-efficient HTF. To increase the efficiency of the solar collector, ionic liquids have great potential as an alternative of the current HHF (Wu, Reddy et al. 2001; Moens, Blake et al. 2003; Valkenburg, Vaughn et al. 2005;Wishart 2009).

Ionic liquids (ILs) are the group of salts which are liquid at ambient temperature (less than 100^{o}C) and consist of ionic species (Rogers and Seddon 2003). Typically ILs contains large organic cations, such as imidazolium, pyrazolium, triazolium, thiazolium, oxazdium, pyridinium, pyridazinium, pyrimidinium, pyrazinium, and halogen, fluorinated or organic anions. These ILs have excellent physical and chemical properties including high thermal stability, negligible vapor pressure and volatility, exposure to air and moisture stability, low melting point, wide electrochemical window, nonflammability, high ionic conductivities, high solvating capability, corrosion resistance to plastics and carbon steels (Rogers and Seddon 2003; Paulechka, Zaitsau et al. 2005; Valkenburg, Vaughn et al. 2005; Endres and Zein El Abedin 2006). Due to these excellent properties, ILs becomes very useful for material processing (Reddy 2009), as a catalyst for synthesis of inorganic nano-materials (Singh, Kumari et al. 2009), as electrolytes for batteries and solar cells (Wishart 2009), and as lubricants (Jiménez and Bermúdez 2009).

On the other hand, nanofluids are liquids in which a small amount of metallic (Cu, Ag, and Au) or nonmetallic (Al_2O_3, CuO, TiO_2) nanoparticles (one dimension less than 100 nm) are dispersed in base fluids (Choi and Eastman 1995). The nanofluids have

shown significant enhancement of heat transfer, mass transfer, wetting, and spreading characteristics (Wang, Xu et al. 1999; Krishnamurthy, Bhattacharya et al. 2006). Water and ethylene glycol based nanofluids already shows their potential applicability as cooling media for high heat generating electronic devices, nuclear plants, the automobile industry (Chopkar, Das et al. 2006; Buongiorno, Hu et al. 2008; Shen, Shih et al. 2008). These enhanced heat transfer properties of nanofluids encourage the researchers to combine these two (nanoparticles and ionic liquids) growing interests, forming the nanoparticle enhanced ionic liquids (NEILs) by dispersing small amounts of nanoparticles into base ILs for HTF of solar thermal applications. There are several research group works on the thermophysical properties of the ILs based nanofluids which are discussed in literature review section. Although there are several previous studies on thermal properties and stability of the NEILs, none of these studies report heat transfer behavior of NEILs. The heat transfer behavior of NEILs will play an important role in assessing its effectiveness and viability for CSP applications.

1.2 Research Goal and Objectives

The present research work focused on the heat transfer behavior of ILs and NEILs under natural and forced convection. For greater fidelity of the reported results, thermophysical properties such as density, viscosity, heat capacity, and thermal conductivity of the ILs and NEILs were also measured. Natural convection was performed in rectangular cavity heated from below condition and the systematic forced convection was performed in flowing through a circular tube. The objective and specific task of the resarch is divided into following sections:

(1) Experimentally measure the thermophysical properties of ILs and NEILs.

(2) Perform the natural convection heat transfer experiment of ILs and NEILs.

(3) Perform the forced convection heat transfer experiment of ILs and NEILs.

(4) Numerical simulation of natural and forced convection of ILs and NEILs.

1.3 Dissertation Layout

Chapter 2 presents a critical review about the IL and its applications. Literature reviews about the IoNanofluids (Ionic liquid with nanoparticles), or NEILs and the possible reasons for enhanced properties are also discussed.

Chapter 3 includes the experimental facilities to fulfill the current research objectives such as the natural convection experimental setup, forced convection experimental setup. Operating principles of the different measuring devices such as Pycnometer for density, LVDV-II+ProCP viscometer for viscosity, Differential Scanning Calorimetry (DSC) for heat capacity, and KD2 Pro thermal property analyzer for thermal conductivity measurements are also discussed.

Chapter 4 includes the thermophysical properties such as density, viscosity, thermal conductivity, and heat capacity of all four ILs and NEILs.

Chapter 5 includes the experimental results of natural convection of ILs and NEILs.

Chapter 6 includes the experimental results of forced convection of ILs and NEILs.

In chapter 7, the numerical results of natural and forced convection of ILs and NEILs are presented.

Finally, chapter 8 concludes the results from the natural convection and forced convection of IL and NEIL. This chapter also presents the future research direction.

CHAPTER 2

LITERATURE REVIEW

2.1 Introduction

Heat transfer fluids (HTFs) have a greater range of industrial applications. The most common liquid and liquid/vapor based HTFs are glycol based liquid, mineral oil, and Therminol (VP-1) diphenyl oxide/biphenyl fluids. Energy storage capacity of the HTFs is an important property, which increases the system efficiency as well as reduces the operating cost. The focus of the research is to study the heat transfer behavior of ionic liquids (ILs) and nanoparticles enhanced ionic liquid (NEILs) as a potential candidate for HTFs for solar thermal collector. The required targeted properties of HTFs are summarized by National Renewable Energy Laboratory(Herrmann and Kearney 2002).

Table 2.1 Heat-transfer fluid requirements (Herrmann and Kearney 2002)

Storage density	>1.9 MJ/m^3
Freezing point	≤0 ◦C
High temperature stability	≥430 ◦C
Cost goal	≤$15/kW h
Required quantity for a solar plant	460,000m^3
Vapor pressure	<1 atm
Materials compatibility	Carbon and stainless steel
Viscosity	Similar to Therminol, VP-1, 2.48 cSt at 40ºC

There are several studies of ILs where this liquid was proposed as a thermal fluid for solar thermal collectors. Most of the previous studies concerned the physical properties of ILs. Also there are few studies of thermophysical properties of IL with nanoparticles.

The current chapter presents the literature review based on brief history of ILs, thermophysical properties of ionic liquids, applications of ILs, nanofluids, and ILs with nanoparticles.

2.2 Ionic Liquids

Ionic liquids (ILs) are group of salts, which has appreciable liquid ranges. The cations of ILs large organic species and anions are organic or inorganic species. The chemical structure of common cations and anions are shown in Fig. 2.1.

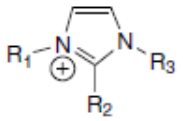

Imidazolium

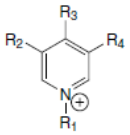

Pyridinium

Pyrrolidinium

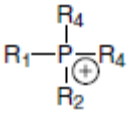

Phosphonium

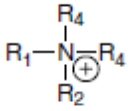

Ammonium

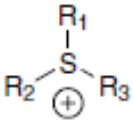

Sulfonium

(a) Cations

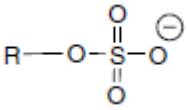

Alkylsulfate

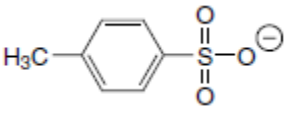

Tosylate

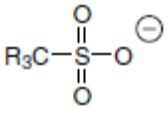

Methanesulfonate

(b) Organic anions

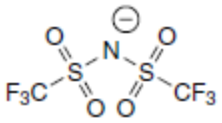

Bis(trifluoromethylsulfonyl)imide

Hexafluorophosphate

Tetrafluoroborate

Halide

(c) Inorganic anions

Figure 2.1 Chemical structure of common (a) cations, (b) organic anions, and (c) inorganic anions

Historically, the term "ionic liquid" was first use in general sense by R. M. Barrer at 1943 (Barrer 1943). Before that the development of ethylammonium nitrates $(C_2H_5)NH^+_3 \cdot NO^-_3$ was synthesized in 1914 (Sugden and Wilkins 1929). Then in 1970 and 1980

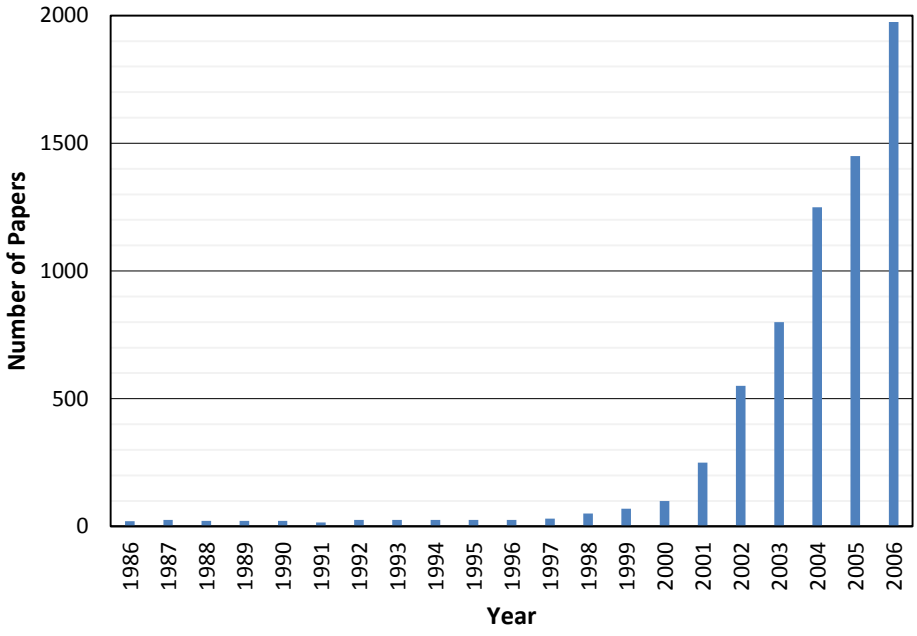

(a)

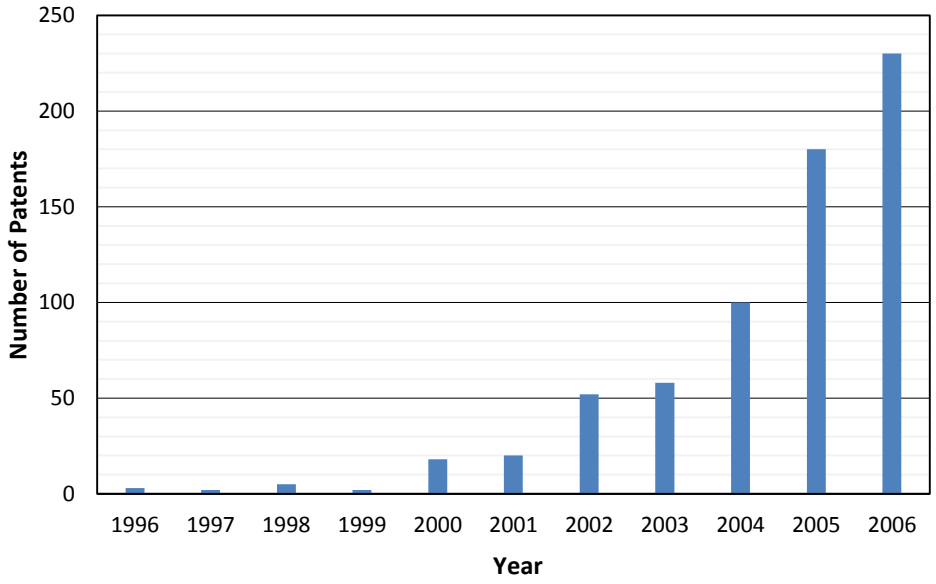

(b)

Figure 2.2 Number of (a) article and (b) patent related to ionic liquids published yearly (Plechkova and Seddon 2008)

imidazolium and pyridiniumcations with halide or trihalogenoaluminateanions based ILs for electrolyte of battery applications were developed (Chum, Koch et al. 1975; Wilkes, Levisky et al. 1982). After that in late 1990s ILs becomes the important solvents for synthesis and in industrial application (Keskin, Kayrak-Talay et al. 2007). The academic and industrial interests of ILs increases starting from 1990s, which is clear from the number of yearly article and patent publications of ILs (1996–2006) shown in Fig.2.2. Dong et al. (Dong, Muzny et al. 2007) also studies a web-based survey to find the thermophysical properties database and report the same scenario.

With combinations of varieties of cations and anions theoretically 10^{18} ILs can be formed but in realistic the number will be lower (Chemfiles 2006). In literature surveys (Zhang, Sun et al. 2006) through 1984-2004, there was 1680 pieces of physical properties data of 588 ILs, with combinations of 276 cations and 55 anions recorded. Firstly ILs was

used for organic synthesis for industrial applications, and also academic research was limited to the synthesis and properties studies but now it becomes promising in different fields such as analytical chemistry, chemical processing, industrial applications etc. That's why the research interest about ILs is booming.

2.3 Thermophysical Properties of Ionic Liquids

The excellent thermophysical properties of ILs make them as potential replacements of organic solvents or conventional heat transfer fluids (HTFs). The properties of modern ILs are presented in Table 2.2 and the properties may vary depending on the selection of cation and anion (Gardas and Coutinho 2009).

Table 2.2 Properties of modern ionic liquids (Johnson 2007)

A salt	Cation and or anion quite large
Freezing point	Preferably below 100°C
Liquidus range	Often > 200°C
Thermal stability	Usually high
Viscosity	Normally < 100 cP, workable
Dielectric constant	Implied < 30
Polarity	Moderate
Specific conductivity	Usually < 10 mScm-1, "Good"
Molar conductivity	< 10 Scm^2 mol^{-1}
Electrochemical window	> 2V, even 4.5 V, except for Brønsted acidic systems
Solvent and/or catalyst	Excellent for many organic reactions
Vapor pressure	Usually negligible

2.4 Melting Point

Melting point is one of the important properties of organic liquids which are considered as solvents for reactions, as heat transfer fluids, and for working fluids for electrochemical applications. ILs has the low melting point which has impact in the higher liquidus range. H. L. Ngo et al. (Ngo, LeCompte et al. 2000) have investigated the melting point of several imidazolium-based ILs by using Differential Scanning Calorimetry (DSC) and reports that the melting point decreases with increasing cations size. The higher chain length cations ILs have great interest in solar cell applications (Yamanaka, Kawano et al. 2007). Lazzús (Lazzús 2012) have studied 200 ILs to predict the melting point by using the group contribution method of anion and cations. The predicted melting point well correlates with the previously published data. Trohalaki (Trohalaki and Pachter 2005) proposed the melting point of ILs by Quantitative Structure-Property Relationships (QSPRs) and found the poor melting point of derived ILs. Melting points also depend on the different anions which are shown in Table 2.3.

Table 2.3 Melting points of ionic liquids depending on different anions (Fredlake, Crosthwaite et al. 2004)

Ionic liquid	Melting points (^{o}C)
[C_4mim]Cl	41
[C_4mim][NTf_2]	-2
[C_4mim][OTf]	13

2.5 Density

The density of ILs is a basic physical property which needs to be known before being used for any application. There are several literature data on the density of ILs, Pereiro et al. (Pereiro, Veiga et al. 2009) have measured the density of 1-butyl-1-methylpyrrolidiniumbis(trifluoromethylsulfonyl)imide, $[C_4mpyrr][NTf_2]$, and trihexyl(tetradecyl) phosphoniumdicyanamide, $[P_{66614}][dca]$ and found that the density data was correlated well with a quadratic function with the temperature. Kumełan et al. (Kumełan, Tuma et al. 2009) also have mentioned the temperature dependent density of $[C_4mpyrr][NTf_2]$ IL with the solubility of the CO_2 and H_2. This density data was used to compare the present experimental data. Bazito et al. (Bazito, Kawano et al. 2007) synthesize two ILs and measured the chemical stability in metallic lithium. To perform the chemical stability study, they measured the density and found the density with the temperature is non-linear . Anthony et al. (Anthony, Anderson et al. 2005) have performed the density measurements to find the gas stability in ILs with different anions. Kilaru et al. (Kilaru, Baker et al. 2007) have studied the density of imidazolium-, quaternary ammonium-, andphosphonium-based ILs. They observed that the highest density is for the ammonium based ILs and lowest density is for phosphonium base ILs. Liu et al. (Liu, Maginn et al. 2012) have studied the density experimentally and molecular dynamic simulation of six ILs and have reported trend in $[N4_{COOH}111][Tf2N]\sim[bmim][Pf_2N]>[bmim][Tf_2N]>[bmmim][Tf_2N]>[bmpyr][Tf_2N]\sim[N_{4111}][Tf_2N]$. The density of different imidazolium, pyridinium, ammonium, phosphonium and pyrrolidium based ILs varies from 1.05 to 1.64g/cm^3 at 293 K to 1.01 and 1.57 g/cm^{3}at 363 K (Rooney, Jacquemin et al. 2010) and slightly decreases with temperature.

Cation type has a strong effect on density, and density decreases with increasing alkyl chain length as observed by Fredlake et al. (Fredlake, Crosthwaite et al. 2004). They also reported that the introduction of a third alkyl substitutes on the imidazolium ring at the C2 position reduces the density. J. Jacquemin et al. (Jacquemin, Husson et al. 2006) studies several dried and water saturated ILs and conclude that the densities of the water-saturated ILs are somewhat lower compared to the dried samples, and also the minor change in density independent of temperature.

2.6 Viscosity

Viscosity of any liquid is the internal resistance to flow. Viscosity of ILs is most important physical properties for design heat transfer equipment, process piping, and liquid-liquid extractor system. Generally it is desired to have low viscosity liquid for applications in piping to reduce the pumping cost, and higher viscosities may apply for lubrication. The RTILs are mostly the high viscous liquid viscosity ranging from 10 to 726 cP (Bonhôte, Dias et al. 1996). Jacquemin et al. (Jacquemin, Husson et al. 2006) have studied the viscosity of dry and water saturated six ILs and the decreased viscosity of water saturated ILs compared to the dry ILs. Tokuda et al (Tokuda, Hayamizu et al. 2005) have studied the viscosity of ILs with different alkyl chain length and the viscosity shows the trend as $[C_8mim][(CF_3SO_2)_2N]$>$[C_6mim][(CF_3SO_2)_2N]$>[bmim]$[(CF_3SO_2)_2N]$> [mmim]$[(CF_3SO_2)_2N]$>[emim]$[(CF_3SO_2)_2N]$. The similar study was observed by Crosthwaite et al. (Crosthwaite, Muldoon et al. 2005) and found that viscosity depends on the alkyl chain length of imidazoliumcations and increases with chain length. Liu et al. (Liu, Maginn et al. 2012) have also measured the viscosity of six ILs by experimentally and molecular dynamic simulation and found the trend in $[N4_{COOH}111][Tf_2N]$>[bmmim]

[Tf_2N]~[bmim][Pf_2N]>[N_{4111}][Tf_2N]>[bmpyr][Tf_2N]>[bmim][Tf_2N]. They also conclude that the ILs viscosity is the reverse order of self-diffusivity and revealed that the macroscopic property like viscosity was dominated by the microscopic ion dynamics. Harris et al. (Harris, Kanakubo et al. 2007) studied temperature and pressure dependency of viscosity of 1-Hexyl-3-methylimidazolium Hexafluorophosphate and1-butyl-3-methylimidazolium bis{(trifluoromethyl) sulfonyl}imide ILs and shows Arrhenius temperature dependence relation. All of the reported results show that the viscosity of ILs is highly temperature dependent and decreases sharply with temperature increases.

2.7 Surface Tension

For better understanding of the versatility of RTILs it is necessary to have a detailed idea of surface properties. Surface tension of ILs is an important property for understand the vapor-liquid interface. Sanchez et al. (Sánchez, Espel et al. 2009) have studied the surface tension of 13 ILs containing imidazolium, pyridinium, or pyrrolidiniumcations and dicyanamide (DCA-), tetrafluoroborate (BF4-), thiocyanate (SCN-), methylsulfate (MeSO4-), and trifluoroacetate (TFA-) anions. All of the ILs reported decreased surface tension with increasing temperature and having lower surface tension than water. Marsh et al. (Marsh, Boxall et al. 2004) have reported in the literature review that the surface tension of [C_8mim][Cl] ILs is 33.8N/m and[bmim][I] ILs is 54.7N/m. Rooney et al. (Rooney, Jacquemin et al. 2010) have studied surface tension of several imidazolium ILs and reported that surface tension decreases with increase alkyl chain length of imidazoliumcation. Carvalho et al. (Carvalho, Neves et al. 2010) studied experimentally surface tension of six imidazolium, pyridinium, pyrrolidinium, andphosphonium based ILs with bis {(trifluoromethyl) sulfonyl}imide (NTf_2) anion,

reports that introducing methyl group in $[C_4mim][NTf_2]$ IL increases the surface tension and makes it more temperature dependent. Wandschneider et al. (Wandschneider, Lehmann et al. 2008) have measured surface tension of pure ILs by pendant drop method and reported surface tension values between 25-48 mN/m. Kilaru et al. (Kilaru, Baker et al. 2007) have reported the surface tension of imidazolium-, quaternary ammonium-, andphosphonium-based ILs and mentioned that there is negligible effect of anion change on surface tension. Gardas et al. (Gardas and Coutinho 2008) experimentally measured the surface tension of ILs and develop Quantitative structure–property relationship to predict the surface tension of ILs. Their predicted data matches within the maximum deviation 5.75%.

2.8 Specific Heat Capacity

The amount of energy per molecule that any liquid can store before the unit temperature increase of the liquid is defined as heat capacity. Heat capacity is one of the basic and most important thermodynamic properties of ILs used as heat transfer fluids for heat exchange in chemical plants and solar thermal power generation. In literature there is not enough data for the heat of ILs and there are a lot of discrepancies in the heat capacity measurement data. In most of the literatures, the heat capacity of ILs was measured by differential scanning calorimetry (DSC) or modulated differential scanning calorimetry (MDSC) (Waliszewski, Stępniak et al. 2005; Diedrichs and Gmehling 2006;Ge, Hardacre et al. 2008). Diedrichs et al. (Diedrichs and Gmehling 2006) have studied heat capacity of nine pyridinium and imidazolium based ILs using DSC, MDSC, and Tian–Calvet calorimeter. The measurement results present as a function of temperature and shows linear increments of heat capacity with temperature. The study also concludes that the

DSC and MDSC are less time consuming and need smaller sample, whereas Tian–Calvet calorimeter is more time consuming and has a larger sample size and gives more accurate measurements. Waliszewski et al. (Waliszewski, Stępniak et al. 2005) have experimentally measured heat capacity of ILs and estimated by the group contribution method, and found estimated values almost 12% higher than the measured value. The higher values of heat capacity are because the estimation of heat capacity considered only ion–ion interactions. Ge et al. (Ge, Hardacre et al. 2008) have measured the heat capacity and extend the Joback (Joback 1984), Gardas et al. (Gardas and Coutinho 2008) group contribution method; they concluded that ILs with new parameters P, B, and-SO_2- groups using group contribution methods. Liu et al (Liu, Maginn et al. 2012) have reported experimental and molecular dynamic simulation measurements of heat capacity of six ILs and found that heat capacity increases with temperature.

2.9 Thermal Conductivity

Thermal conductivity is one of the most important thermophysical properties of any heat transfer fluids. There are different techniques in the literature to measure thermal conductivity of ILs such as the transient hot wire method (Valkenburg, Vaughn et al. 2005; Ge, Hardacre et al. 2007; Tomida, Kenmochi et al. 2007; Tomida, Kenmochi et al. 2007; Chen, He et al. 2008; Nieto de Castro, Lourenço et al. 2009; Paul, Morshed et al. 2011), guarded parallel plate instrument (Fröba, Rausch et al. 2010), Transient Grating Technique (Frez, Diebold et al. 2006). Chen et al. (Chen, He et al. 2008) have measured the thermal conductivity of 1-butyl-3-methylimidazoliumbis{(trifluoromethyl)sulfonyl} imide, [C_4mim][NTf_2] within the temperature limit 25-40^{o}C and thermal conductivity value was 0.13 $W.m^{-1}K^{-1}$. Ge et al. (Ge, Hardacre et al. 2007) have experimentally

measured the thermal conductivity of eleven ILs within temperature limit 293 K to 353 K. The thermal conductivity of all ILs was found within 0.1 to 0.2 $W.m^{-1}K^{-1}$ and slightly decreases with increasing temperature. They also studied the water and chloride impurity effects on thermal conductivity and reports lower thermal conductivity compared to that of pure ILs. Tomida et al. (Tomida, Kenmochi et al. 2007) studied the thermal conductivity of ILs with function of pressure and temperature for a series of 1-alkyl-3-methylimidazoliumhexafluorophosphates having butyl, hexyl, and octyl groups and reports the negligible effect of alkyl chain length on thermal conductivity of ILs. They also report the weak temperature and pressure effect on thermal conductivity of ILs. Fröba et al. (Fröba, Rausch et al. 2010) have studied 1-ethyl-3-methylimidazolium-based ILs with different anions and reported that for same anion there is a slight increase in thermal conductivity with a higher molar mass of cations. Liu et al. (Liu, Maginn et al. 2012) have reported the thermal conductivity of six ILs within 0.09-0.13 W/m.K and have the trend $[N4_{COOH}111][Tf_2N]$>[bmmim][Tf_2N]>[bmim][Tf_2N]>[bmpyr][Tf_2N]> $[N_{4111}]$ [Tf_2N]>[bmim][Pf_2N]. All of the literature have reported that the thermal conductivity of ILs is much lower than water.

2.10 Applications and Uses of Ionic Liquids

The research areas and publications of ILs increase rapidly because of their unique chemical and physical properties. The researchers also have interest because making combinations with cations' and anions' different physical properties ILs can be synthesis based on the specific purposes. The application of ILs includes material processing (Reddy 2009), as a catalyst for synthesis of inorganic nano-materials (Zhou 2005; Singh, Kumari et al. 2009), as electrolytes for battery and solar cells (Chen, Officer

et al. 2005; Lewandowski and Świderska-Mocek 2009), and as lubricants (Jiménez and Bermúdez 2009). Other than those specific applications the possible applications of ILs are shown in Fig.2.3. Reddy (Reddy 2009) has used C_4mimCl-$AlCl_3$ IL to recycling of Aluminum and found greater than 99.9% purity of the deposits. Singh et al. (Singh, Kumari et al. 2009) have prepared Cu nanoparticles in ILs and mentioned that the use of ILs makes the nanoparticles preparation more easy and environmently friendly. Chen et al. (Chen, Officer et al. 2005) firstly incorporates IL electrolyte in solar cell and found overall conversion efficiency 0.14%. Jimenez et al. (Jiménez and Bermúdez 2009) studied the wear behavior of titanium and steel in contact with IL. The experimental results were compared with the conventional mineral oil and reported 60% reduction in mean friction value. Plechkova et al. (Plechkova and Seddon 2008) have given an overall idea of chemical industry application of ILs and current supplier of ILs. Bhatt et al. (Bhatt and Gohil 2013) have used the ILs as phase change materials (PCMs) in solar cookers and found that ILs makes the process slower to achieve the cooking temperature and remain the heat for a long time which is important in late hour cooking. Wishart (Wishart 2009) has summarized all of the types of energy applications of ILs; including electrolyte in solar photovoltaic cell, solar thermal conversion, and fuel cell.

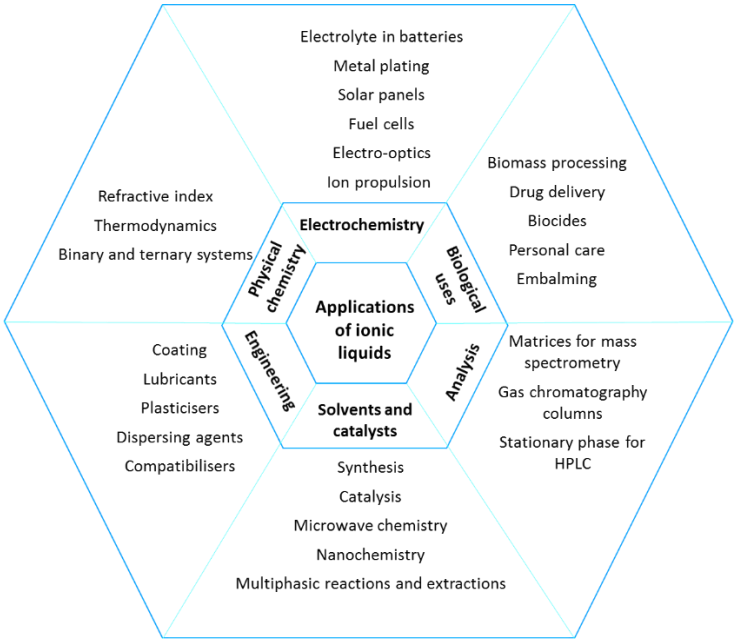

Figure 2.3 Applications of ionic liquids (Plechkova and Seddon 2008)

There are few studies on the applicability of ILs in solar collector applications (Wu, Reddy et al. 2001; Blake, Moens et al. 2002;Moens, Blake et al. 2003). Wu et al. (Wu, Reddy et al. 2001) have studied the applicability of [C_4min][PF_6], [C_8mim][PF_6], [C4min][bistrifluromethaneSul- flonimide], [C_4min][BF_4], [C_8mim][BF_4], and [C_4min][bistrifluromethanesulflonimide] ILs as a heat storage medium for solar collector. They calculate the storage density of [C_8mim][PF_6] IL which is 378 MJ/m^3. Moens et al. (Moens, Blake et al. 2003) have performed an overall assessment study of ILs to use as heat transfer fluid is solar parabolic trough systems and found high thermal stability which is an important issue for solar thermal collectors. Blake et al. (Blake, Moens et al. 2002) analyzed the levelized electricity cost (LEC) of different fluids and found ILs potentially reduce the operating cost due to low freezing point.

2.11 Nanofluids

The concept of nanoparticles with fluid called nanofluids was first proposed by Choi (Choi and Eastman 1995) which defined as dilute suspensions of particles with at least one dimension smaller than about 100 nm. The nanofluids have the great interest in heat transfer research because of its enhanced heat transfer properties such thermal conductivity and heat capacity, which are very important for any heat transfer fluids (Lee, Hwang et al. 2008). There are various metallic and nonmetallic nanoparticles such as Al_2O_3, CuO, TiO_2, carbon nanotubes, carbon nanofibers, Cu, Ag, and Au used for stable nanofluids (Xie, Lee et al. 2003; Murshed, Leong et al. 2005; Lee, Yoon et al. 2007; Wei and Wang 2010; Mazumder, Davis et al. 2013). The interest of nanofluids as heat transfer fluids is still growing which is clear from the number research article publications in Fig. 2.4.

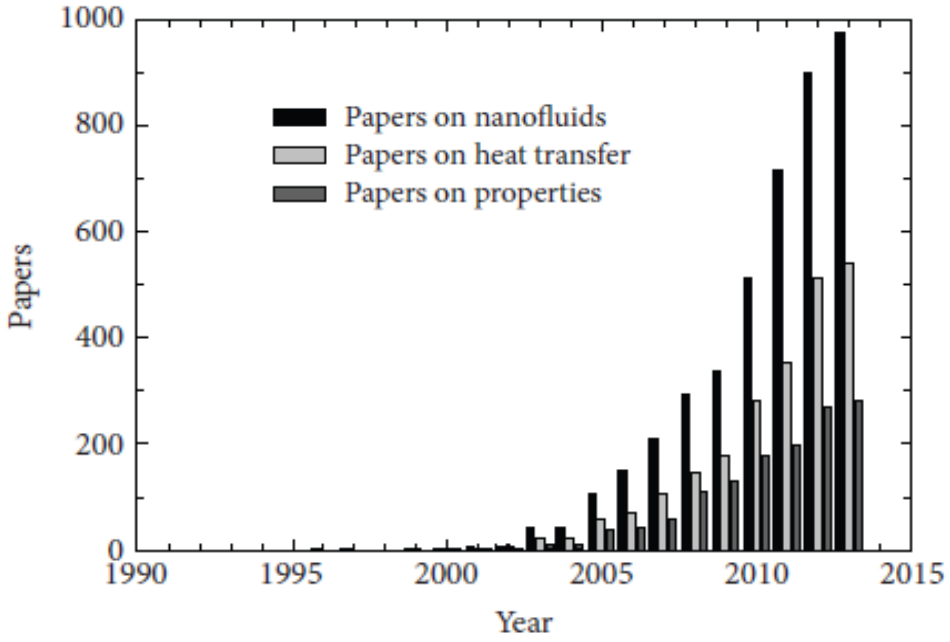

Figure 2.4 Number of publicationsof nanofluids, heat transfer in nanofluids, and properties of nanofluids (Manca, Jaluria et al. 2014)

The main focus of the nanofluids is the enhanced thermophysical properties and heat transfer behavior. Among those literatures, there are few investigations emphasized which are related to the nanoparticles, shape of the particles, natural convection, and forced convection study. Lee et al. (Lee, Hwang et al. 2008) have studied experimentally the viscosity and thermal conductivity of water based Al_2O_3 nanofluids at low concentration 0.01 to 0.3 vol.% and reported enhanced thermophysical properties of nanofluids compare to base fluid. The thermal conductivity of TiO_2-water nanofluids was observed by Murshed et al. (Murshed, Leong et al. 2005). Two different particle shapes (spherical and rod) were investigated and they concluded that the rod like particles containing nanofluids higher thermal conductivity compare to spherical nanofluids. Srivastava (Srivastava 2012) has also theoretically investigated the thermal conductivity and viscosity of TiO_2-water nanofluids. In that study, the enhanced thermal conductivity and viscosity was predicted by the aggregation of nanoparticles in nanofluids. Leong et al. (Leong, Yang et al. 2006) proposed interfacial layer of nanoparticles model to predict the thermal conductivity of nanofluids and experimental results predicted well by the model. Chen et al. (Chen, Ding et al. 2007) have studied the rheological behavior of ethylene glycol based TiO_2 nanofluids and reported Newtonian behavior of nanofluids. They also predicted the experimental viscosity with aggregation model.

There are few experimental studies of the natural convection of water based nanofluids in literature (Putra, Roetzel et al. 2003; Wen and Ding 2005; Nnanna 2007; Ho, Liu et al. 2010; Li and Peterson 2010; Paul, Morshed et al. 2013). Putra et al. (Putra, Roetzel et al. 2003) have experimentally studied the natural convection of Al_2O_3 and CuO-water nanofluids in a cylindrical enclosure placed horizontally and heated from one

side with other side kept cold. They reported systematic degradation of natural convection heat transfer and mentioned that particle fluid slip and sedimentation of nanoparticles are the possible reason of the degradation. Wen et al. (Wen and Ding 2005) performed both transient and steady state natural convection experiments of TiO_2-water nanofluids and they found lower heat transfer coefficients of nanofluids compared to the base fluid and they explained several possible reasons of those degradation including: nanofluids thermophysical properties, convection by concentration difference, pH influence, and particle-surface interactions. Nnanna (Nnanna 2007) investigated natural convection of Al_2O_3-water nanofluids in the differentially heated enclosure and reported that the concentration>2% degrades the natural convection heat transfer due to the higher kinematic viscosity of nanofluids. Li et al.(Li and Peterson 2010) and Ho et al. (Ho, Liu et al. 2010) studied the natural convection of Al_2O_3 nanofluids in cylindrical and square enclosure respectively; they also reported decreased natural convection heat transfer coefficient. Paul et al. (Paul, Morshed et al. 2013) have investigated the natural convection of ZnO-water nanofluids in a rectangular cavity heated from below and found the degrade behavior of nanofluids and degradation increases with nanoparticle concentration.

The enhancement of heat transfer coefficient under forced convection was also reported by other researchers, where experiments were carried out for Al_2O_3-water nanofluids at laminar (Wen and Ding 2004; Zeinali Heris, Nasr Esfahany et al. 2007; Lai, Phelan et al. 2008) and turbulent (Torii 2010) flow regime. Wen et al. (Wen and Ding 2004) have performed the forced convection study with constant heat flux flow through a copper tube under laminar flow region and reported up to ~47% enhanced heat transfer of

1.6 vol% Al_2O_3-water nanofluids. They also found that the heat transfer behavior could not predict by the conventional Shah's equation (Shah 1975). Lai et al. (Lai, Prasher et al. 2009) investigated forced convection of Al_2O_3-water nanofluids in a 1.02mm diameter tube under constant heat flux conditions and reported the enhanced heat transfer coefficient of nanofluids. Heriset al (Zeinali Heris, Nasr Esfahany et al. 2007) reported the enhanced heat transfer coefficient of Al_2O_3-water nanofluids performing forced convection in circular tube with the constant temperature boundary condition. Torii(Torii 2010) studied the forced convection of diamond, CuO, and Al_2O_3nanofluids in the turbulent flow regime and reported 9.8%, 6.6%, and 5.4% enhancement of Nusselt number for 1 vol% nanofluids respectively at $Re = 6000 \pm 100$. He et al. (He, Jin et al. 2007) have investigated the forced convection behavior of TiO_2 nanofluids in a vertical tube under laminar and turbulent flow region and found enhanced heat transfer in both cases. They also found that the particle size does not affect much of heat transfer but the thermal conductivity decreases with particle size. Chen et al. (Chen, Yang et al. 2008) have studied the rheological behavior of nanofluids with rod like TiO_2 nanoparticles and observed shear thinning behavior of nanofluids. Shear viscosity reaches a constant at a shear rate around ~100–1000 s^{-1} based on the nanoparticles concentration. The forced convection experimental investigation of multi wall carbon nanotube (CNT) based nanofluids was observed by Ding et al. (Ding, Alias et al. 2006) and a maximum 350% enhancement at $Re = 800$ was found for 0.5 wt% nanofluids. The possible mechanism of enhancement of heat transfer behavior of nanofluids were discussed in the entire above experimental enhancement studies, which includes enhancement of thermal conductivity, enhancement of thermal conduction in flow condition, non-uniform shear across the tube,

enhancement of wettability of the flowing tube, boundary layer thickness reduction, and particle aggregation. The exact mechanism of the heat transfer behavior of nanofluids is still under investigation.

2.12 Ionic Liquids with Nanoparticles

The favorable thermophysical properties of ILs and enhanced heat transfer behavior of nanofluids have encouraged the researchers to blend those two materials (ILs and nanoparticles) to form ILs based nanofluids named nanoparticle enhanced ionic liquids (NEILs). There are several groups working on the thermophysical properties of NEILs based on different applications. Nieto de Castro et al. (Nieto de Castro, Lourenço et al. 2009; Nieto de Castro, Murshed et al. 2012) and Murshed et al. (Murshed, de Castro et al. 2011)reports the thermal conductivity and heat capacity of 1-hexyl-3-methylimidazolium tetrafluoroborate $[C_6mim][BF_4]$, 1-butyl-3-methylimidazoliumhexafluorophosphate $[C_4mim][PF_6]$, 1-hexyl-3-methylimidazol iumhexafluorophosphate $[C_6mim][PF_6]$, 1-butyl-3-methylimidazolium trifluorome thanesulfonate$[C_4mim][CF_3SO_3]$, and 1-butyl-1-methylpyrrolidiniumbis {(trifluoromethyl)sulfonyl}imide $[C_4mpyrr][(CF_3SO_2)_2N]$, ILs and multiwalled carbon nanotubes (MWCNTs) based IoNanofluids, shows the thermal conductivity enhancements of IoNanofluid5 to 35 % and heat capacity enhanced up to 8%. Wittmar et al. (Wittmar, Ruiz-Abad et al. 2012) have studied the rheological behavior of SiO_2 nanoparticles in hydrophobic and hydrophilic imidazolium-based ILs and reported strong effect of ILs hydrophilicity, nanoparticles surface, concentration of the nanoparticles, and temperature on rheological behavior; improved colloidal stability of nanofluids containing SiO_2 nanoparticles with hydrophobic ILs. Fox et al (Fox, Visser et al. 2013)

have investigated the thermophysical properties including thermal stability, viscosity, and thermal conductivity of NEILs containing 1-butyl-2,3-methylimidazolium bis(trifluoromethylsulfonyl)imide ([C_4mmim][Tf_2N])IL and different nanoparticles such as: spherical Al_2O_3, whiskers Al_2O_3, carbon black, MWCNT, single walled carbon nanotube (SWCNT), stacked grapheme nanofiber, ZnO, Fe_2O_3, SiO_2, CuO, and Au. They observed that whiskers NEILs have the highest thermal conductivity enhancement and carbon black have the highest viscosity. The aggregation and strong interaction between ILs and nanoparticles are the possible reason of the viscosity and thermal conductivity enhancement, respectively. Wang et al. (Wang, Wang et al. 2011) have reported enhanced thermal conductivity but lower heat capacity of graphene (GE) and MWCNTs IoNanofluids compare to base ILs. Bridges et al.(Bridges, Visser et al. 2011) have studied the heat capacity and thermal stability of NEILs made of 1-Butyl-2,3-dimethylimidazolium bis{(trifluoromethyl)sulfonyl}imide ([C_4mmim][NTf_2]) with Al_2O_3 and carbon black (CB) nanoparticles; they have reported higher heat capacity values for Al_2O_3 NEILs and lower heat capacity of CB NEILs. They also reported no detrimental effect on thermal stability of NEILs. Ueno et al. (Ueno, Hata et al. 2008; Ueno, Imaizumi et al. 2008; Ueno, Inaba et al. 2008) studied the colloidal stability of silica nanoparticlesin1-alkyl-3-methylimidazolium ([$C_n$mim])-based ILswith different anionic structures; ionic transport and viscoelastic properties of nanofluids containing 1-ethyl-3-methyl imidazoliumbis(trifluoromethanesulfonyl) amide ([C_2mim][NTf_2]) IL (Ueno, Inaba et al. 2008) and [BF_4] anion-based ILs (Ueno, Hata et al. 2008) with silica nanoparticles. They exhibit the silica nanoparticles have long term colloidal stability in ILs and higher ionic conductivity of nanofluids compare to base [C_2mim][NTf_2];

reaction-limited cluster aggregation (RLCA) model also was proposed for the viscoelastic response. Wang et al.(Wang, Wang et al. 2010; Baogang Wang 2011; Wang, Wang et al. 2011) studied the thermal conductivity, rheological and tribological behavior of 1-butyl-3-methylimidazolium hexafluorophosphate ([Bmim][PF_6]) IL based nanofluids with different size gold nanoparticles (Baogang Wang 2011), gold nanoparticles with different stabilizing agents (Wang, Wang et al. 2011), and functionalized MWCNTs (Wang, Wang et al. 2010); they reported enhanced thermal conductivity, shear thinning behavior and favorable friction-reduction properties of nanofluids compare to base IL. Paul et al. (Paul, Morshed et al. 2012; Paul, Morshed et al. 2013) have recently reported enhanced thermal conductivity and heat capacity of NEILs made with 1-butyl-3-methylimidazolium bis{(trifluoromethyl)sulfonyl}imide ([C_4mim][NTf_2]) and N-butyl-N-methylpyrrolidiniumbis{(trifluoromethyl)sulfonyl} imide, ([C_4mpyrr][NTf_2]) ILs with 0.5 and 1 wt% Al_2O_3 nanoparticles, respectively. Shin et al. (Shin and Banerjee 2010; Shin and Banerjee 2011) and Tiznobaik et al. (Tiznobaik and Shin 2013) reported enhanced heat capacity of nanofluids synthesized by lithium carbonate and potassium carbonate (62:38 ratio) and alkali chloride salt eutectic with SiO_2 nanoparticles (1%by wt.) for solar thermal applications.

2.13 Summary

In the brief literature of ionic liquids and nanoparticle enhanced ionic liquids, it was observed that the ILs has favorable thermophysical properties, which makes them potential thermal fluids for solar collector and many other applications. The thermophysical properties of ILs were enhanced by the dispersion small amount of nanoparticles in it. Although there are a lot of research articles on thermophysical

properties of ILs and NEILs there are few studies on heat transfer and thermal performance. Based on the literature of ILs and NEILs the heat transfer performance under natural and forced convection experiments was performed in the present research.

CHAPTER 3

EXPERIMENTAL FACILITY

3.1 Introduction

In the present dissertation thermophysical properties of ionic liquids (ILs) and nanoparticle enhanced ionic liquids (NEILs) were measured experimentally. The author also performs the natural and forced convection of ILs and NEILs. For natural convection an experimental setup was designed and built in a rectangular cavity heated from below condition with two different aspect ratios. Forced convection experimental loop facility was equipped with pump, heat exchanger, storage tank, heater, and power supply. The thermophysical property measurement equipment's are pycnometer, LVDV-II+ProCP Viscometer, KD2 Pro thermal property analyzer, and Differential Scanning Calorimetry. In the present chapter the detail working principle of the equipment and the experimental procedure of the test facilities are discussed.

3.2 Measurements of Density

The density of ILs and NEILs were measured using a 1 mL Pycnometer from Thomas Scientific and presented in Fig. 3.1. The pycnometer and the samples were placed in a thermal bath (Thermo NESLAB) to maintain a uniform temperature. The weight of the sample was measured by using METTLER TOLEDO balance which has a precision of 0.01 mg. Before using for ionic liquid the pycnometer was calibrated with

water and was found to be accurate to within 0.5%. The volumetric thermal expansion coefficient was calculated by using equation:

$$\beta = -\frac{1}{\rho}(\frac{\partial \rho}{\partial T})_p \quad (3\text{-}1)$$

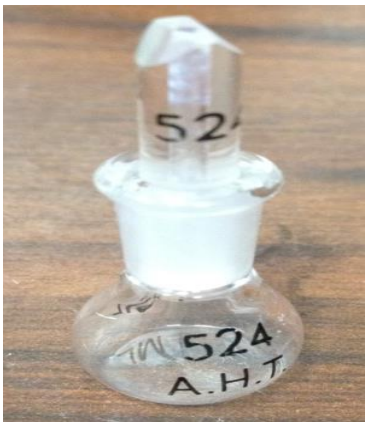

Figure 3.1 Pycnometer

3.3 Measurements of Viscosity

The viscosity of the ILs and NEILs were measured by using a cone and plate type rotary viscometer (LVDV-II+ProCP, from Brookfield Engineering Co.) and presented in Fig. 3.2.

Figure 3.2 LVDV-II+ProCP Viscometer

The sample size of the cone and plate arrangement is 1mL. The cone and plate arrangement has a thermal jacket to maintain a constant sample temperature and it has the temperature accuracy within ±0.1^{o}C. For temperature control a thermal bath (Thermo NESLAB) was used with temperature accuracy within ±0.01K. The viscometer was calibrated by using company standard liquid.

3.4 Measurements of Thermal Conductivity

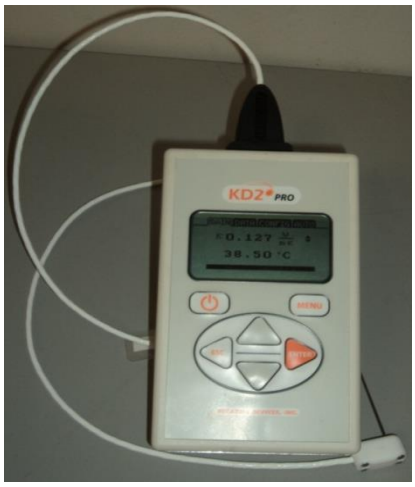

Figure 3.3 KD2 Pro thermal property analyzer

Thermal conductivity of ILs and NEILs were measured by using the KD2 Pro thermal property analyzer (Decagon Device, USA) and presented in Fig. 3.3. The measurements principle is based on the transient hot wire method. The meter has a probe with 60 mm length and 1.3 mm diameter with a heating element and a thermoresistor which is inserted vertically into the test sample. The probe is connected with a microcontroller for controlling and conducting the measurements. Before using for IL and NEIL the meter was calibrated with distilled water and company supplied standard glycerin. A thermal bath (Thermo NESLAB) was used to maintain a constant temperature of the measuring sample. The temperature accuracy of the bath is within ±0.01 K. The

thermal bathused to control temperature for all experimental measurements is presented in Fig. 3.4.

Figure 3.4 Thermo NESLAB thermal bath

3.5 Measurements of Heat Capacity

Heat capacity of ILs and NEILs were measured using Differential Scanning Calorimetry (DSC Q2000 from TA instruments Inc.). The sample was placed in a standard aluminum hermetic pan covered with lid and the average sample size was 12.98-16.35mg. Nitrogen was used as cooling system at flow rate of 40 mL/min. The DSC run was performed from 25^{o}C to 345^{o}C at a heating rate of 10^{o}C/min. There were three different runs performed and the experimental procedure was the same as described by Shin et al.(Shin and Banerjee 2011).

3.6 Synthesis of Nanoparticle Enhanced Ionic Liquids (NEILs)

The experiment used base ionic liquids (ILs) 1-butyl-3-methylimidazolium bis{(trifluoromethyl)sulfonyl}imide ([C_4mim][NTf_2]);Chemical Abstracts Service(CAS) registry number: 174899-83-3; molecular formula: $C_{10}H_{15}F_6N_3O_4S_2$; molecular weight:419.37 g/mol,N-butyl-N-methylpyrrolidiniumbis{trifluoromethyl)sulfonyl} imide

([C_4mpyrr][NTf_2]);CAS: 223437-11-4; molecular formula: $C_{11}H_{20}F_6N_2O_4S_2$; molecular weight:422.41 g/mol, N-butyl-N,N,N-trimetylammoniumbis(trifluormethylsulfonyl)imide ([N_{4111}][NTf_2]); CAS: 258373-75-5; molecular formula: $C_9H_{18}F_6N_2O_4S_2$; molecular weight: 396.37 g/mol, and 1-butyl-2, 3-dimethylimidazolium bis(trifluoromethylsulfonyl)imide, ([C_4mmim][NTf_2]) CAS 350493-08-2 molecular formula: $C_{11}H_{17}F_6N_3O_4S_2$molecular weight:433.39 g/mol. 99% pure ILs are purchased from IoLiTec Company (Germany). The chemical structure of cation and anion of all ILs is shown in Fig.3.5.

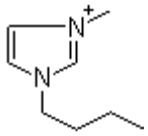

$[C_4mim]^+$

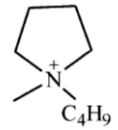

$[C_4mpyrr]^+$

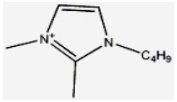

$[N_{4111}]^+$

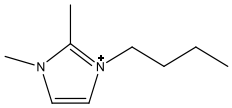

$[C_4mmim]^+$

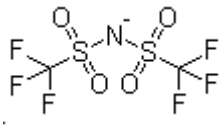

$[NTf_2]^-$

Anion

Figure 3.5 Chemical structure of cation and anion of all ionic liquids

Al_2O_3 nanoparticles were purchased from Sigma-Aldrich, USA. Spherical shaped nanoparticles are γ-phase with particle size<50nm (TEM) and surface area >40 m^2/g (BET); whiskers nanoparticles having diam. × L, 2-6 nm × 200-400 nm and aspect ratio>

100 (TEM). Al_2O_3 were dispersed in the base ILs using a vortex mixture (Mini Vortexture from Fisher Scientific) to produce NEILs which was further agitated for ~90 min to break any possible agglomeration of nanoparticles. The weight percentage of nanoparticles were 0.5, 1.0, and 2.5. The thermophysical properties were measured just after synthesis of NEILs. SEM image of the Al_2O_3 nanoparticles is presented in Fig. 3.6, where a flow diagram of NEILs preparation is also presented.

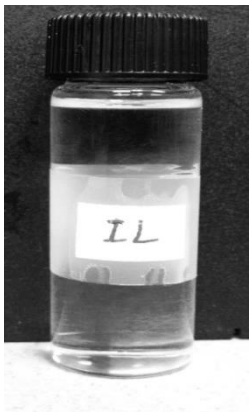

Base ionic liquid

+

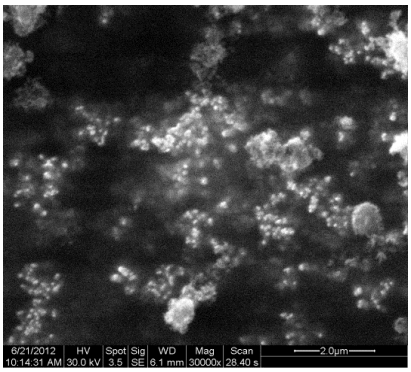

SEM image of Al_2O_3 nanoparticles

Vortex mixture

Nanoparticle Enhanched Ionic Liquids (NEILs)

Figure 3.6 Sysnthesis of NEILs, IL sample, SEM image, vortex mixture, and NEILs sample

3.7 Characterization of NEILs

The nanoparticles' size was characterized by using FEI Quanta200 Scanning Electron Microcsope (SEM). Also the NEILs was characterized by using Hitachi H8000 Transmission Electron Microscope (TEM). The SEM and TEM image of Al_2O_3 nanoparticles are presented in Fig. 3.7 and Fig. 3.8 respectively.

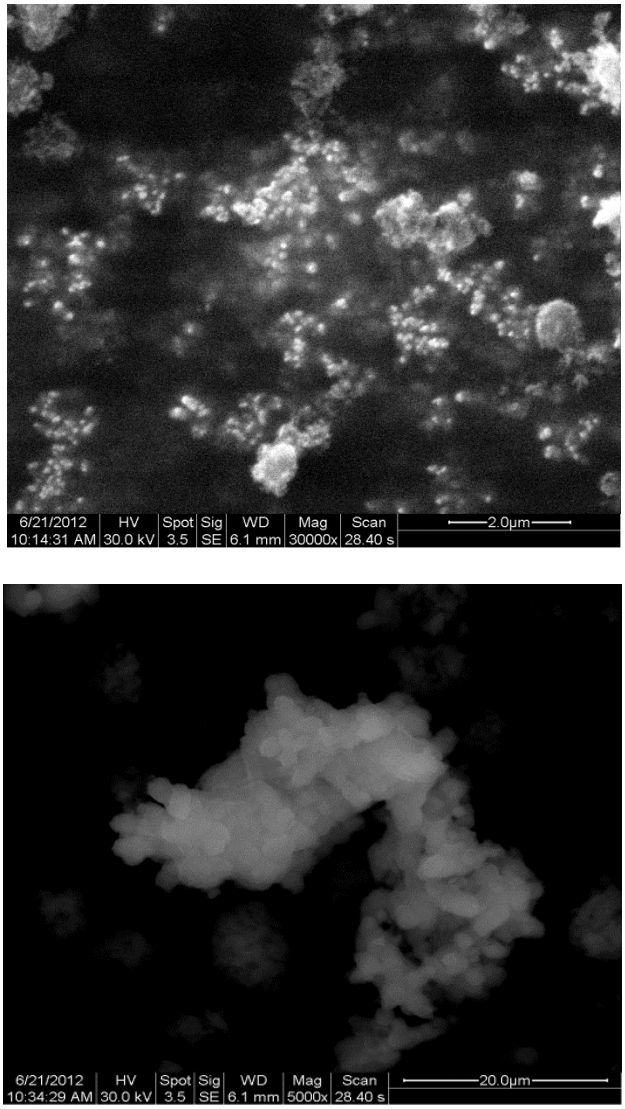

Figure 3.7 SEM image of Al_3O_3 nanoparticles (a) spherical (b) whiskers

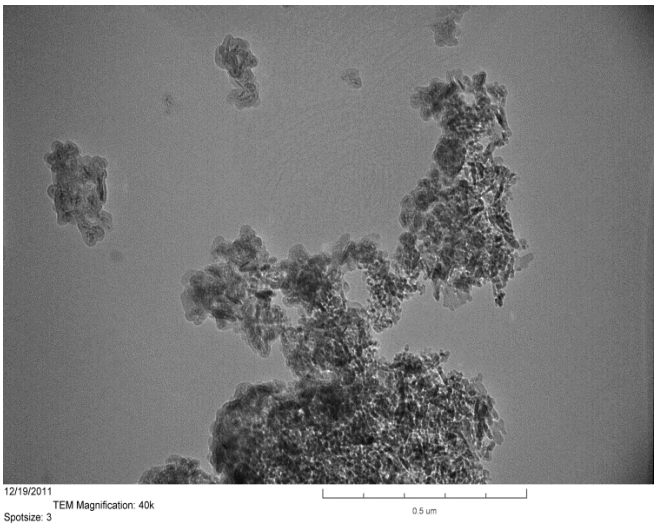

Figure 3.8 TEM image of 0.5 wt% NEIL ([C_4mim][NTf_2]+spherical Al_2O_3)

Dispersion of nanoparticles in iILs was observed by an Olympus ix70 inverted microscope. Also the nanoparticles' size distribution on NEILs was observed by using the time resolved dynamic light scattering (TRDLS) technique.

3.8 Natural Convection Experimental System

Fig. 3.9(a) shows the schematic of the rectangular enclosure used in the experimental investigations; Fig. 3.9(b) is the photograph of experimental setup, which includes test enclosure, heater, insulation, thermal bath, flow meter, power supply, data acquisition system, and thermocouples. The experimental test sections are rectangular enclosures, made with clear polycarbonate Lexan sheet and the dimensions are (length×width×height) 50×50×50mm and 50×50×75mm.

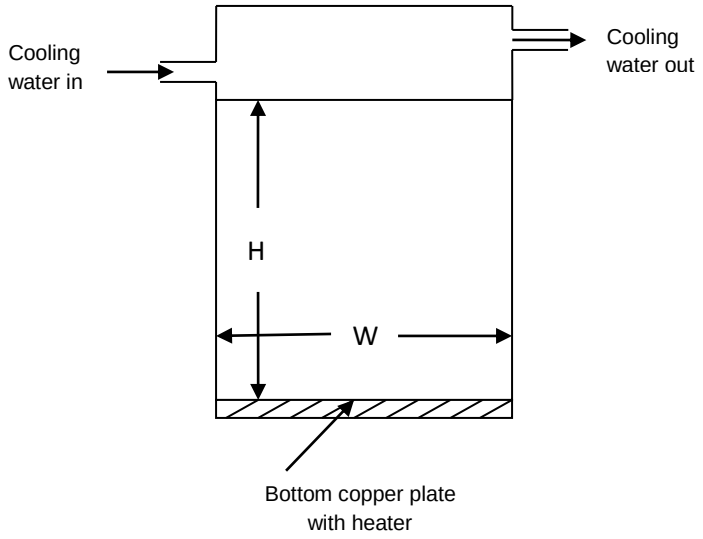

(a)

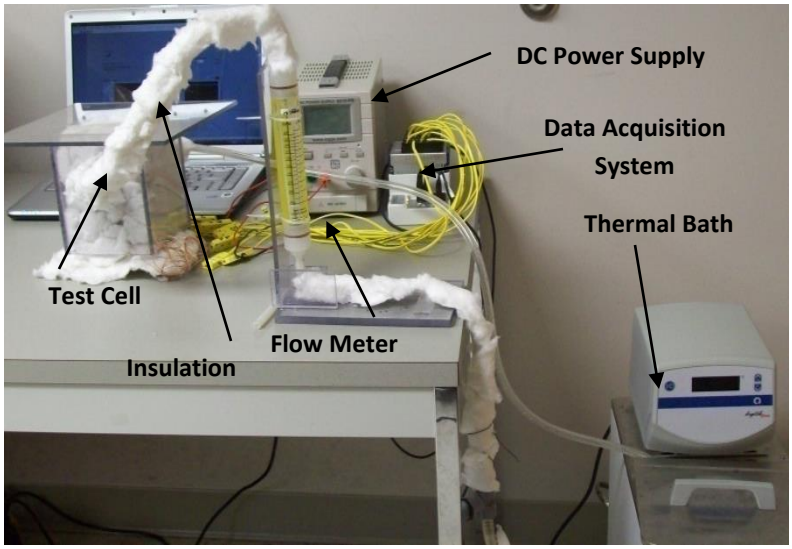

Figure 3.9 Schematic of experimental cavity (b) Photograph of experimental setup

Two ends of the enclosure are made with conductive copper plates of thickness 3 mm to perform as hot and cold surfaces. There are two openings in the top copper sheet which are for filling liquid and removing air bubbles from the enclosure. The top copper sheet is maintained at a uniform temperature by flowing cold water through a secondary

enclosure of 25 mm height situated on top of the copper sheet. A flexible silicone rubber fiberglass insulated heater (20W, from OMEGA) is closely attached to the lower copper surface. The heating power is supplied from a DC power supply (30W, E3612A, from Agilent Inc). The heating and cooling surface temperatures are measured by using K-type thermocouples of 0.13 mm diameter. There are two other thermocouples which are connected to the cold water inlet and outlet lines to measure the inlet and outlet temperatures of the cold water. All of the thermocouples are calibrated using a constant temperature bath (Thermo NESLAB) and thermocouples are connected to the data acquisition system by Labview software. All of the thermocouples are connected to a National Instrument (NI) data acquisition system cDAQ 9178 via a temperature card NI 9211 which was interfaced with a computer. Labview software was used for collecting and recording the data. The input voltage and current were measured from the display of the power supply. The whole system was insulated with the fiberglass insulation to reduce the heat loss to the environment.

3.9 Data Processing of Natural Convection

Before performing any experiment the test enclosure was rinsed thoroughly several times with DI water and the liquid was poured into the test enclosure with care to avoid entrapment of any air bubbles into the enclosure. The NEILs was shaken very well before filled into the enclosure. After preparing the test section, turn on the power supply and set the desired voltage. During the experiment the hot and cold surface temperatures were monitored and recorded until a steady state was reached. After recording the data, the voltage increases to the next desired value. In the experiment different Rayleigh numbers

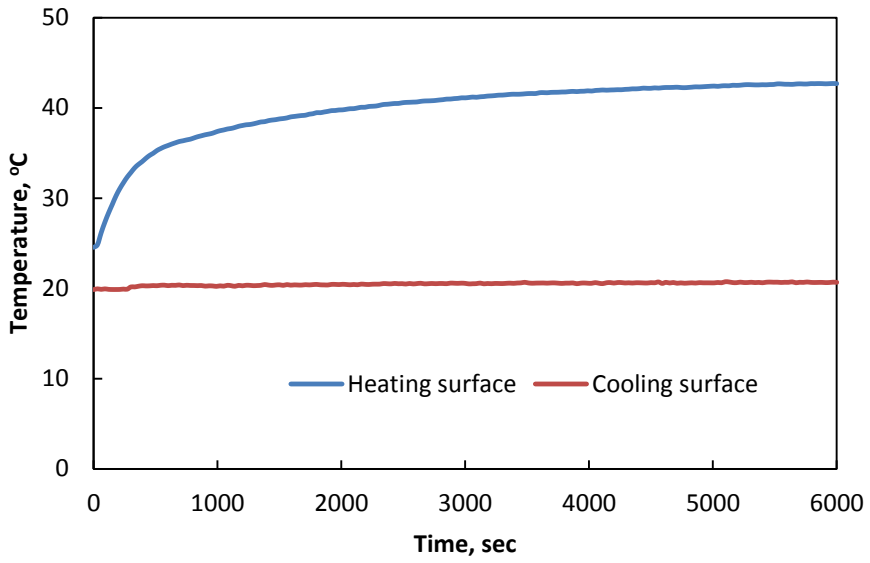

Figure 3.10 Initial transient hot and cold surface temperature

have been achieved by changing the heat flux. During the experiment the hot and cold surface temperatures are monitored and recorded until a steady state is reached. Fig. 3.10 shows the typical hot and cold surface temperature profiles. Heat flux $q^{"}$ was calculated from the input power of the heater and dividing by the surface area of the copper plate.

$$q^{"} = \frac{VI}{A} \tag{3-2}$$

where, V is the input voltage, I is the input current, A is the surface area of the heater. Considering the heat loss, corrected heat flux ($q^{"}_{corr}$) was calculated from the heat removed by the cold water and actual input heat. Hot surface temperature, T_{hf} and cold surface temperature, T_{cf} of the internal surface have been calculated from the thermocouple readings and using the one dimensional (1-D) steady state heat conduction equation:

$$T_{hf} = T_h - (\frac{q^{"}_{corr}}{k_c} x) \quad (3\text{-}3a)$$

$$T_{cf} = T_c + (\frac{q^{"}_{corr}}{k_c} x) \quad (3\text{-}3b)$$

Finally the heat transfer coefficient h was calculated by:

$$h = \frac{q^{"}_{corr}}{(T_{hf} - T_{cf})} \quad (3\text{-}4)$$

3.10 Forced Convection Experimental Setup

Fig. 3.11(a) and (b) presents the photograph of test section and schematic of the flow loop used in thermal performance of ILs and NEILs experiment. The loop consisted of a pump, test section, heat exchanger, collection tank, and pressure transducer. The pump was connected to a frequency inverter which was calibrated for the pump using a stopwatch and bucket method. The test section was a stainless steel tube of 3.86 mm inner diameter, 6.35 mm outer diameter, and 990.6 mm length. Uniform heat flux was applied to the test section using a flexible heating tape (OMEGA Engg. FGS101-040). Power was supplied to the heater using a DC power (Agilent Technologies: 6655A) supply. To reduce the heat loss to the ambient and to ensure constant heat flux condition, the entire test section was insulated with fiberglass insulation. Five thermocouples were mounted on the tube surface to measure surface temperature. The thermocouples' position was at a normalized axial distance with respect to tube diameter (x/D) of 23.03 (T_1), 75.65 (T_2), 128.28 (T_3), 180.92 (T_4), and 233.55 (T_5) from the test section inlet. Another two thermocouples were inserted into the tube to measure the inlet and outlet liquid bulk temperatures. A differential pressure transducer was connected between the inlet and outlet of the test section to measure the pressure drop within the test section. All

thermocouples and the pressure transducer were connected to a National Instrument (NI) data acquisition system cDAQ-9178 via a temperature card NI 9211 and pressure card NI 9203 which were interfaced with a computer. Labview software was used for recording all data.

(a)

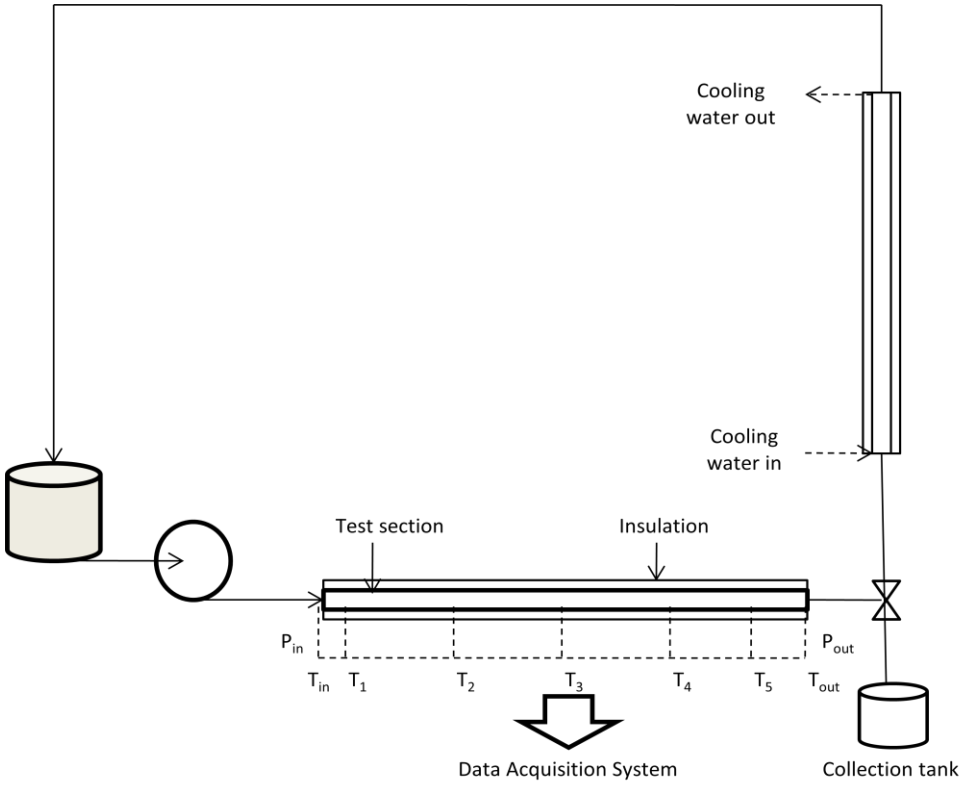

(a)

Figure 3.11 (a) Photograph of test section (b) Schematic of the forced convection experimental setup

To perform the experiment with base ILs and NEILs the whole test loop was washed out with DI-water andthe pump was run for several hours to remove all water bubbles from the test loop. After that the experimental liquid was placed in the tank and the pump was set to run at a desired flow rate. At the same time the desired power input from the DC power supply was applied. The test section was allowed to reach steady state before the temperature data were recorded, which was monitored by the LabView software. After recording the data, the next pump flow rate was increased. The same procedure was repeated up to maximum allowable flow rate of the pump.

3.11 Data Processing of Forced Convection

The test section was allowed to reach a steady state before the temperature data were recorded. Heat flux ($q^{"}$) was calculated from input power (Q) of the heater and heating surface area (A) using the following equation:

$$q^{"\prime\prime} = \frac{Q}{A} = \frac{VI}{\pi D_o L} \tag{3-5}$$

where V and I are the input voltage and current respectively, D_o is the outer diameter of tube, and L is the heating length.

Local heat transfer coefficient at an axial distance x, along the test section, $h(x)$, was calculated using the equation:

$$h(x) = \frac{q^{"\prime\prime}}{T'_w(x) - T_f(x)} \tag{3-6}$$

where $T'_w(x)$ and $T_f(x)$ are the local temperatures of the inner surface and liquid respectively.

The inner surface temperature was calculated using the steady state one-dimensional heat conduction equation with the constant heat flux boundary condition for which the governing equation is (Incropera, Lavine et al. 2011):

$$\frac{1}{r}\frac{d}{dr}\left(r\frac{dT}{dr}\right) = 0 \tag{3-7}$$

The solution for the inner surface temperature becomes

$$T_w'(x) = T_w(x) - \frac{Q.\ln(r_o/r_i)}{2\pi L k_s} \tag{3-8}$$

where $T_w(x)$ is the local temperature of outer surface as measured by the thermocouples, r_o and r_i are the outer and inner radius of the test tube respectively, and k_s is the thermal conductivity of stainless steel.

Meanwhile, the local temperature of the liquid was calculated using the energy balance relation:

$$T_f(x) = T_{fi} + \frac{Q}{\rho C_p V'}\frac{x_1}{L} \tag{3-9}$$

where T_{fi} is the liquid inlet temperature of the test section, C_p is the heat capacity of the liquid, and V' is the volumetric flow rate. All the fluid properties were evaluated at the average ($T_{av} = \frac{T_{in}+T_{out}}{2}$) of the inlet and outlet fluid temperature of the test section.

3.12 Measurement Uncertainties

In the natural and forced convection two different power supplies were used. The power supply that is used for natural convection has uncertainty of voltage and current ±0.1V, and ±0.001A respectively. The power supply that is used for forced convection has uncertainty of voltage and current ±0.01V, and ±0.001A respectively. The measurement uncertainty of thermocouples are ±0.18^{o}C to ±0.2^{o}C. A systematic

uncertainty analysis was performed using standard Kline and McClintock method (Kline and McClintock 1953):

$$W_p = \sqrt{\sum_{i=1}^{n} \left(\frac{\partial p'}{\partial a'} w'\right)^2} \tag{3-10}$$

where W_p is the total uncertainty of calculated parameter, p', and a' variables of functional dependence, and w' is the uncertainty of the independent variables. Since the dimensionless numbers are the functions of numerous measured quantities and physical properties, therefore the uncertainty will propagate. The maximum uncertainty calculated from for the input power, heat transfer coefficient, Nusselt number, Rayleigh number, and Reynolds number are presented in Table 3.1.

Table 3.1 Maximum uncertainty of experimental measurements

Natural convection		Forced convection	
Power	±1.62%	Power	±0.15%,
Heat transfer coefficient	±2.23%	Heat transfer coefficient	±0.89%.
Nusselt number	±4.59%	Nusselt number	±4.35%
Rayleigh number	±11.58%	Reynolds number	±5.86%

CHAPTER 4

THERMOPHYSICAL PROPERTIES OF ILS AND NEILS

4.1 Introduction

Thermophysical properties of any heat transfer fluids (HTFs) are very important to assess their potentiality in any system. Density and volumetric thermal expansion coefficient plays an essential role in buoyancy driven heat transfer character. Viscosity and thermal conductivity are important in fluid flow and heat conduction measurements. Heat capacity is the measure of amount of heat storage capacity by the HTFs. There are a lot of studies of thermophysical properties of ionic liquids (ILs) and nanoparticle enhanced ionic liquids (NEILs). Here, the main purpose of the dissertation is to investigate the thermal performance under natural and forced convection of ILs and NEILs. For greater fidelity of the thermal performance, thermophysical properties such as density, viscosity, heat capacity, and thermal conductivity of the ILs and NEILs were measured experimentally and reported.

Here, two different shapes (spherical and whiskers) of Al_2O_3 naoparticles are used to form NEILs with $[C_4mpyrr][NTf_2]$IL to see the shape particle shape effect on thermophysical properties. The experimental thermophysical properties of ILs are compared with previously published data and found in reasonably good agreement with the previous data. The experimental effective thermophysical properties of NEILs

are compared with the existing theoretical model and the plausible mechanism of thermophysical properties enhancement are discussed.

4.2 Density of ILs

The density of all four ILs are measured within temperature range from 10-70^{o}C. Fig. 4.1 (a-d) shows the density of ILs as a function of temperature and the density data were compared with the previous published data (Anthony, Anderson et al. 2005; Tokuda, Hayamizu et al. 2005; Jacquemin, Husson et al. 2006; Tokuda, Tsuzuki et al. 2006; Bazito, Kawano et al. 2007; Kilaru, Baker et al. 2007; Wandschneider, Lehmann et al. 2008; Katsuta, Shiozawa et al. 2009; Kumełan, Tuma et al. 2009; Pereiro, Veiga et al. 2009; Liu, Maginn et al. 2012). The present experimental data was found to be in reasonably good agreement with the previous published data. Present density data have trends in $[C_4mim][NTf_2]$>$[C_4mmim][NTf_2]$>$[C_4mpyrr][NTf_2]$>$[N_{4111}][NTf_2]$. All of the measured temperature and the different ILs the density varies from 1.4405 g/cm^3-1.3424g/cm^3. It is clear from the Fig. 4.1 (a-d) that density decreases slightly as the temperature increases and the density data can be presented as a correlation of:

$$\rho = aT + b \tag{4-1}$$

where ρ is the density in g/cm^{3}unit, T is temperature in Kelvin unit, and a and b are the constants listed in Table 4.1 for all ILs. All of the ILs' density was measured at least three times at any single temperature and the density data is presented with the standard deviation in Table 4.2.

Table 4.1 Constants of density and temperature correlation

ILs	a	b
$[C_4mim][NTf_2]$	-1.08×10^{-3}	1.748
$[C_4mmim][NTf_2]$	-8.99×10^{-4}	1.686
$[C_4mpyrr][NTf_2]$	-7.77×10^{-4}	1.6129
$[N_{4111}][NTf_2]$	-8.42×10^{-4}	1.629

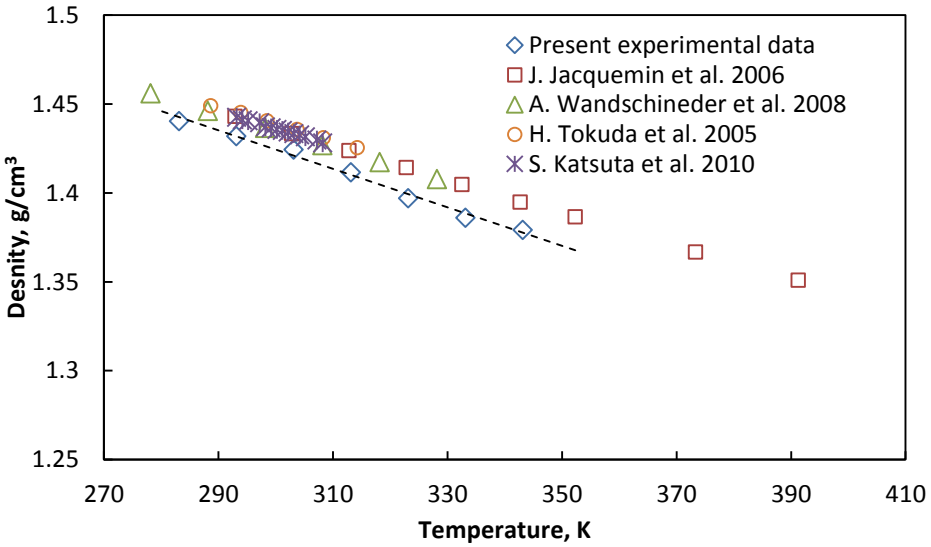

(a)

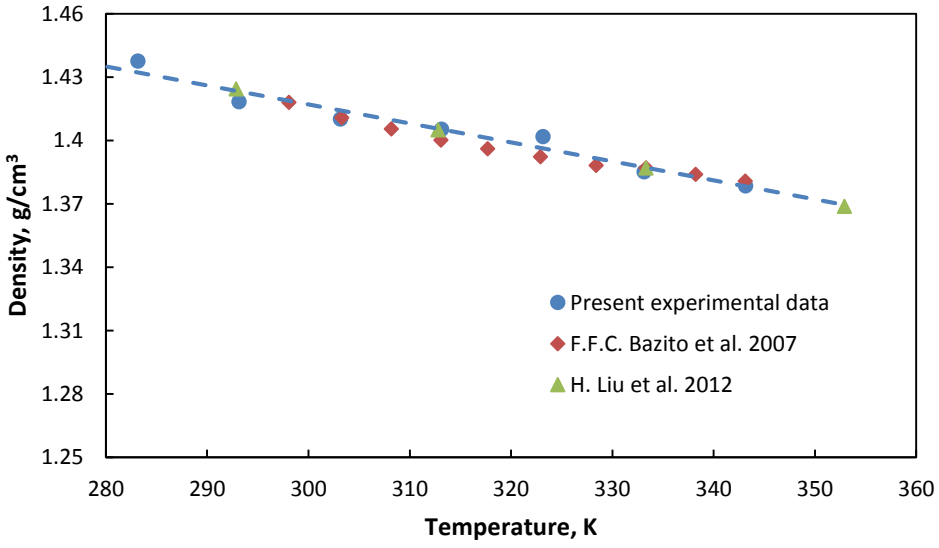

(b)

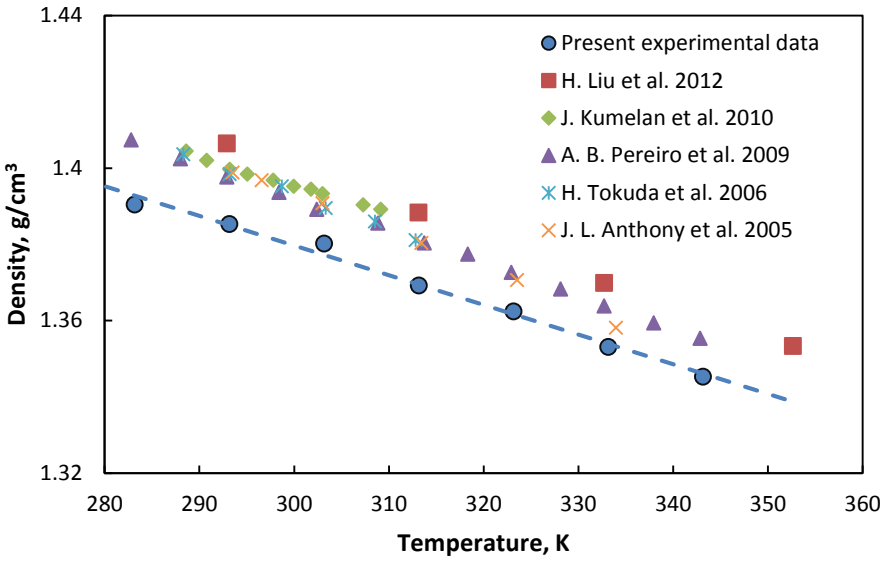

(c)

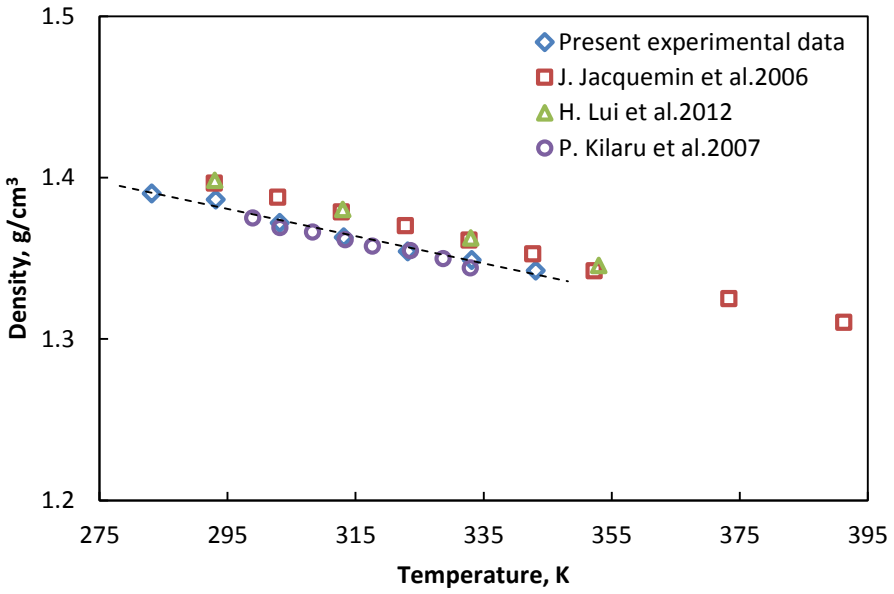

(d)

Figure 4.1 Density of ILs as a function of temperature (a) $[C_4mim][NTf_2]$, (b) $[C_4mmim][NTf_2]$, (c)$[C_4mpyrr][NTf_2]$, and (d) $[N_{4111}][NTf_2]$

Table 4.2 Density of four ILs with standard deviation

Density, g/cm^3				
T,K	**[C$_4$mim][NTf$_2$]**	**[N$_{4111}$][NTf$_2$]**	**[C$_4$mpyrr][NTf$_2$]**	**[C$_4$mmim][NTf$_2$]**
283.15	1.4405±0.0071	1.39017±0.0082	1.39046±0.0103	1.43755±0.003
293.15	1.41198±0.0154	1.38636±0.0073	1.38536±0.0067	1.41831±0.006
303.15	1.40446±0.0064	1.37206±0.0092	1.38029±0.0034	1.40841±0.0056
313.15	1.39164±0.0062	1.36306±0.0104	1.36924±0.0035	1.40493±0.0086
323.15	1.38706±0.076	1.35426±0.0108	1.36244±0.0041	1.39683±0.0094
333.15	1.38606±0.091	1.34896±0.0079	1.35312±0.0045	1.38513±0.0074
343.15	1.37926±0.086	1.34244±0.0052	1.34534±0.0062	1.37853±0.0068

Fig. 4.2 presents the volumetric thermal expansion coefficient of [C$_4$mim][NTf$_2$]. Fig. 4.2 shows the volumetric thermal expansion coefficient as a function of temperature and volumetric thermal expansion coefficient slightly increases with temperature.

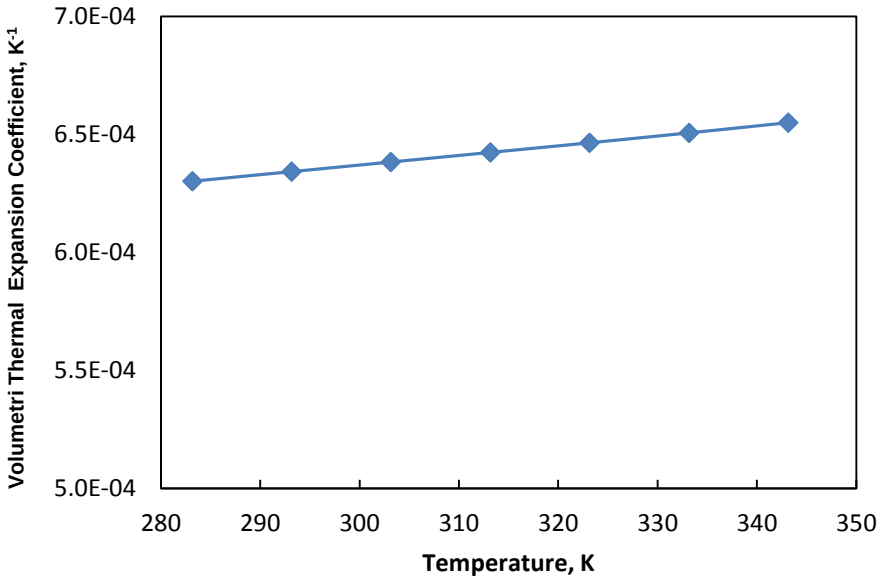

Figure 4.2 Temperature dependent volume expansion coefficient of [C$_4$mim][NTf$_2$]

4.3 Viscosity of ILs

The rheological behavior and shear viscosity of all four ILs are measured at 20-90^{o}C and the viscosity data is compared with the literature (Jacquemin, Husson et al. 2006; Bazito, Kawano et al. 2007; Katsuta, Shiozawa et al. 2009; Pereiro, Veiga et al. 2009; Liu, Maginn et al. 2012). The present experimental data of viscosity well correlates with the literature and shows trends in $[N_{4111}][NTf_2]$>$[C_4mmim][NTf_2]$>$[C_4mpyrr][NTf_2]$>$[C_4mim][NTf_2]$. Fig.4.3 shows the shear rate as a function of shear stress of all four ILs at 30^{o}C. The linear behavior of shear stress and shear rate proves the Newtonian behavior of ILs.

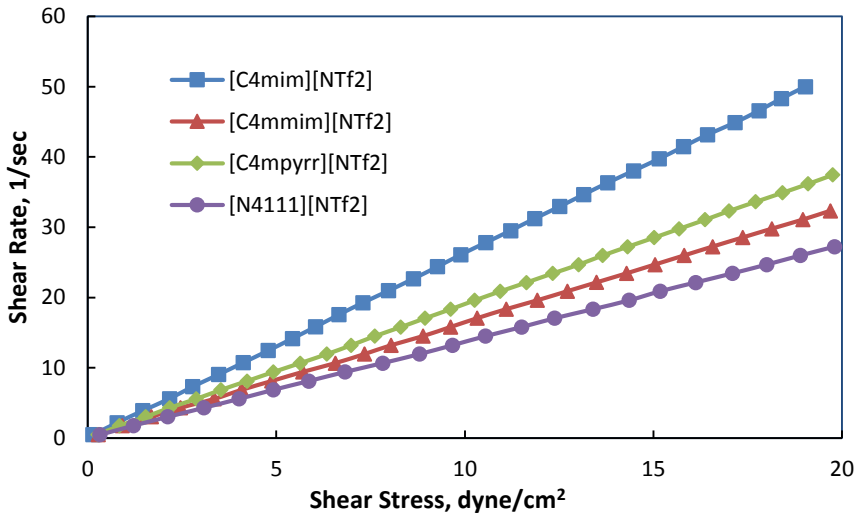

Figure 4.3 Shear rate as a function of shear stress of all ILs at 30^{o}C

Fig. 4.4 (a-d) shows the shear viscosity as a function of temperature which indicates the strong temperature effect on viscosity of the ILs and the viscosity depends on temperature with an exponential manner which follows the Andrade equation (4-2):

$$ln\mu = A + B\frac{100}{T} \quad (4.2)$$

where A , B are constant and T is the temperature in Kelvin. The constant of all four ILs are presented in Table 4.3. All of the ILs' viscosity was measured at least three times at any single temperature and the density data is presented with the standard deviation in Table 4.4.

Table 4.3 Constants of viscosity and temperature correlation

ILs	A	B
$[C_4mim][NTf_2]$	-6.807	3.165
$[C_4mmim][NTf_2]$	-8.449	3.833
$[C_4mpyrr][NTf_2]$	-7.171	3.377
$[N_{4111}][NTf_2]$	-7.596	3.589

Table 4.4 Viscosity of four ILs with standard deviation

Viscosity, CP				
T,K	**$[C_4mim][NTf_2]$**	**$[C_4mmim][NTf_2]$**	**$[C_4mpyrr][NTf_2]$**	**$[N_{4111}][NTf_2]$**
293.05	62.83±3.5595	119.97±3.307	84.16±3.8527	125.3±5.2086
303.05	40.64±3.7027	70.6±0.8622	52.81±1.2741	78.6±5.1733
312.95	28.7±2.3643	45.6±0.6429	35.55±1.365	50.4±2.9462
322.85	21.5±1.3204	31.6±0.7572	25.16±0.7234	34.4±1.5695
332.85	16.2±0.8622	23.2±0.6928	18.62±0.7638	24.9±1.0214
343.05	12.4±0.4	17.4±0.4163	14.21±0.3215	19±0.4583
353.15	8.94±0.3721	11.51±03918	11.12±0.2962	12.87±0.3126
263.15	7.26±0.2903	9.27±0.3187	9.03±0.2638	10.47±0.2154

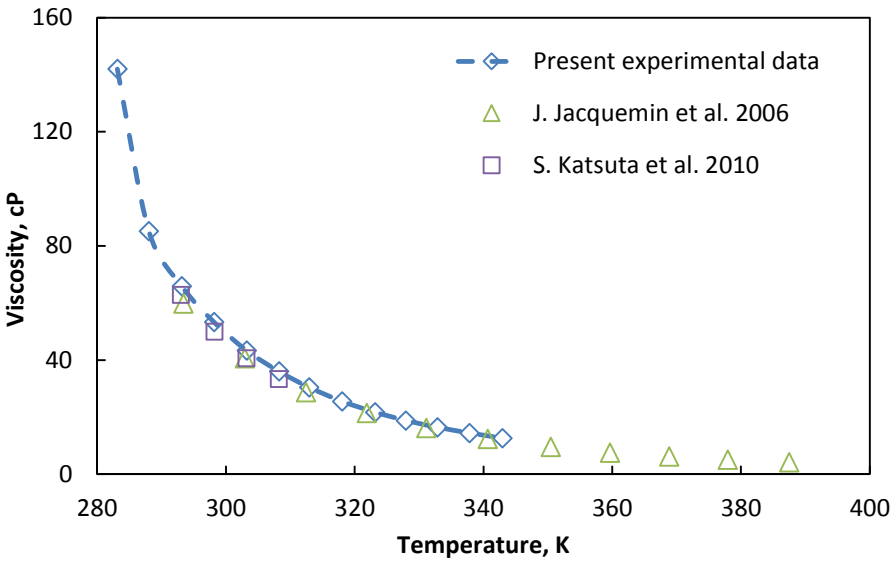
160
120
80
40
0
Viscosity, cP
280
300
320
340
360
380
400
Temperature, K
Present experimental data
J. Jacquemin et al. 2006
S. Katsuta et al. 2010

(a)

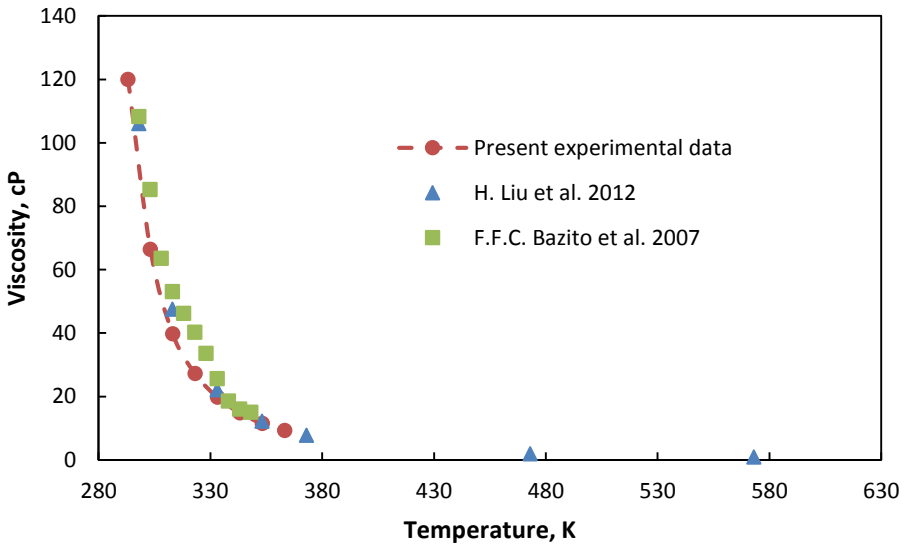
140
120
100
80
60
40
20
0
Viscosity, cP
280
330
380
430
480
530
580
630
Temperature, K
Present experimental data
H. Liu et al. 2012
F.F.C. Bazito et al. 2007

(b)

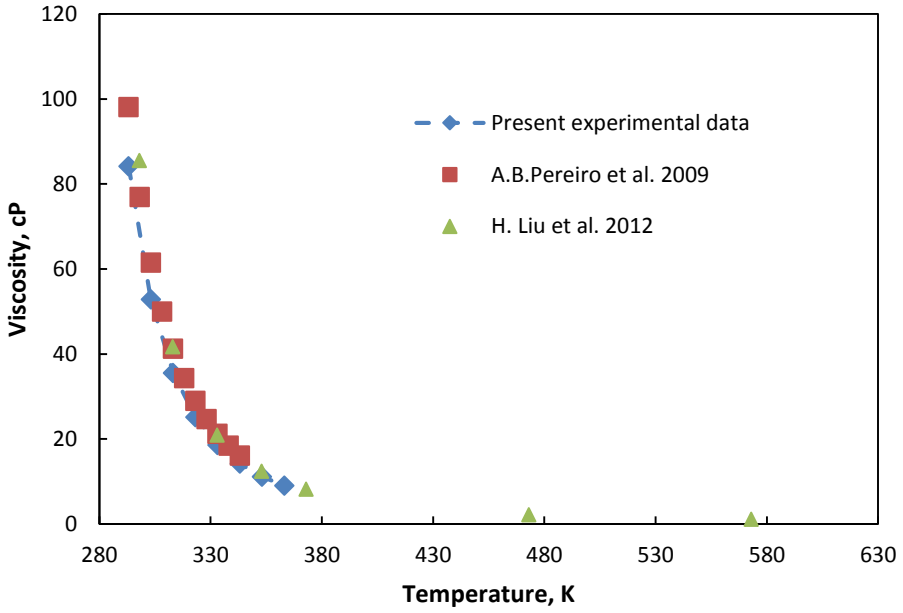

(c)

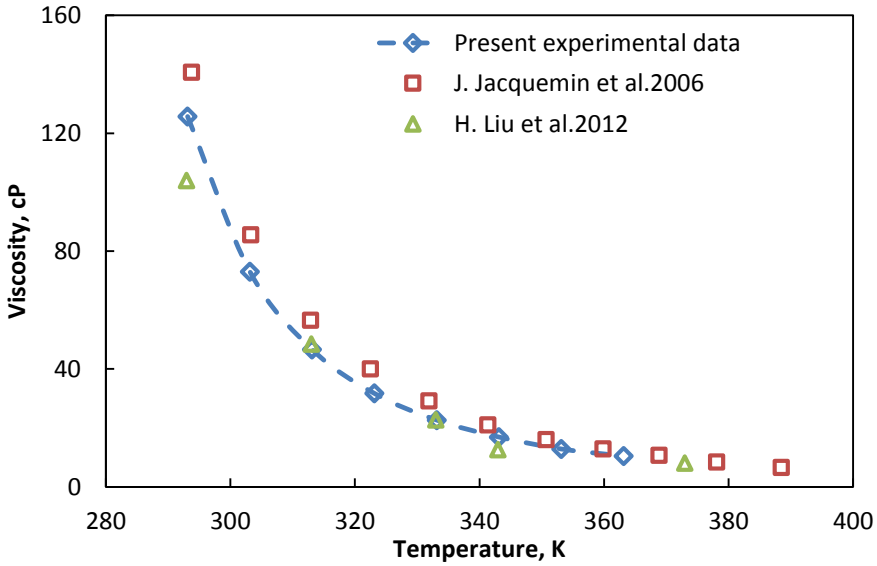

(d)

Figure 4.4 Shear viscosity of ILs as a function of temperature (a) $[C_4mim][NTf_2]$, (b) $[C_4mmim][NTf_2]$, (c)$[C_4mpyrr][NTf_2]$, and (d) $[N_{4111}][NTf_2]$

4.4 Heat Capacity of ILs

Heat capacity of all four ILs are measured within the temperature range 25-345^{o}C and within the measured temperature range heat capacity increases almost linearly with temperature. The experimental heat capacity trend is [C_4mim][NTf_2]>[N_{4111}][NTf_2]> [C_4mpyrr][NTf_2]>[C_4mmim][NTf_2]. The experimental results are presented in Fig. 4.5(a-d) and data were compared with the previously published data (Troncoso, Cerdeiriña et al. 2006; Ge, Hardacre et al. 2008; Holbrey, Reichert et al. 2010;Liu, Maginn et al. 2012). But in literature there is no sufficient data for all of the ILs. Only for [C_4mim][NTf_2] IL was found many data and all of the data are scattered which can be seen in Fig.4.5 (a). The same scattered heat capacity data were reported for other IL and a recent study report by IUPAC mentioned that such variation in heat capacity measurement is typical (Marsh 2009). For [C_4mmim][NTf_2] and [C_4mpyrr][NTf_2] the experimental results matches well with H. Liu et al.'s (Liu, Maginn et al. 2012) data.

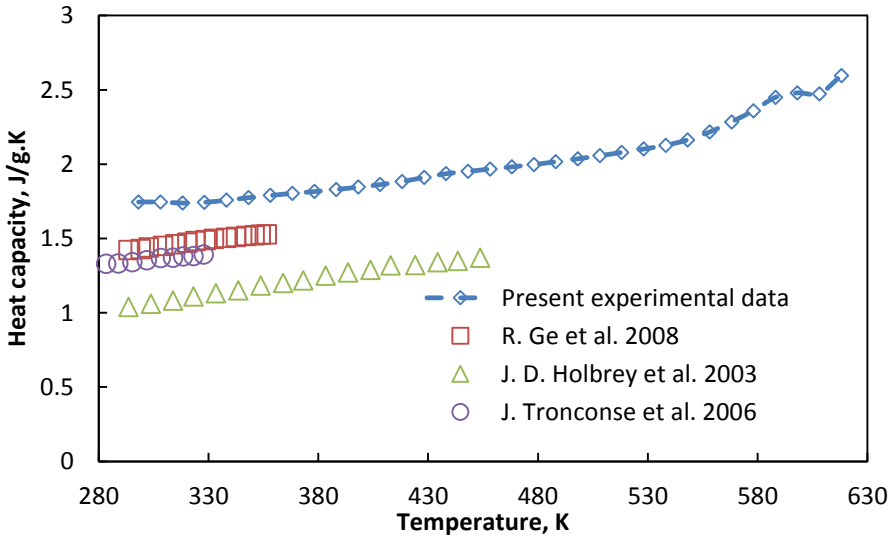

(a)

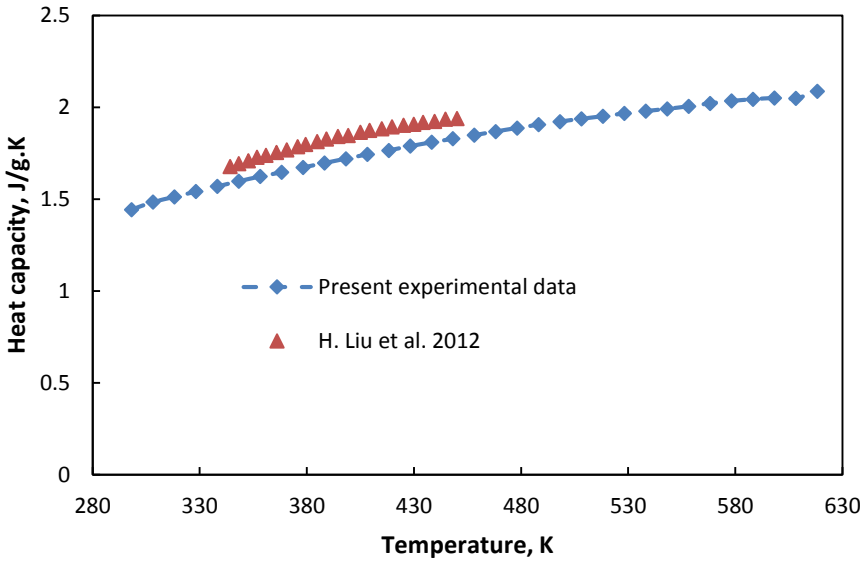
2.5
2
1.5
1
0.5
0
Heat capacity, J/g.K
280
330
380
430
480
530
580
630
Temperature, K
Present experimental data
H. Liu et al. 2012

(b)

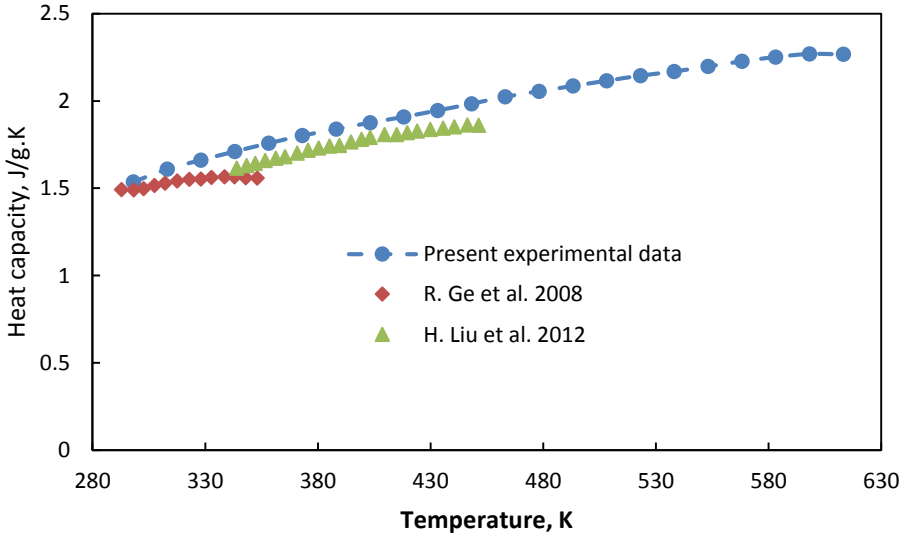
2.5
2
1.5
1
0.5
0
Heat capacity, J/g.K
280
330
380
430
480
530
580
630
Temperature, K
Present experimental data
R. Ge et al. 2008
H. Liu et al. 2012

(c)

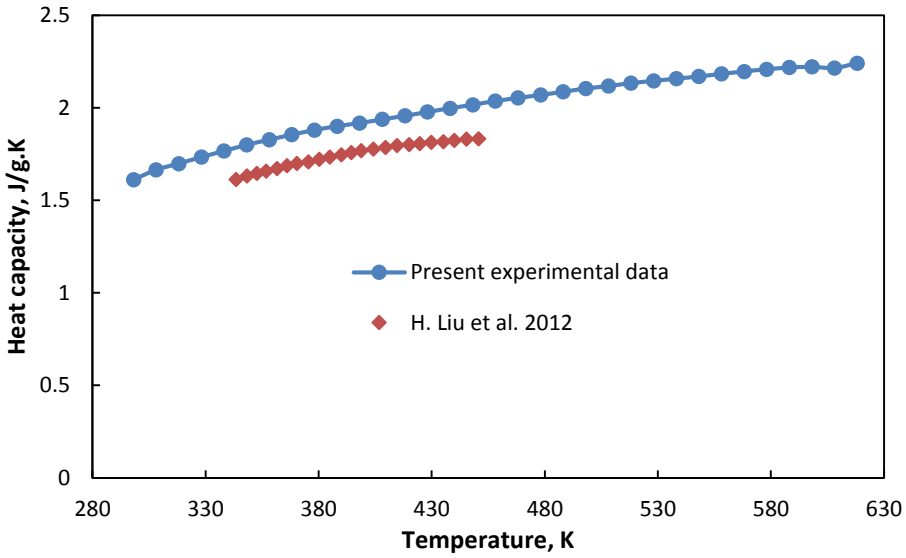

(d)

Figure 4.5 Heat capacity of ILs as a function of temperature (a) [C_4mim][NTf_2], (b) [C_4mmim][NTf_2], (c)[C_4mpyrr][NTf_2], and (d) [N_{4111}][NTf_2]

4.5 Thermal Conductivity of ILs

The thermal conductivity of all four ILs are investigated within the temperature range 10-70^{o}C and presented in Fig. 4.6(a-d) where thermal conductivity is presented as a function of temperature. The experimental thermal conductivity values' trend is [C_4mim][NTf_2]>[C_4mmim][NTf_2]>[N_{4111}][NTf_2]>[C_4mpyrr][NTf_2]. The maximum thermal conductivity was found 0.127W/m.K which means the thermal conductivity of ILs are less than De-Ionized (DI) water and has thermal conductivity of approximately 21% of that of DI water at room temperature. In Fig. 4.6(a-d) it is apparent that within the temperature limit studied the thermal conductivity slightly decreases with temperature or has a very low temperature effect. The temperature dependent thermal conductivity can be represented by the linear equation:

$$k_f = aT + b \tag{4-3}$$

where k_f is the thermal conductivity in W/m.K unit, T is temperature in Kelvin unit, and a and b are the constants listed in Table 4.5 for all ILs. Moreover, the thermal conductivity of ILs is not a strong function of temperature which was reported by a lot of researchers for different imidazolium and pyrrolidinium based ILs using the same method and same device (Ge, Hardacre et al. 2007; Chen, He et al. 2008; Nieto de Castro, Lourenço et al. 2009) and same transient hot wire method but different experimental setups (Valkenburg, Vaughn et al. 2005; Rooney, Jacquemin et al. 2010). Other measurements using techniques like parallel-plate instruments (Fröba, Rausch et al. 2010) and transient grating technique(Frez, Diebold et al. 2006) also report the same behavior of thermal conductivity of ILs. Similar to the temperature effect on thermal conductivity of ILs, the thermal conductivity of ILs also has very small pressure dependence (Tomida, Kenmochi et al. 2007; Tomida, Kenmochi et al. 2007). The present experimental data were compared with the previously published data (Ge, Hardacre et al. 2007; Chen, He et al. 2008; Nieto de Castro, Lourenço et al. 2009; Liu, Maginn et al. 2012) and matches well with Liu et al.'s (Liu, Maginn et al. 2012) data. All of the ILs' thermal conductivity was measured at least three times at any single temperature and the density data is presented with the standard deviation in Table 4.6.

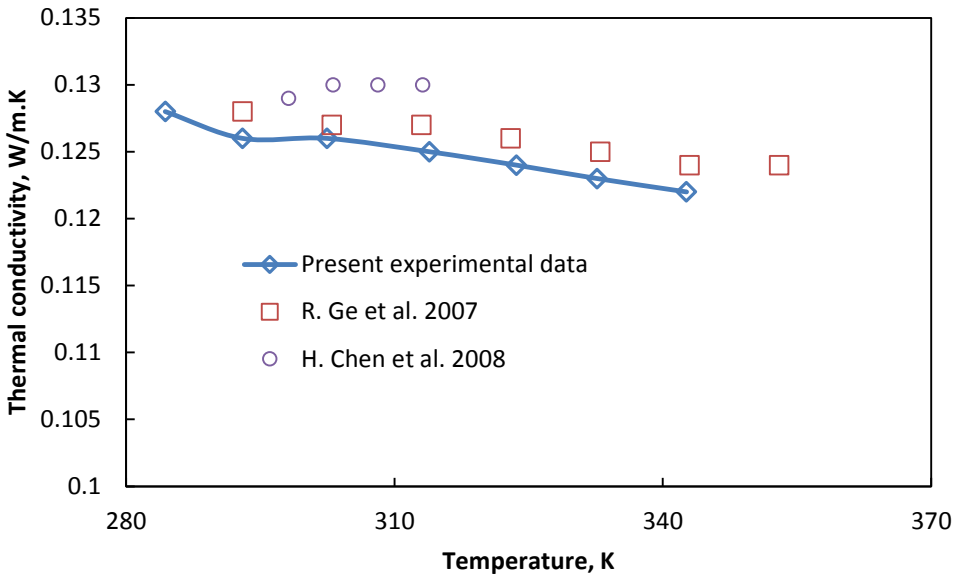
0.135
0.13
0.125
0.12
0.115
0.11
0.105
0.1
Thermal conductivity, W/m.K
280
310
340
370
Temperature, K
Present experimental data
R. Ge et al. 2007
H. Chen et al. 2008

(a)

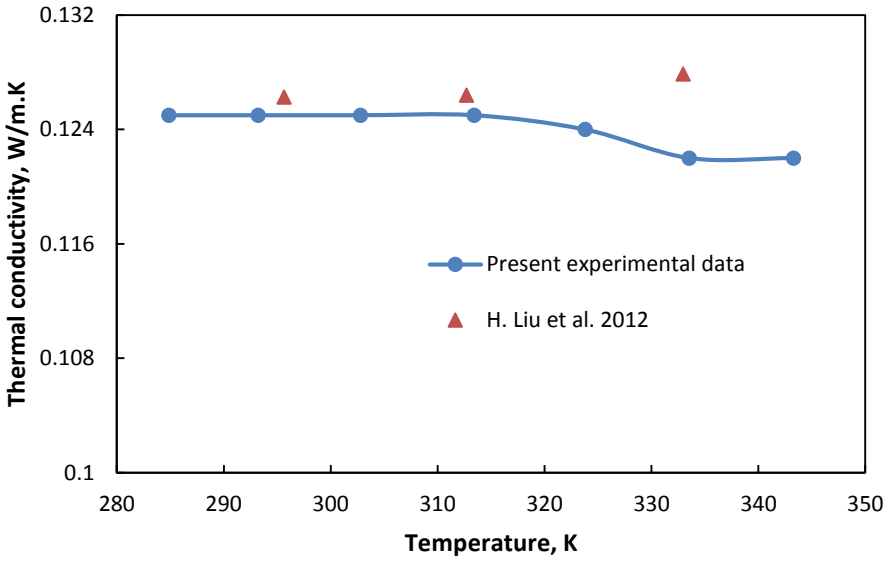
0.132
0.124
0.116
0.108
0.1
Thermal conductivity, W/m.K
280
290
300
310
320
330
340
350
Temperature, K
Present experimental data
H. Liu et al. 2012

(b)

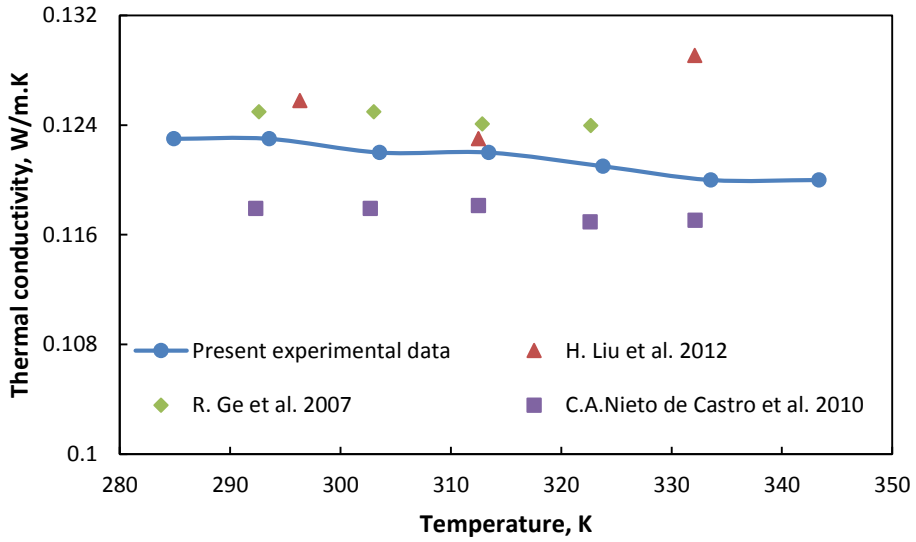

(c)

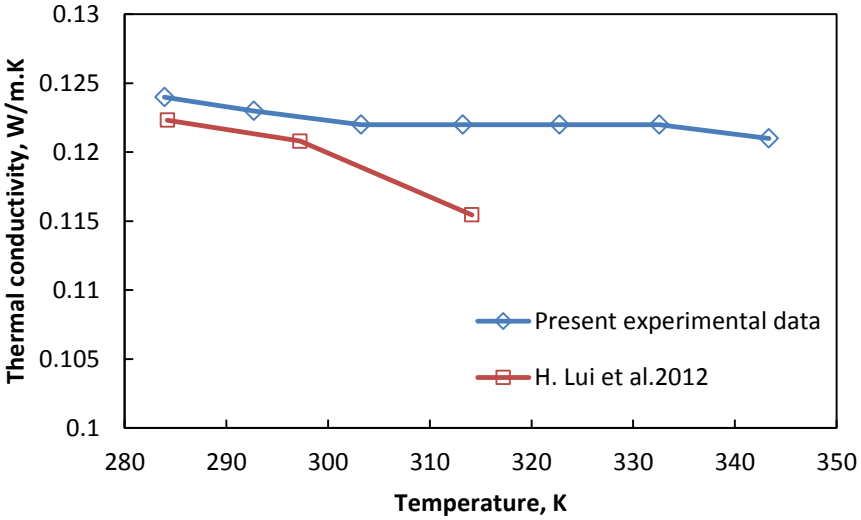

(d)

Figure 4.6 Thermal conductivity of ILs as a function of temperature (a) [C_4mim][NTf_2], (b) [C_4mmim][NTf_2], (c)[C_4mpyrr][NTf_2], and (d) [N_{4111}][NTf_2]

Table 4.5 Constants of thermal conductivity and temperature correlation

ILs	a	b
$[C_4mim][NTf_2]$	-9×10^{-5}	0.1544
$[C_4mmim][NTf_2]$	-6×10^{-5}	0.1422
$[C_4mpyrr][NTf_2]$	-6×10^{-5}	0.1398
$[N_{4111}][NTf_2]$	-4×10^{-5}	0.1347

Table 4.6 Thermal conductivity of four ILs with standard deviation

T,K	**$[C_4mim][NTf_2]$**	**$[C_4mmim][NTf_2]$**	**$[C_4mpyrr][NTf_2]$**	**$[N_{4111}][NTf_2]$**
284.38	0.128±0.0021	0.125±0.001	0.123±0.0006	0.124±0.0006
293.01	0.126±0.0023	0.125±0.0006	0.123±0.0006	0.123±0.0012
302.45	0.126±0.002	0.125±0.0006	0.122±0.0012	0.122±0.001
313.92	0.125±0.0015	0.125±0.0012	0.122±0.0006	0.122±0.001
323.64	0.124±0.0015	0.124±0.0006	0.123±0.0006	0.122±0.0006
332.64	0.123±0.0015	0.122±0.0026	0.121±0.0006	0.122±0.0006
342.65	0.122±0.0006	0.12±0.0707	0.119±0.0006	0.121±0.0006

4.6 Properties of nanoparticle enhanced ionic liquids (NEILs)

The thermophysical properties of NEILs with spherical Al_2O_3 nanoparticles were measured for all four ILs. To see the particle shape effect on thermophysical properties of NEILs, whiskers Al_2O_3 nanoparticles were also dispersed on $[C_4mpyrr][NTf_2]$ IL. Here the thermophysical properties of all NEILs as well as particle shape effect on thermophysical properties are presented.

4.7 Density of NEILs

The density of all four spherical NEILs as a function of temperature is presented in Fig. 4.7 (a-d). The density of base ILs and NEILs decreases with temperature within the measured temperature 10-70^{o}C. It is clear that the NEILs have higher density

compared to the base IL because of high density Al_2O_3 nanoparticles. Density decreasing with temperature becomes less prominent with nanoparticles concentration, which means the Al_2O_3 particles are less sensitive with variation of temperature compare to the base IL. The density of NEILs as a function of nanoparticle volume fraction is presented in Fig. 4.8 and experimental data matches well with the calculated effective density using the mixing theory (Ho, Liu et al. 2010):

$$\rho_{NEIL} = \phi\rho_n + (1-\phi)\rho_{BL} \tag{4-4}$$

Fig. 4.9 presents the density of NEILs with Al_2O_3 whiskers nanoparticles and [C_4mpyrr][NTf_2] IL as a function of temperature; these density data were used for natural convection heat transfer parameter calculations. No variations were observed in the density data for different shapes of particles.

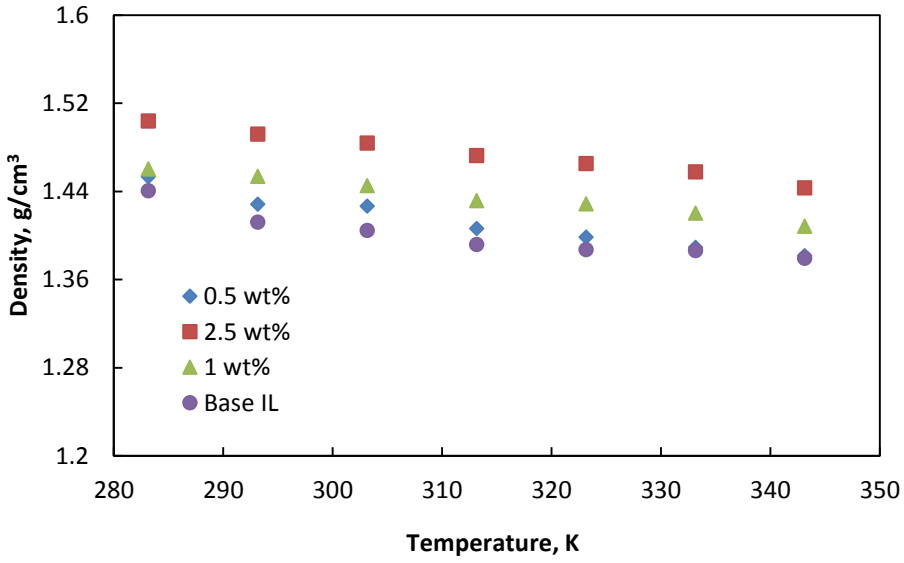

(a)

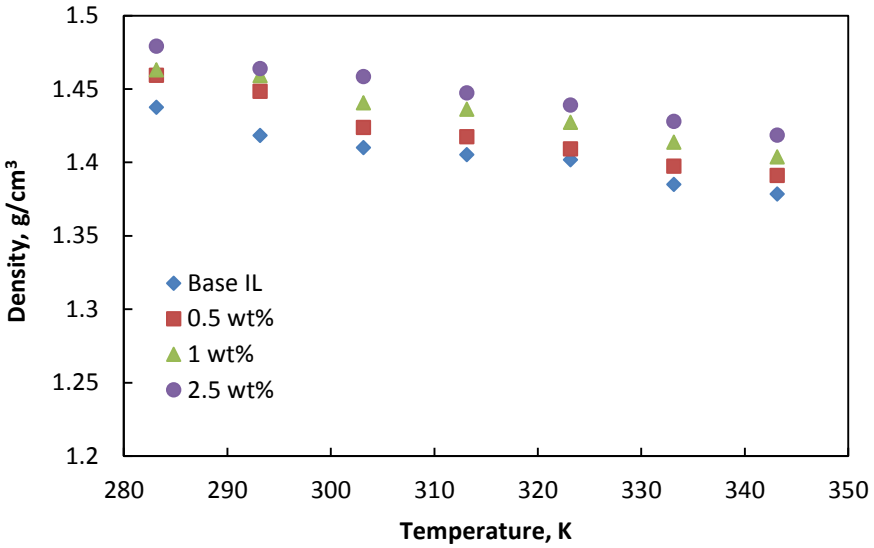
1.5
1.45
1.4
1.35
1.3
1.25
1.2
Density, g/cm³
Base IL
0.5 wt%
1 wt%
2.5 wt%
280
290
300
310
320
330
340
350
Temperature, K

(b)

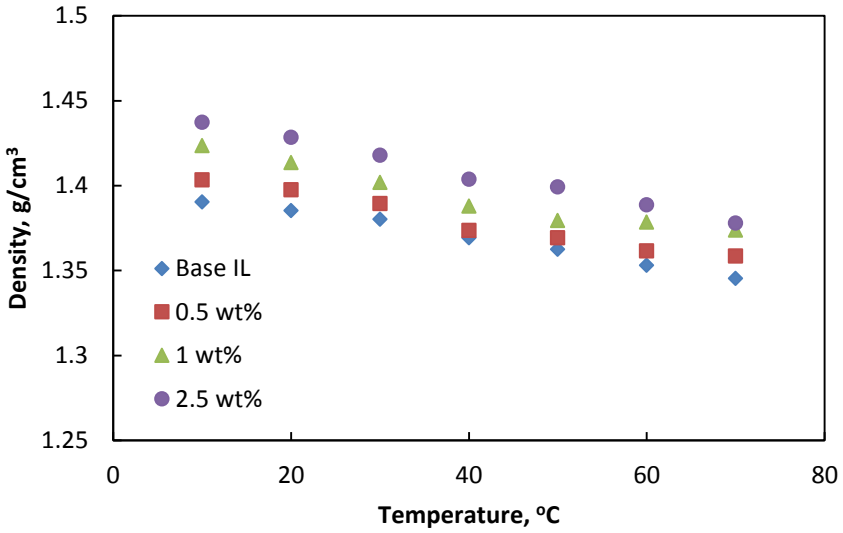
1.5
1.45
1.4
1.35
1.3
1.25
Density, g/cm³
Base IL
0.5 wt%
1 wt%
2.5 wt%
0
20
40
60
80
Temperature, °C

(c)

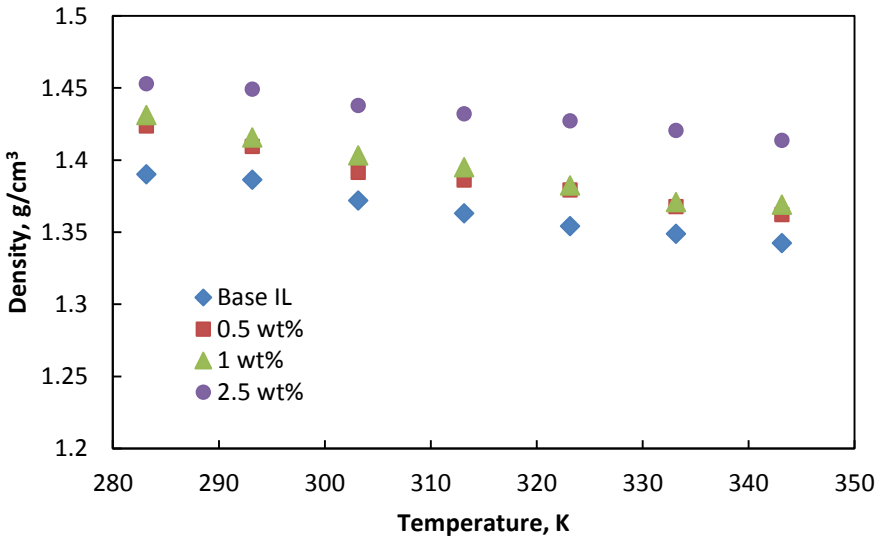

(d)

Figure 4.7 Density of base ILs and spherical Al_2O_3 NEILs as a function of temperature (a) [C_4mim][NTf_2], (b) [C_4mmim][NTf_2], (c)[C_4mpyrr][NTf_2], and (d) [N_{4111}][NTf_2]

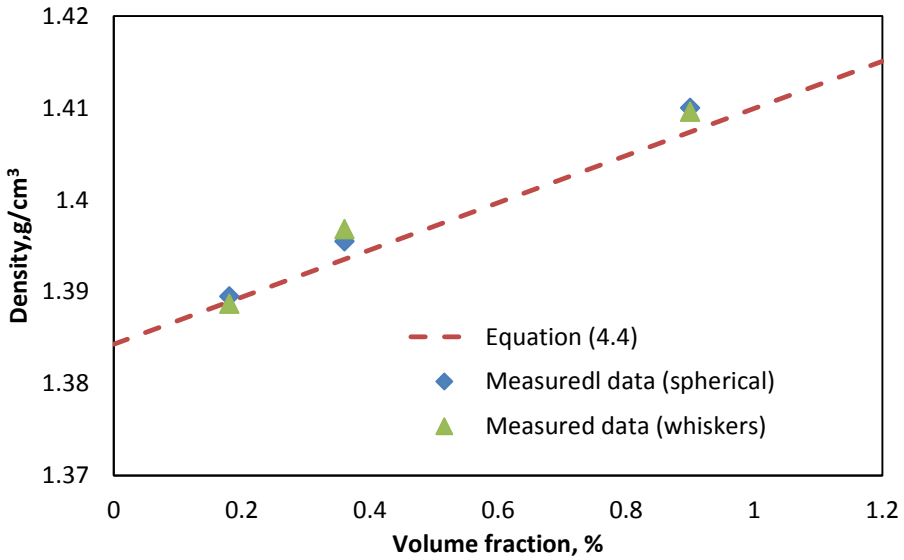

Figure 4.8 Density of NEILs as a function of nanoparticle volume fraction

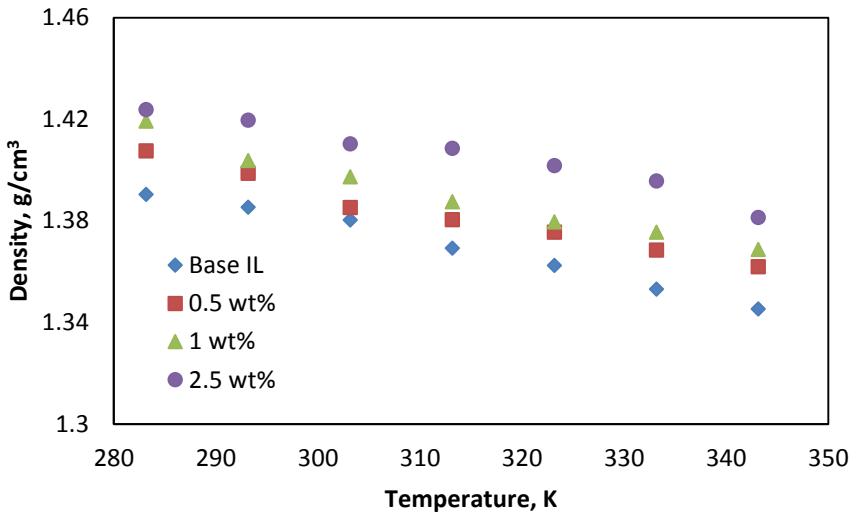

Figure 4.9 Density of base ILs and whiskers Al_2O_3 NEILs as a function of temperature

4.8 Viscosity of NEILs

The rheological behavior of base ILs and 0.5, 1.0, and 2.5 wt% Al_2O_3 NEILs were measured for different temperatures ranging from 20-90^oC. Fig. 4.10(a) shows the rheological behavior of [C_4mmim][NTf_2] IL and NEILs at 30^oC. The base IL shows that the shear viscosity is independent on shear rate which shows the Newtonian behavior of the IL. It is clear from the Fig that NEILs shows non Newtonian shear thinning behavior which means at a low shear rate, shear viscosity shows higher value and at an increasing shear rate, viscosity decreases. It is also clear from the Fig. 4.10(a) that 2.5 wt% NEILs shows stronger shear thinning behavior than lower concentration. Fig. 4.10(b) represents the rheological behavior of 0.5 wt% of four NEILs at 30^oC and it is clear that all of the NEILs shows shear thinning behavior. The rheological behavior of 1.0 wt% [C_4mmim][NTf_2] NEILs at different temperatures is presented in Fig. 4.10(c). The shear thinning behavior occurs at all the measured temperatures and the shear thinning increases with temperature. The same shear thinning behavior of ionic liquid based

nanofluids are observed by Wang et al. (Wang, Wang et al. 2010). It is also observed that the shear viscosity shows strong temperature dependency which is clearer in Fig. 4.10(d), where viscosity of base $[C_4mmim][NTf_2]$ IL and NEILs is presented as a function of temperature. The temperature dependent viscosity data of NEILs was found to fit very well with the equation (Chen, Ding et al. 2007) and presented in Fig. 4.10(e):

$$\ln \mu = A + \frac{1000.B}{(T+C)} \tag{4-5}$$

where μ is the shear viscosity, T is temperature in Kelvin (K) unit, and A, B, and C are constants.

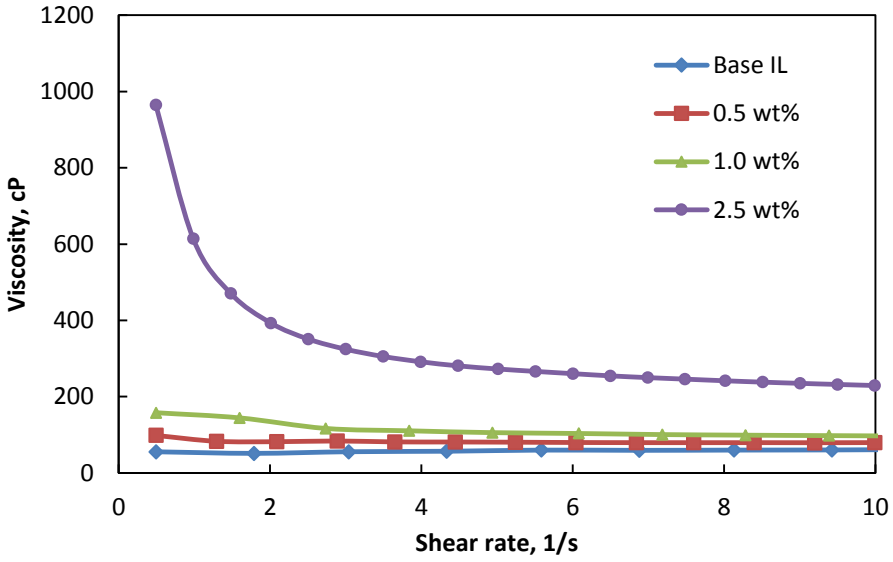

(a)

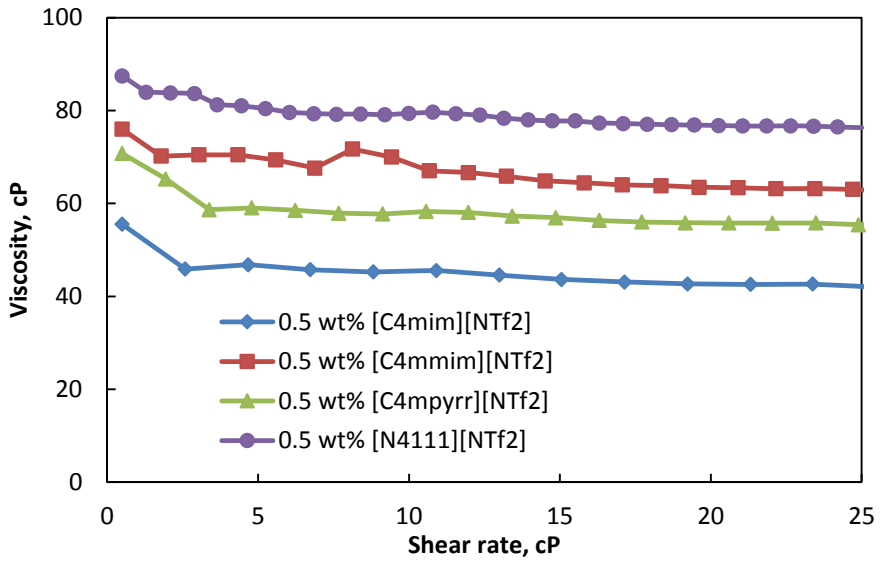
100
80
60
40
20
0
Viscosity, cP
0
5
10
15
20
25
Shear rate, cP
0.5 wt% [C4mim][NTf2]
0.5 wt% [C4mmim][NTf2]
0.5 wt% [C4mpyrr][NTf2]
0.5 wt% [N4111][NTf2]

(b)

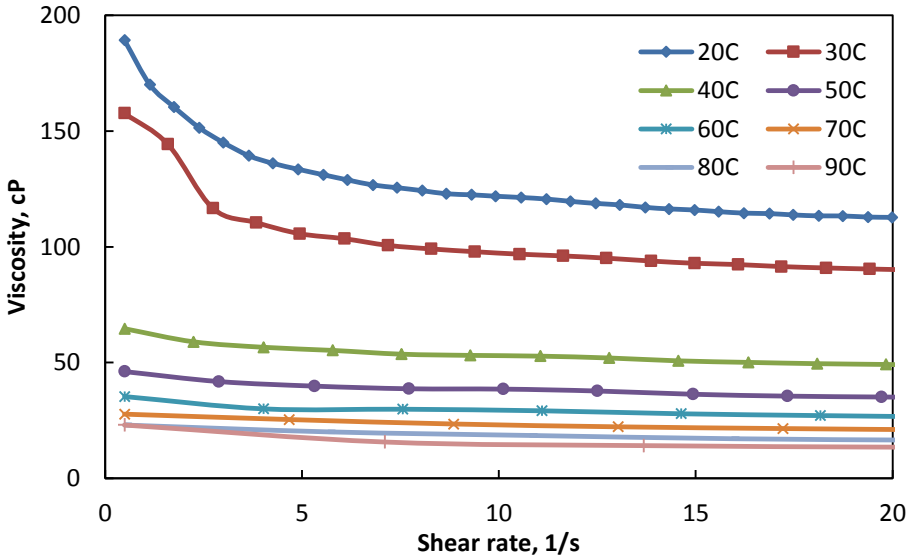
200
150
100
50
0
Viscosity, cP
0
5
10
15
20
Shear rate, 1/s
20C
30C
40C
50C
60C
70C
80C
90C

(c)

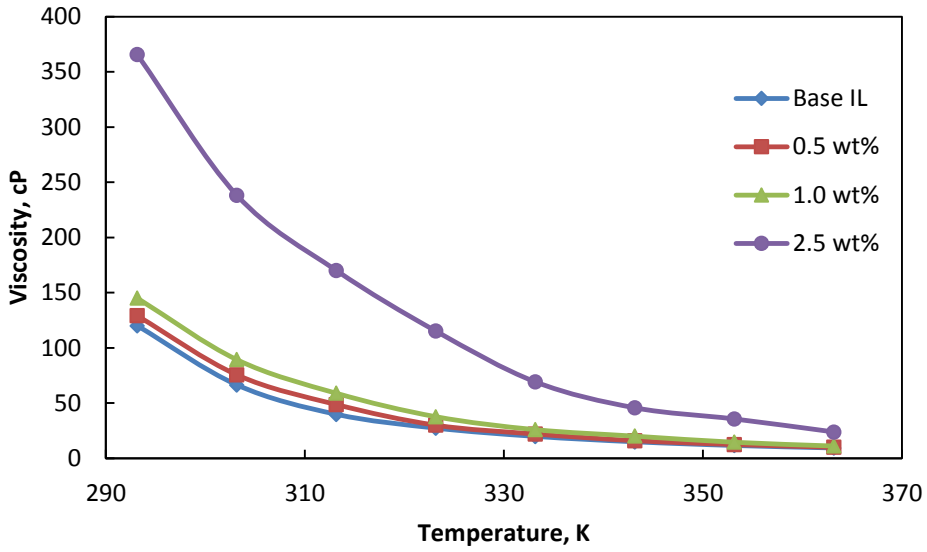

(d)

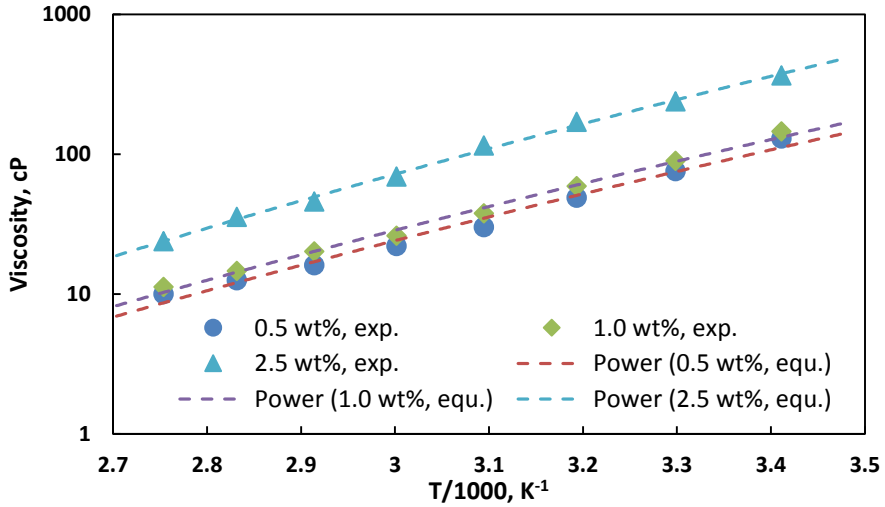

(e)

Figure 4.10 Rheological behavior of a) base [C_4mmim][NTf_2] IL and NEILs at 30°C b) 0.5 wt% Al_2O_3 loading of four ILs c) 1 wt% [C_4mmim][NTf_2] NEILs at different temperature d) viscosity of [C_4mmim][NTf_2] NEILs as a function of temperature, e) viscosity of [C_4mmim][NTf_2]

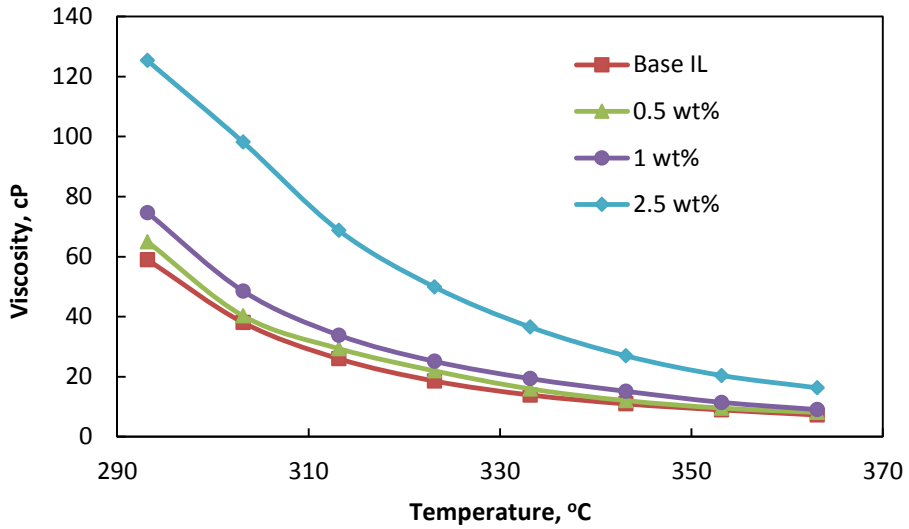
140
120
100
80
60
40
20
0
290
310
330
350
370
Viscosity, cP
Temperature, °C
Base IL
0.5 wt%
1 wt%
2.5 wt%

(a)

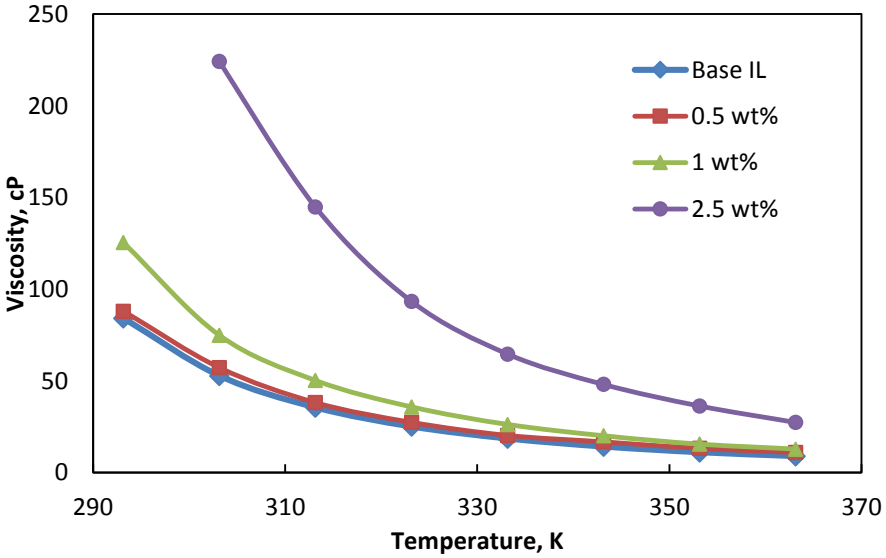
250
200
150
100
50
0
290
310
330
350
370
Viscosity, cP
Temperature, K
Base IL
0.5 wt%
1 wt%
2.5 wt%

(b)

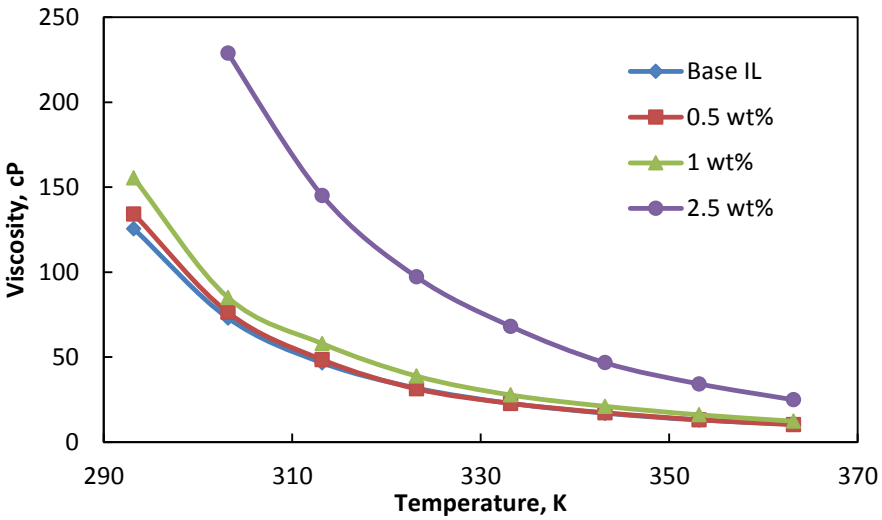

(c)

Figure 4.11 Viscosity of NEILs as a function of temperature (a) [C_4mim][NTf_2], (b) [C_4mpyrr][NTf_2], and (c) [N_{4111}][NTf_2]

Fig. 4.11 (a-c) shows the viscosity of three other ILs and NEILs as a function of temperature. The particle shape effect on shear viscosity was observed for NEILs with [C_4mpyrr][NTf_2] and spherical and whiskers Al_2O_3. The effective shear viscosity and nanoparticle volume fraction of two different particles are presented in Fig. 4.12 and the temperature dependent viscosity of whiskers NEILs is presented in Fig. 4.13. From Fig. 4.12, it can be seen that the effective viscosity of spherical nanoparticles NEILs shows higher values compared to that of whiskers nanoparticles NEILs which contradict with previous study of conventional water-Al_2O_3 nanofluids with different shape of nanoparticles by Timofeeva et al. (Timofeeva, Routbort et al. 2009). They reported that nanofluids with rodlike nanoparticles shows higher viscosity because restriction of rotational and translational Brownian motion of nanoparticles shows lower shear thinning behavior as well as higher viscosity. But the same higher viscosity of NEILs with

spherical nanoparticles compare to whiskers nanoparticles was reported by Fox et al. (Fox, Visser et al. 2013), where they have presented optical micrograph of NEILs and have seen that the whiskers particle cluster diameter was smaller than the spherical particles.

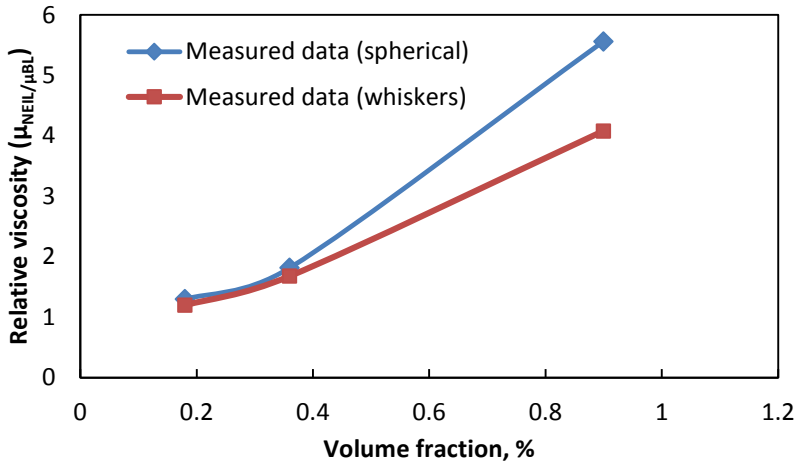

Figure 4.12 Effective shear viscosity as a function of nanoparticle volume fraction of two different particles

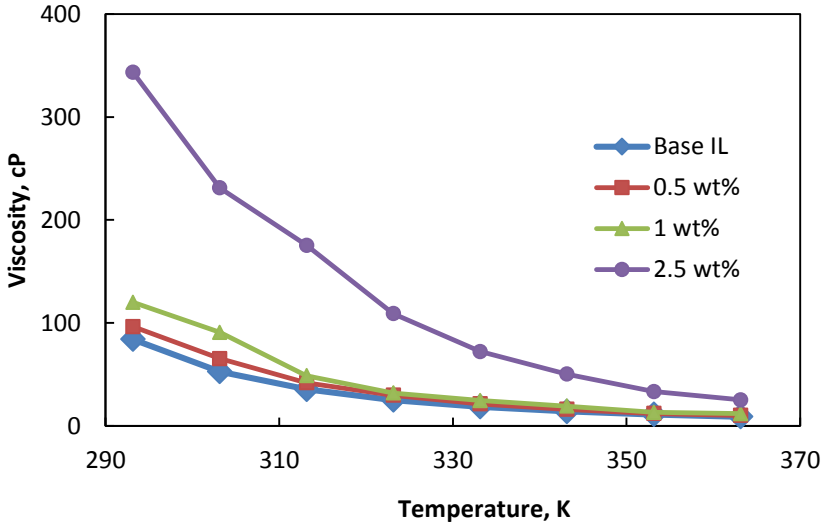

Figure 4.13 Viscosity of base ILs and whiskers Al_2O_3 NEILs as a function of temperature

The effective viscosity of [C_4mmim][NTf_2] NEILs at 30°C as a function of nanoparticles volume fraction is presented in Fig. 4.14 and it is clear that viscosity enhancement with nanoparticle volume fraction is nonlinear. The experimental results of viscosity enhancement with nanoparticles concentration was compared with numerous theoretical models.

Firstly the Einstein model (Einstein 1906) for calculationg viscosity of fluid containing low volume fraction (<0.02) of spherical particles is considered:

$$\frac{\mu_{NEIL}}{\mu_{BL}} = 1 + 2.5\phi \tag{4-6}$$

Brinkman (Brinkman 1952) modified the Einstein model for fluid containing high concentration nanoparticles:

$$\frac{\mu_{NEIL}}{\mu_{BL}} = \frac{1}{(1-\phi)^{2.5}} \tag{4-7}$$

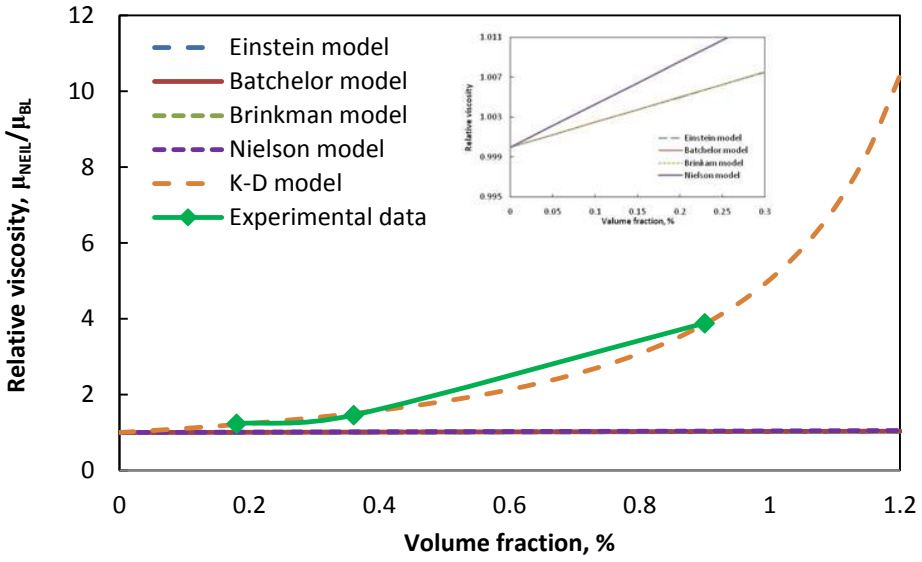

Figure 4.14 Effective viscosity as a function of nanoparticle volume fraction

After that, Batchelor (Batchelor 1977) modified the Einstein model by considering Brownian motion of particles in nanofluids:

$$\frac{\mu_{NEIL}}{\mu_{BL}} = 1 + 2.5\phi + 6.2\phi^2 \quad (4\text{-}8)$$

where μ_{NEIL} and μ_{BL} are the viscosity of NEIL and base liquid, and ϕ is the nanoparticle volume fraction. Fig.4.14 shows that the above mentioned model could not predict the experimental results. Predicted results were found to be lower compared to the experimental values as all of the models only take into account the volume fraction of nanoparticles and does not take into account nanoparticles clustering which is very common for the NEILs. The similar high enhancement of viscosity with a small amount of loading of nanoparticles behavior was also observed by Fox et al. (Fox, Visser et al. 2013), Bridges et al.(Bridges, Visser et al. 2011), and Wang et al. (Wang, Wang et al. 2011) for ionic liquid containing Al_2O_3 and Gold (Au) nanoparticles respectively.

The present experimental results then tried to explain considering the agglomeration of nanoparticles in NEILs. Nielson (Nielsen 1970) proposed the power low model considering the agglomeration packing fraction for higher concentration of nanoparticles:

$$\frac{\mu_{NEIL}}{\mu_{BL}} = (1 + 1.5\phi)e^{\frac{\phi}{(1-\phi_m)}} \quad (4\text{-}9)$$

where ϕ_m is the maximum particle packing fraction which is typically considered 0.605. This model also underpredicts the experimental results which can be observed in Fig.4.14.

Finally the Krieger-Dougherty (K-D) model (Krieger and Dougherty 1959) was considered to predict the experimental results which take into consideration the maximum packing fraction and effect of variable packing fraction:

$$\frac{\mu_{NEIL}}{\mu_{BL}} = (1 - \frac{\phi_a}{\phi_m})^{-[\eta]\phi_m} \quad (4\text{-}10)$$

where the typical value of the intrinsic viscosity$[\eta]$ is 2.5 and ϕ_a is the effective volume fraction of aggregates which is given by ratio of the radii of the aggregate and primary nanoparticles:

$$\phi_a = \phi(\frac{r_a}{r_n})^{3-D'} \quad (4\text{-}11)$$

where r_a and r_n are the average radii of the aggregate and primary nanoparticles respectively, D' is the fractal index, and the typical value of fractal index is 1.8 for nanofluids. Finally the model can be rearranged as:

$$\frac{\mu_{NEIL}}{\mu_{BL}} = (1 - \frac{\phi}{0.605}(\frac{r_a}{r_n})^{1.2})^{-1.5125} \quad (4\text{-}12)$$

The experimental results were fitted with the equ. (4.12) at aggregation factor $(\frac{r_a}{r_n} = 21.5)$ and presented in Fig. 4.14. In literature, aggregation factor was observed up to 16 for nitrate-silica nanofluids (Jo, Jung et al. 2011). The aggregation of NEILs was also observed by Fox et al. (Fox, Visser et al. 2013), and they found the $[C_4mmim][NTf_2]$+Al_2O_3 NEILs cluster size average 100μm where the primary particle size<50nm. For better observation, an optical image of 0.5 wt% NEILs was also taken and presented in Fig. 4.15. It is clear that the nanoparticles agglomerated in IL. The same particle agglomeration of NEIL was also observed by the DLS particle size in Fig.4.16. It

was observed that the average hydrodynamic radii of nanoparticles increases with time. The measurements were taken just after synthesis of NEILs. So, from the observation it is clear that the particles have a huge tendency to agglomerate and this might be one reason for the large enhancement of viscosity. However, including this phenomenon, there may be other variables that need to be taken into consideration for further discussion.

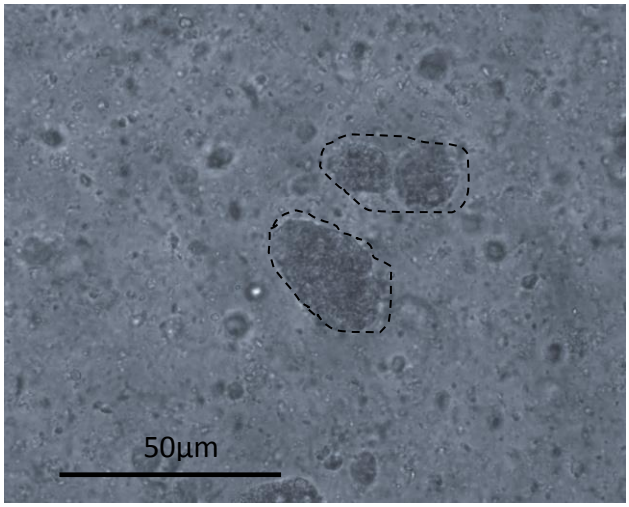

Figure 4.15 Optical image of 0.5 wt% NEILs

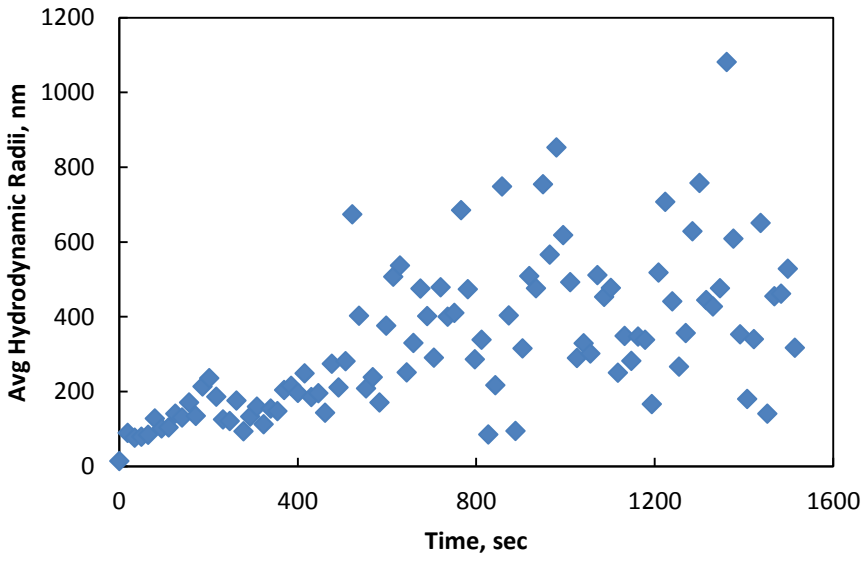

Figure 4.16 Nanoparticle size with respect to time

4.9 Thermal Conductivity of NEILs

The thermal conductivity of all base ILs and NEILs are measured within 10-70^{o}C temperature range. Fig. 4.17(a-d) shows the thermal conductivity of four NEILs as a function of temperature where the effective thermal conductivity was normalized with respect to the corresponding thermal conductivity of base IL. It is clear from the Fig.4.17(a-d) that the thermal conductivity increases with the wt% of nanoparticles over the measured temperature range and there is not a strong temperature dependency observed. The maximum enhancement was observed ~11% for 2.5 wt% NEIL.

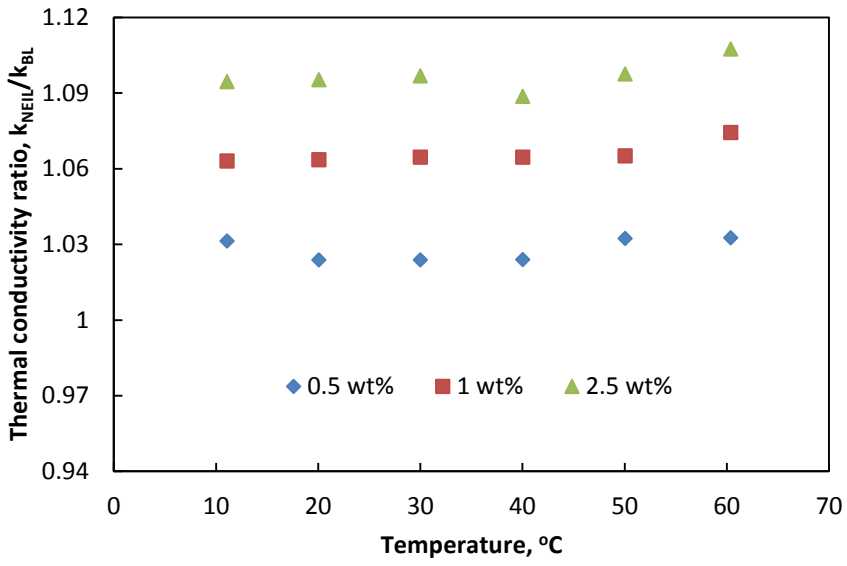

(a)

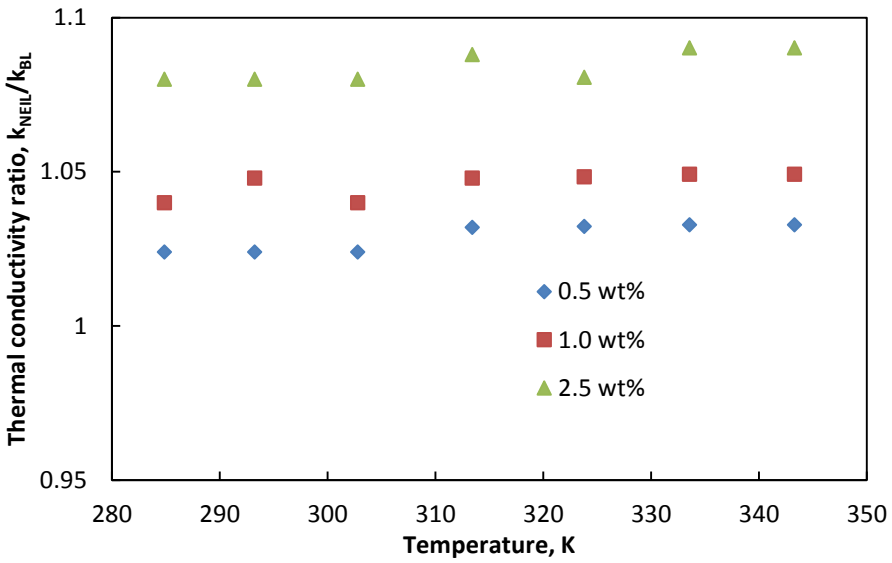
1.1
1.05
1
0.95
Thermal conductivity ratio, k_{NEIL}/k_{BL}
280
290
300
310
320
330
340
350
Temperature, K
0.5 wt%
1.0 wt%
2.5 wt%

(b)

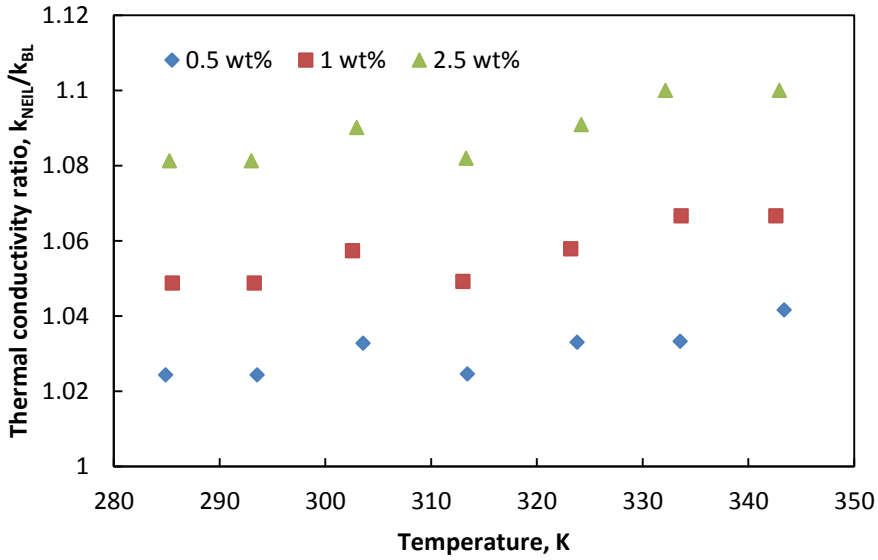
1.12
1.1
1.08
1.06
1.04
1.02
1
Thermal conductivity ratio, k_{NEIL}/k_{BL}
280
290
300
310
320
330
340
350
Temperature, K
0.5 wt%
1 wt%
2.5 wt%

(c)

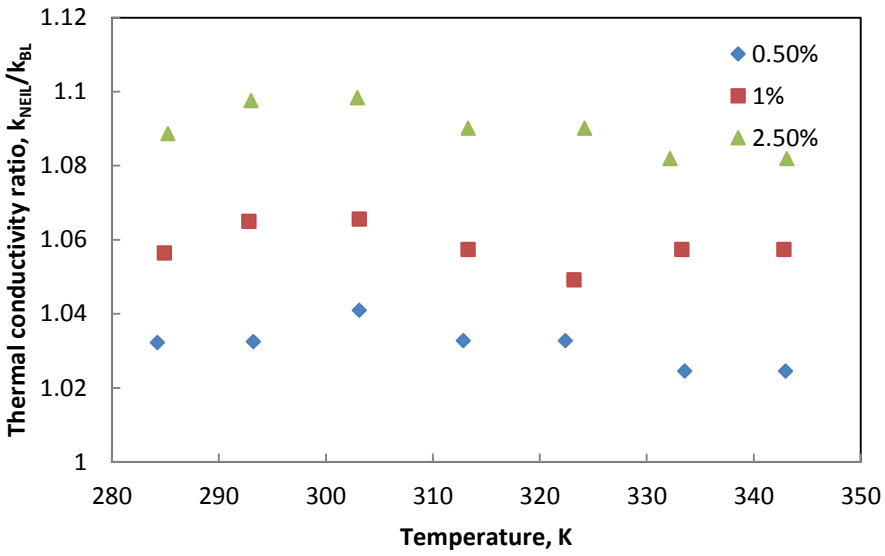

(d)

Figure 4.17 Effective thermal conductivity of NEILs as a function of temperature (a) [C_4mim][NTf_2], (b) [C_4mmim][NTf_2], (c) [C_4mpyrr][NTf_2] and (d) [N_{4111}][NTf_2]

The particle shape effect on thermal conductivity of NEILs was observed for [C_4mpyrr][NTf_2] IL with spherical and whiskers Al_2O_3 nanoparticles. The comparison of effective thermal conductivity of two different NEILs as function of volume fraction is presented in Fig.4.18, and normalized thermal conductivity of whiskers NEILs as function of temperature is presented in Fig.4.19. From the Fig. 4.18 it is also clear that thermal conductivity enhancement of whiskers nanoparticles is always higher than the spherical nanoparticles. It is noted by Timofeeva et al.(Timofeeva, Routbort et al. 2009) that increasing the particle aspect ratio has a positive effect on the thermal conductivity enhancement.

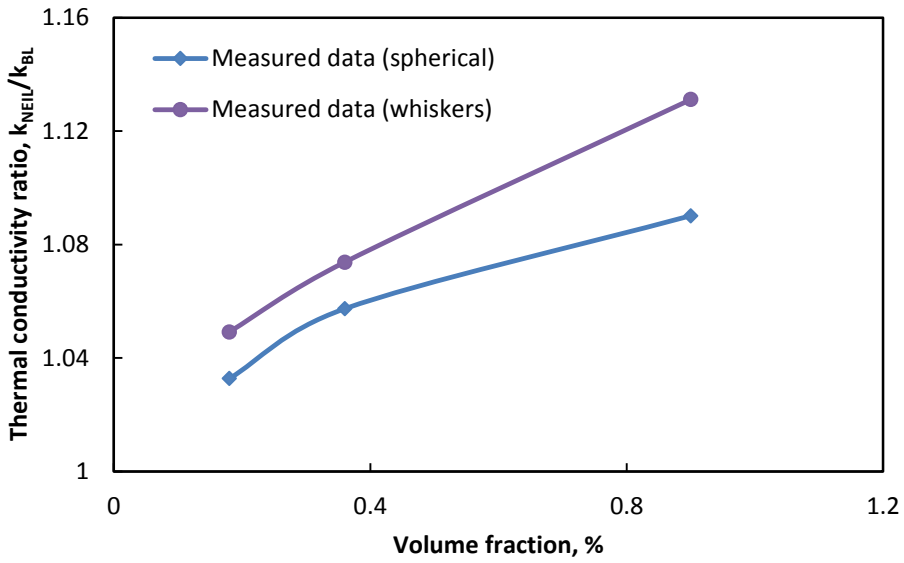

Figure 4.18 Effective thermal conductivity as a function of nanoparticle volume fraction of two different particles

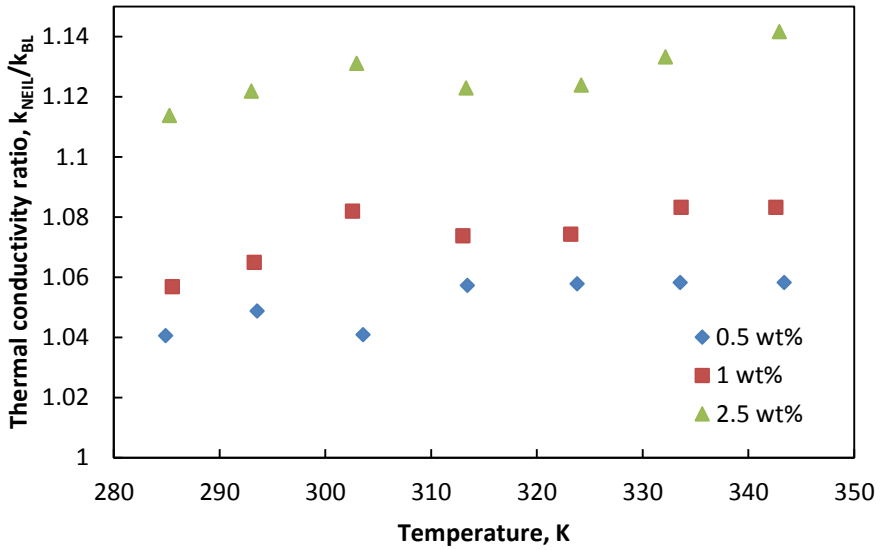

Figure 4.19 Effective thermal conductivity whiskers Al_2O_3 NEILs as a function of temperature

The mechanism of thermal conductivity enhancement of traditional nanofluids has been discussed by numerious researchers. The possible mechanisms include the

Brownian motion of nanoparticles, liquid layering in liquid/nanoparticle surface interface, the nature of heat transport to the nanoparticles, and the effect of nanoparticle clustering and structuring (Das, Putra et al. 2003; Jang and Choi 2004; Murshed, Leong et al. 2005; Leong, Yang et al. 2006; Murshed, Leong et al. 2008). To understand the exact mechanism of thermal conductivity enhancement, the experimental results were compared with the conventional models for thermal conductivity prediction and presented in Fig.4.20. The Maxwell model (Maxwell 1873) for spherical nanoparticles with homogeneous suspension was considered:

$$\frac{k_{NEIL}}{k_{BL}} = \frac{k_n+2k_{BL}-2\phi(k_{BL}-k_n)}{k_n+2k_{BL}+\phi(k_{BL}-k_n)} \tag{4-13}$$

where K_{NEIL}, K_{BL}, , $k_n = 36\ {}^{W}/_{mK}$ are the thermal conductivity of NEIL, base IL, and Al_2O_3 nanoparticles respectively. Φ is the nanoparticle volume fraction. This model underpredicts the experimental results because it only considers the nanoparticles volume fraction and thermal conductivity of base liquid and nanoparticles.

The Bruggeman model (Bruggeman 1935) predicted little bit more enhancement than the Maxwell model because it considers the clustering of nanoparticles. The model for calculating the thermal conductivity of nanofluids is:

$$k_{NEIL} = \frac{1}{4}[(3\phi-1)k_n + (2-3\phi)k_{BL}] + \frac{k_{BL}}{4}\sqrt{\Delta} \tag{4-14}$$

$$\Delta = \left[(3\phi-1)^2(\frac{k_n}{k_{BL}})^2 + (2-3\phi)^2 + 2(2+9\phi-9\phi^2)(\frac{k_n}{k_{BL}})\right] \tag{4-15}$$

The aggregation of nanoparticles was considered to predict the effective thermal conductivity (Chen, Ding et al. 2007) and the aggregation factor ($\frac{r_a}{r_n} = 21.5$) was

considered the same as the shear viscosity predicted. With the aggregation factor the Maxwell model can be rearranged as:

$$\frac{k_{NEIL}}{k_{BL}} = \frac{k_a+2k_{BL}-2\phi_a(k_{BL}-k_a)}{k_a+2k_{BL}+\phi_a(k_{BL}-k_a)} \tag{4-16}$$

where k_a is the aggregates thermal conductivity.

The aggregates thermal conductivity was calculated from the correlation:

$$\frac{k_a}{k_{BL}} = \frac{1}{4}\left\{(3\phi_{in}-1)\frac{k_n}{k_{BL}} + (3(1-\phi_{in})-1) + \left[\left((3\phi_{in}-1)\frac{k_n}{k_{BL}} + (3(1-\phi_{in})-1)\right)^2 + 8\frac{k_n}{k_{BL}}\right]^{1/2}\right\} \tag{4-17}$$

where $\phi_{in}(=(\frac{r_a}{r_n})^{D-3})$ is the aggregates solid volume fraction.

Although considering clustering and aggregation gives higher effective thermal conductivity compared to the Maxwell model (Maxwell 1873), it is clear from the Fig.4.20 that still the model could not predict the experimental effective thermal conductivity. However, the predicted and experimental results are consistent with Nieto de Castro et al. (Nieto de Castro, Lourenço et al. 2009; Nieto de Castro, Murshed et al. 2012), Fox et al. (Fox, Visser et al. 2013), and Wang et al. (Wang, Wang et al. 2010; Baogang Wang 2011; Wang, Wang et al. 2011) where they use carbon nanotube, Al_2O_3, and gold nanoparticles with different base ionic liquids.

Then the interfacial layer of nanoparticles in NEILs is considered to predict the effective thermal conductivity of NEILs by Murshed et al.'s model (Murshed, Leong et al. 2008):

$$k_{NEIL} = \frac{(k_n - k_{lr})\phi k_{lr}[2\gamma_1^2 - \gamma^2 + 1] + (k_n + 2k_{lr})\gamma_1^2[\phi\gamma^2(k_{lr} - k_{BL}) + k_{BL}]}{\gamma_1^2(k_n + 2k_{lr}) - (k_n - k_{lr})\phi[\gamma_1^2 + \gamma^2 - 1]} \tag{4-18}$$

where k_{lr} is the thermal conductivity of interfacial layer which would be $k_{BL} < k_{lr} < k_n$; here we consider $k_{lr} = 3k_{BL}$

$$\gamma = 1 + \frac{t}{r_n} \tag{4-19a}$$

$$\gamma_1 = 1 + \frac{t}{2r_n} \tag{4-19b}$$

where t is the interfacial layer thickness, taking into consideration $t = 2\,nm$ and $r_n = 20\,nm$.

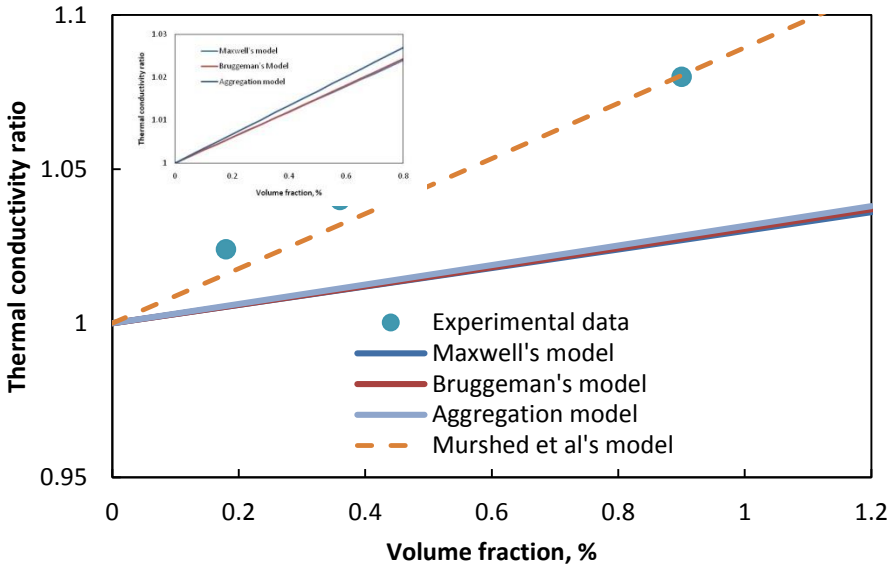

Figure 4.20 Effective thermal conductivity as function of nanoparticles volume fraction

As of Fig. 4.20 the enhancement of thermal conductivity of NEILs is predicted well with the interfactial layer model. Nieto de Castro et al. (Nieto de Castro, Murshed et al. 2012) also use the Murshed's model (Murshed, Leong et al. 2008) to predict the thermal conductivity of $[C_4mim][NTf_2]$ and multi wall carbon nanotubes (MWCNT) considering $t = 1\ nm$and $k_{lr} = 1.2k_{BL}$ and found reasonably good predictions. Although the interfacial layer model predicted well the experimental thermal conductivity with arbitrary interfacial layer thickness and thermal conductivity, there may be other parameter like complex interactions of nanoparticles surface with ILs which should be considered. In literature there is evidence of strong interactions of nanoparticles and ILs (Carper, Wahlbeck et al. 2011; Pensado and Pádua 2011). Molecular dynamic simulations of nanofluids containing ruthenium nanoparticle in ILs were performed by Pensado et al. (Pensado and Pádua 2011) and they reported that nanoparticles are in contact with the anion and cation of ILs. Carper et al. (Carper, Wahlbeck et al. 2011) theoretically modeled IL and Al_2O_3 surfaces and reported complex interaction formation of IL with Al–O surface.

4.10 Heat Capacity of NEILs

The heat capacity of all four ILs and 0.5, 1.0, and 2.5 wt% NEILs are measured within the temperature limit 25-345^{o}C. The heat capacity of all four NEILs over 25-345^{o}C with an interval of 10^{o}C is presented in Fig. 4.21(a-d). It is clear from the Fig. 4.21(a-d) that the heat capacity of NEILs is much higher than the base IL over the measured temperature range and heat capacity increases almost linearly with temperature. The average enhancements of heat capacity are ~9%, ~28%, and ~62% of 0.5, 1, and 2.5 wt% NEILs respectively. Fig. 4.22 shows the whiskers Al_2O_3 NEILs as function of

temperature and observed that the 0.5 and 1.0 wt% whiskers NEILs shows higher heat capacity compared to spherical NEILs. Measured heat capacities of NEILs were compared with the existing classical theoretical model of heat capacity for a mixture where base IL and nanoparticles are assumed at thermal equilibrium (Zhou and Ni 2008):

$$C_{p,NEIL} = \frac{\phi_n \rho_n C_{p,n} + \phi_{BL} \rho_{BL} C_{p,BL}}{\phi_n \rho_n + \phi_{BL} \rho_{BL}} \quad (4\text{-}20)$$

where $c_{p,NEIL}$, $c_{p,n} = 0.791\ {}^{J}/_{g.K}$, and $c_{p,BL}$ are the heat capacity of NEILs, nanoparticles, and base IL respectively, ϕ is the nanoparticles volume fraction, ρ_n and ρ_{BL} are the density of nanoparticles and base IL respectively. Most of the previous studies for water based nanofluids shows lower heat capacity and are predicted well by the theoretical model (Zhou and Ni 2008). The predicted heat capacity of NEILs based on the equation shows slightly lower value than the base IL but the experimental measured heat capacity of NEILs shows much higher value compared to the base IL. That means the significant enhancement of heat capacity of NEILs cannot be predicted by the model and more sophisticated investigations will be required to explain these enhancements. Meanwhile, similar enhancement in heat capacity of NEILs containing spherical Al_2O_3 nanoparticles with [C_4mmim][NTf_2] IL was observed by Bridges et al. (Bridges, Visser et al. 2011). Nieto de Castro et al. (Nieto de Castro, Lourenço et al. 2009; Nieto de Castro, Murshed et al. 2012) also report up to 8% enhancement heat capacity of IoNanofluids ([C_4mim][PF_6]+1wt% MWCNT). Shin et al. (Shin and Banerjee 2011) have reported ~26% enhancement of heat capacity with 1 wt% of silica nanoparticles in eutectic of lithium carbonate and potassium carbonate (62:38 ratio) and proposed that the enhancement is due to the high specific surface energy of nanoparticles. In another

observation Shin et al. (Shin and Banerjee 2010) proposed three independent models to discuss the heat capacity enhancement: (i) higher specific heat capacity of nanoparticles than bulk material, (ii) solid-fluid interaction energy, and (iii) liquid molecules layer in nanoparticles. In addition to those models Tiznobaik et al. (Tiznobaik and Shin 2013) observed that there are needle-like structure forms in nanofluids that have high specific surface area and contribute in high heat capacity of nanofluids. For NEILs as was discussed of viscosity and thermal conductivity, the complex interaction between nanoparticles surface and ILs may also play a role in the enormous enhancement of heat capacity. However, the heat capacity enhancement of NEILs will help to develop energy efficient heat transfer fluids for the next generation CSP system.

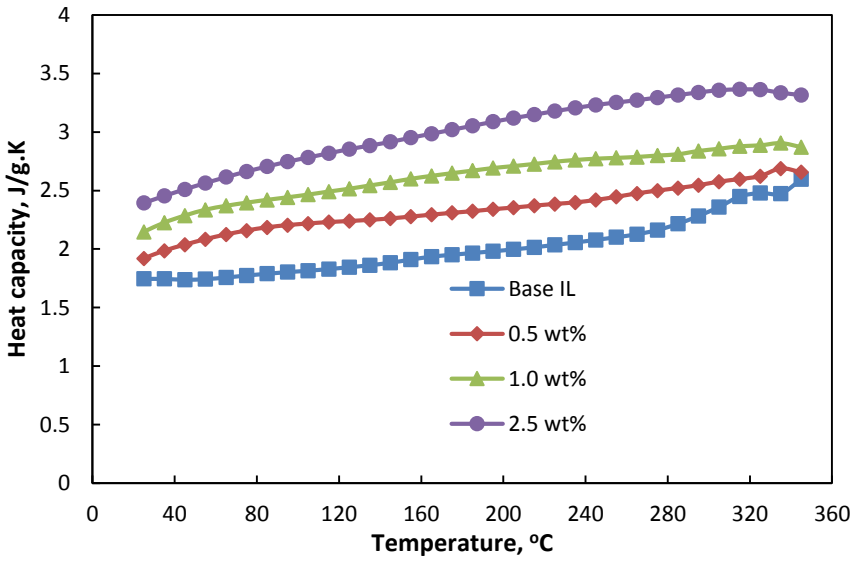

(a)

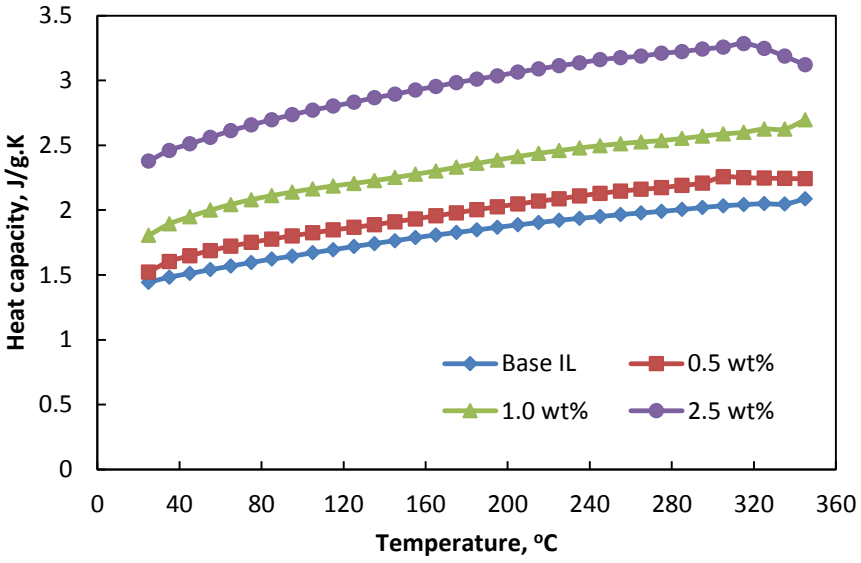
Heat capacity, J/g.K
Temperature, °C
Base IL
0.5 wt%
1.0 wt%
2.5 wt%

(b)

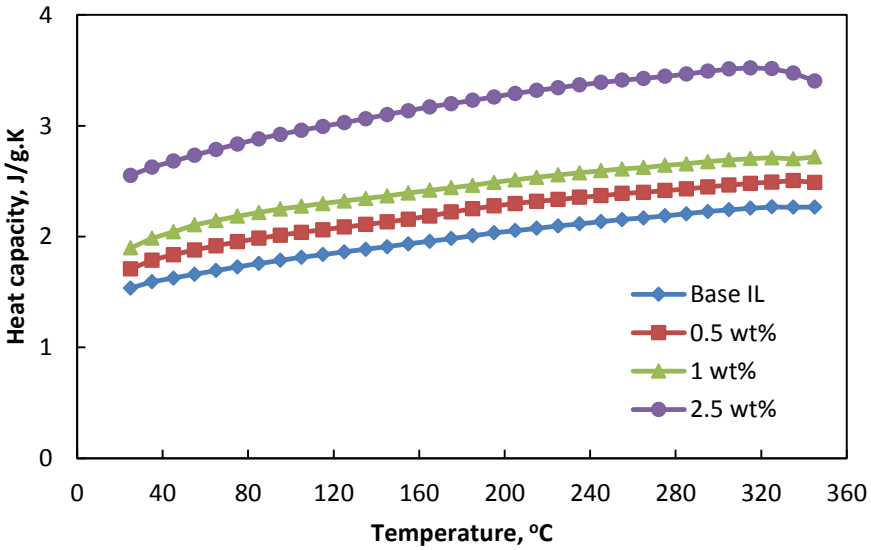
Heat capacity, J/g.K
Temperature, °C
Base IL
0.5 wt%
1 wt%
2.5 wt%

(c)

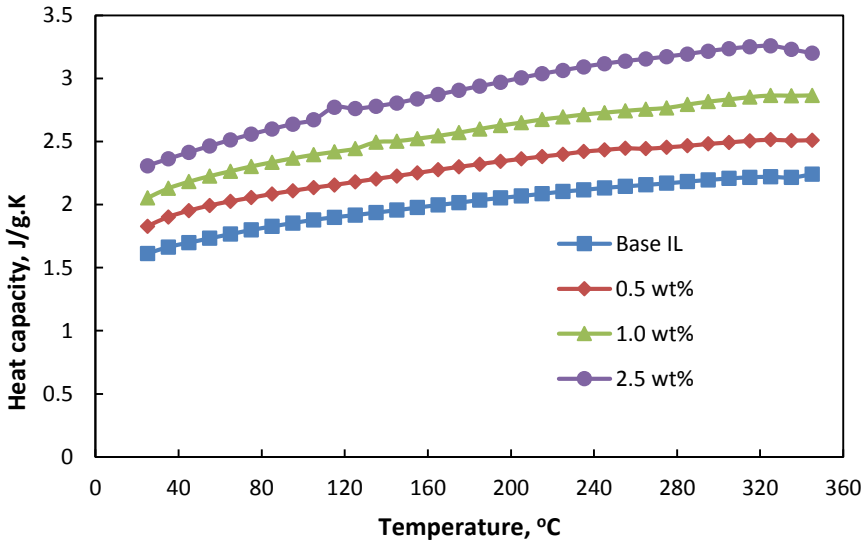

(d)

Figure 4.21 Heat capacity of NEILs as a function of temperature (a) $[C_4mim][NTf_2]$, (b) $[C_4mmim][NTf_2]$, (c) $[C_4mpyrr][NTf_2]$ and (d) $[N_{4111}][NTf_2]$

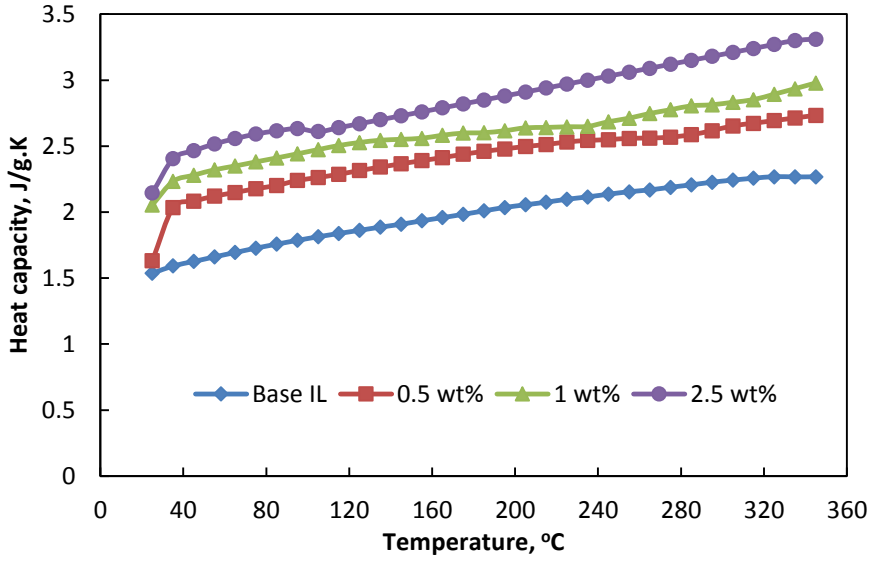

Figure 4.22 Heat capacity of whiskers Al_2O_3 NEILs as a function of temperature

4.11 Summary

The thermophysical properties such as density, viscosity, thermal conductivity, and heat capacity of four ILs and Al_2O_3 nanoparticle enhanced ionic liquids (NEILs) in different concentration (0.5, 1.0, and 2.5 wt%) were measured experimentally and reported. The thermophysical properties of ILs matches well with the previously published data. The ILs shows Newtonian behavior and high temperature dependency where viscosity decreases with increasing temperature. Heat capacity of ILs shows linear relation with the temperature. The thermal conductivity of ILs shows no remarkable variation with temperature and has lower thermal conductivity value compared to DI-water, which is approximately 21% of thermal conductivity of DI-water.

All of the NEILs shows shear thinning behavior in decreased shear viscosity with increasing shear rate. The shear thinning behavior occurs at all measured temperatures and shear thinning increased with temperature. NEILs shows enormous enhancement of shear viscosity with a small volume percentage of nanoparticles and viscosity decreases sharply with temperature increases. The experimental enhanced viscosity of NEILs is predicted well by considering aggregation with high aggregation factor ($\frac{r_a}{r_n} = 21.5$). Thermal conductivity also increases with nanoparticle concentration and shows up to ~11% enhancement for 2.5 wt% NEILs. The thermal conductivity of ILs and NEILs does not show much temperature dependency. The effective thermal conductivity of NEILs has been underpredicted with the same aggregation factor. The better prediction of the effective thermal conductivity was found by considering interfacial layer of nanoparticles on NEILs. Heat capacity of NEILs shows huge enhancements compare to base ILs and up to ~62% enhancement was reported for 2.5 wt% NEILs. The theoretical model for

heat capacity failed to predict the experimental results. However, to explain the exact mechanism of thermophysical properties enhancement there is needed a more sophisticated theoretical model that considers the strong interaction of nanoparticles surface with ILs ions. Although the exact mechanism of enhancement is under investigation, these enhancements will help to assess the applicability of NEILs in CSP system.

CHAPTER 5

NATURAL CONVECTION OF ILS AND NEILS

5.1 Introduction

Natural convection heat transfer behavior is a fundamental study of any heat transfer fluid (HTF), which has wide engineering and industrial applications, i.e. solar energy collection system, geophysics, electronic cooling, thermal storage system, and nuclear energy (Chen, Mikami et al. 2005). There were several natural convection heat transfer experimental studies in literature for water, air, mercury, and nanofluids (Shiina, Fujimura et al. 1994; PallarÈs, Cuesta et al. 1996; Jang and Choi 2004; Calcagni, Marsili et al. 2005; Wen and Ding 2005; Dalal and Das 2006; Wu, Ewing et al. 2006). For the nanofluids study, all of the previous studies discussed water based nanofluids and most of the previous researches for ILs based nanofluids are mainly emphasized on the thermophysical properties and thermal stability. None of these studies report the natural convection heat transfer behavior of ionic liquids (ILs) and nanoparticle enhanced ionic liquids (NEILs). Here, natural convection heat transfer experiments were performed for four ILs and two NEILs.

5.2 Experiments with De-Ionized (DI) Water

Several investigations have been considered for buoyancy driven natural convection of classical fluids in a cavity heated from below (Shiina, Fujimura et al. 1994;

PallarÈs, Cuesta et al. 1996; Jang and Choi 2004; Calcagni, Marsili et al. 2005; Wen and Ding 2005; Dalal and Das 2006; Wu, Ewing et al. 2006). Natural convection in a rectangular cavity heated from below does not depend on the critical temperature difference between the top and bottom surface. The condition of heated from below can be expressed in terms of the critical Rayleigh number which is an important dimensionless parameter in natural convection, and is defined as the ratio of the buoyancy force to the viscous force acting on the fluid. Natural convection in a rectangular cavity heated from below occurs once the Raleigh number exits the critical value Ra>1708 (Bejan and Kraus 2003).

Before performing any experiment the test enclosure was rinsed thoroughly with DI-water and the liquid is poured into the test enclosure with care to avoid entrapment of any air bubbles in the enclosure. Initially the experiment was carried out with DI water and the results have been compared with the other published results (Globe and Dropkin 1959; Putra, Roetzel et al. 2003; Wen and Ding 2005; Ho, Liu et al. 2010) to ensure the credibility of the experimental setup and procedure. Nusselt number (Nu) as a function of Rayleigh number (Ra) for DI-water is compared with that of the published result in Fig.5.1. The Nusselt and the Rayleigh number are computed with the following equations:

$$Nu = \frac{hH}{k_f}; \qquad Pr = \frac{\nu_f}{\alpha}; Gr = \frac{g\beta\Delta T H^3}{\nu_f^2} \tag{5-1}$$

$$Ra = Gr.Pr \tag{5-2}$$

where H is the height of the enclosure, k_f is the thermal conductivity, Pr is the Prandtl number, ν_f is the kinematic viscosity, $\alpha(=\frac{k_f}{\rho C_p})$ is the thermal diffusivity, Gr is the Grashof number, β is the volume expansion coefficient, ρ is the density, C_p is the heat capacity of fluid, ΔT is the temperature difference between hot and cold surface fluid, and g is the gravitational acceleration. All the fluid properties were evaluated at the average ($T_{av} = \frac{T_{heated}+T_{cooled}}{2}$) of the heated and the cooled surface temperature. The natural convection correlation can be represented as $Nu = c'Ra^{n'}$

where c' and n' are the empirical constants. For classical fluid, Globe and Dropkin (Globe and Dropkin 1959) proposed the heat transfer coefficient of natural convection in cavity heated from below.

$$Nu = \frac{hH}{k_f} = 0.069 Ra_{H,f}^{1/3} Pr_f^{0.074} ; 3 \times 10^5 < Ra_{H,f} < 7 \times 10^9 \quad (5\text{-}3)$$

Fig.5.1 shows that the experimental result and reference results have the same trend, and there appears to be differences in the value of empirical constants. Those constants depend on the geometry of the enclosure and on the heating condition. It is clear that the experimental results agree well with the Globe and Dropkin (Globe and Dropkin 1959) correlation over the Rayleigh number range and the maximum deviation is ~9%.

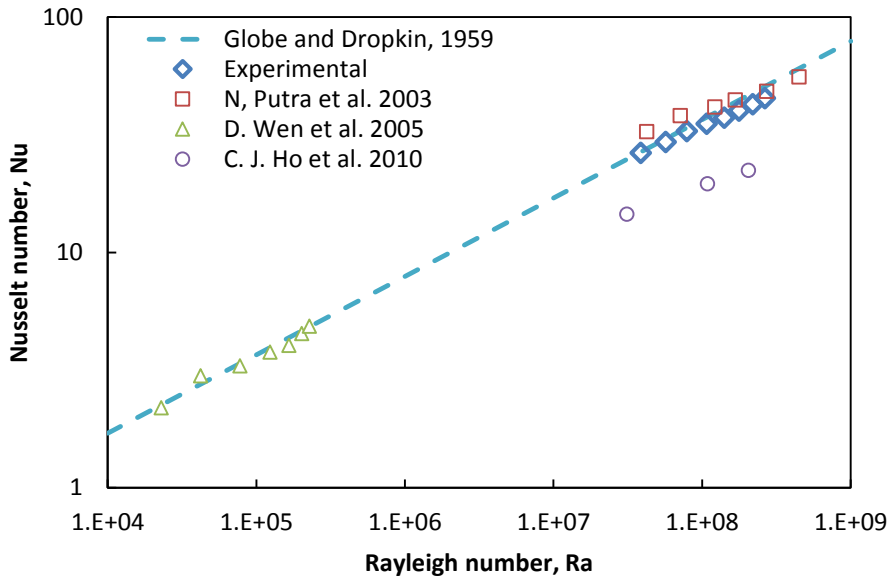

Figure 5.1 Comparison of experimental and published result for natural convection of DI-water

5.3 Experiments with Ionic Liquids

After having confidence with the experimental facilities by DI-water, the systematic natural convection experiments were performed for all four ILs. The experimental results of $[C_4mim][NTf_2]$ IL are presented with respect to input power and temperature differences. The heat transfer coefficients of IL as a function of input power for both aspect ratios are presented in Fig.5.2. Fig.5.2 shows that the heat transfer coefficient of the IL is much lower (approximately 25% for AR=1.5 and 22% for AR=1) than DI-water and the heat transfer coefficient increases with increased input power. The lower heat transfer coefficient of the IL indicates that IL has the lower buoyancy force compare to DI-water, which is clear from the Fig.5.3. Fig.5.3 represents the Rayleigh number as a function of temperature difference between heated and cold surface fluid, which indicates that at the same temperature difference IL has a lower Rayleigh number, suggesting higher viscous force of IL compared to DI-water. The lower heat transfer

coefficient of IL is also an indication from the lower thermal conductivity of IL (Chen, He et al. 2008) which influences the thermal diffusivity. At same temperature the IL has 2.5 times lower thermal diffusivity than DI water.

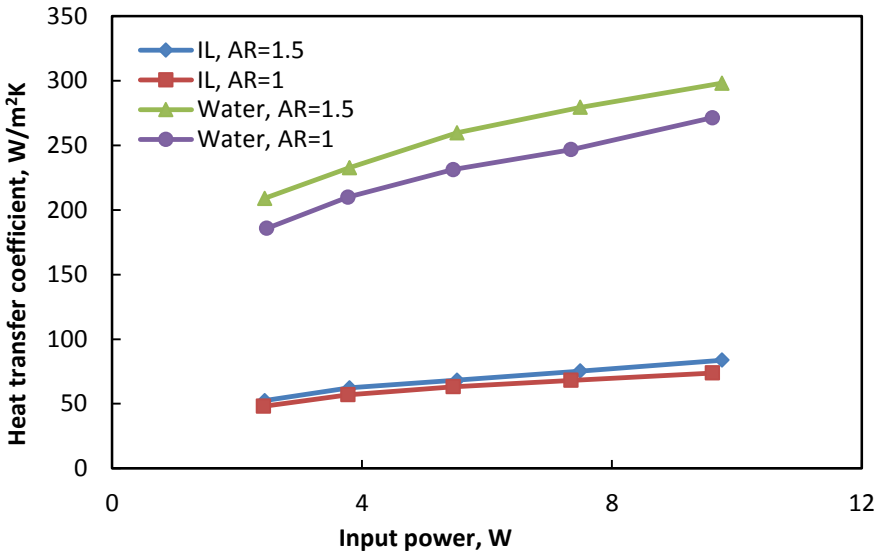

Figure 5.2 Heat transfer coefficient as a function of input power

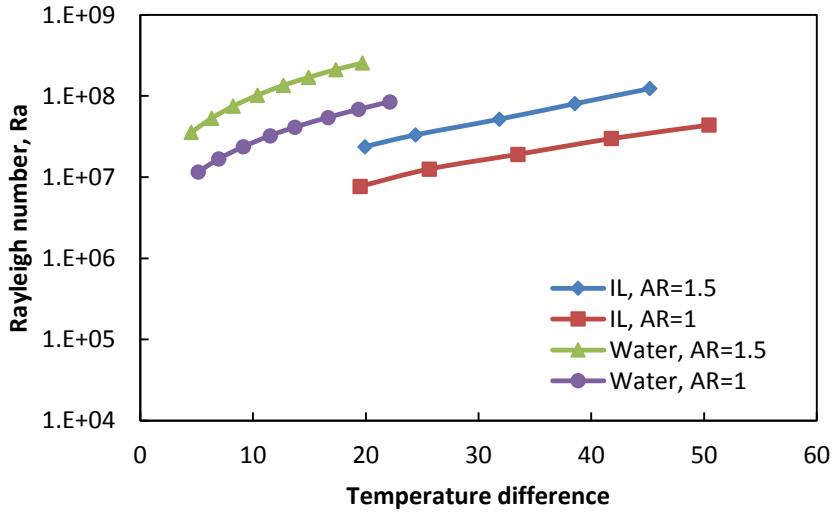

Figure 5.3 Rayleigh number as a function of temperature difference

The Nusselt number as a function of Rayleigh number is presented in Fig.5.4 and it can be noticed that at the same Rayleigh number IL has a higher Nusselt number than DI-water, which is also an indication of lower thermal conductivity of IL. From Fig. 5.2 it is clear that IL has lower convective heat transfer coefficient which implies that the higher Nusselt number is obtained due to much lower thermal conductivity of the IL. The thermal conductivity ratio of water to IL is approximately 4.662 (0.606/0.125) and the heat transfer coefficient ratio of water to IL is approximately 4. That means from the Nusselt number equation the IL has approximately 1.17 (4.662/4) times higher Nusselt number than DI-water which is also clear from the experimental results.

The heat transfer coefficient has the same trend for both aspect ratios and increases with aspect ratios. That means at higher aspect ratio the liquid circulation due to natural convection is higher compared to lower aspect ratio. The evidence of high circulation is obvious from the lower temperature difference at higher aspect ratio as of Fig.5.5. It is also noticed from Fig.5.5 that the temperature difference curve diverges more at higher heat input. The natural convection of all four ILs and water are presented in Fig.5.6 and Fig.5.7 for both AR=1 and AR=1.5 respectively. The Nusselt number and Rayleigh number correlation of IL follows the conventional natural convection correlation form of: $Nu = cRa^n$ with different n and c values for different aspect ratios. The constants are presented in Table. 5.1 within the Rayleigh number range studied.

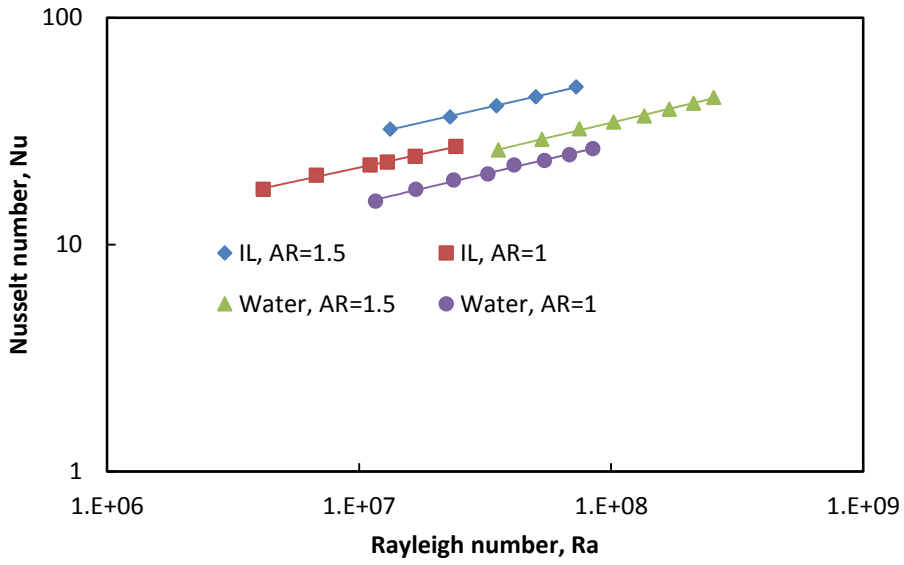

Figure 5.4 Nusselt number as a function of Rayleigh number

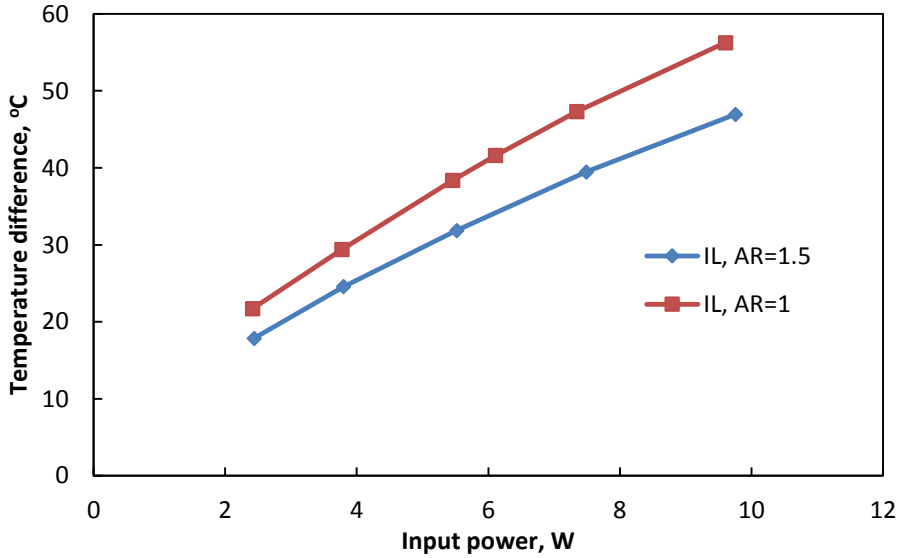

Figure 5.5 Temperature difference as a function of input power

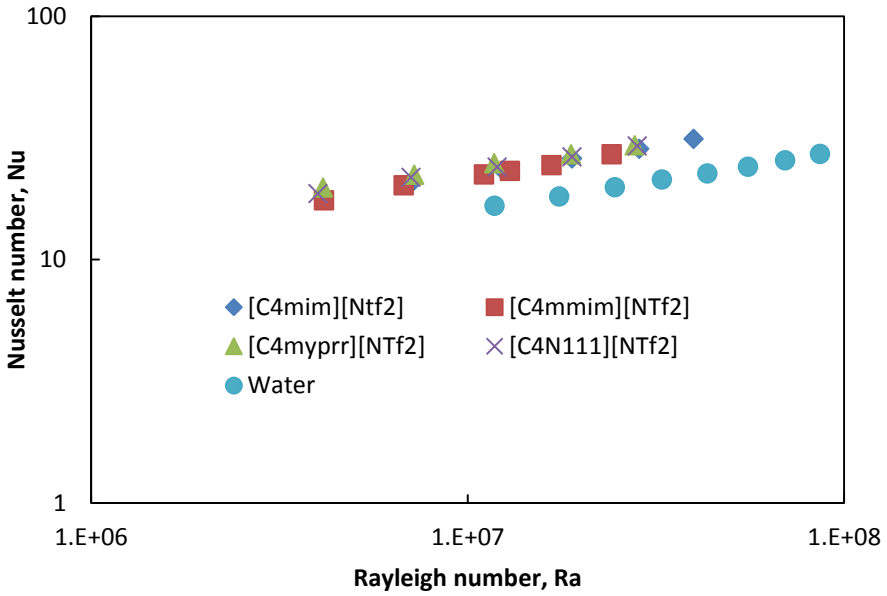

Figure 5.6 Nusselt number as a function of Rayleigh number at AR=1

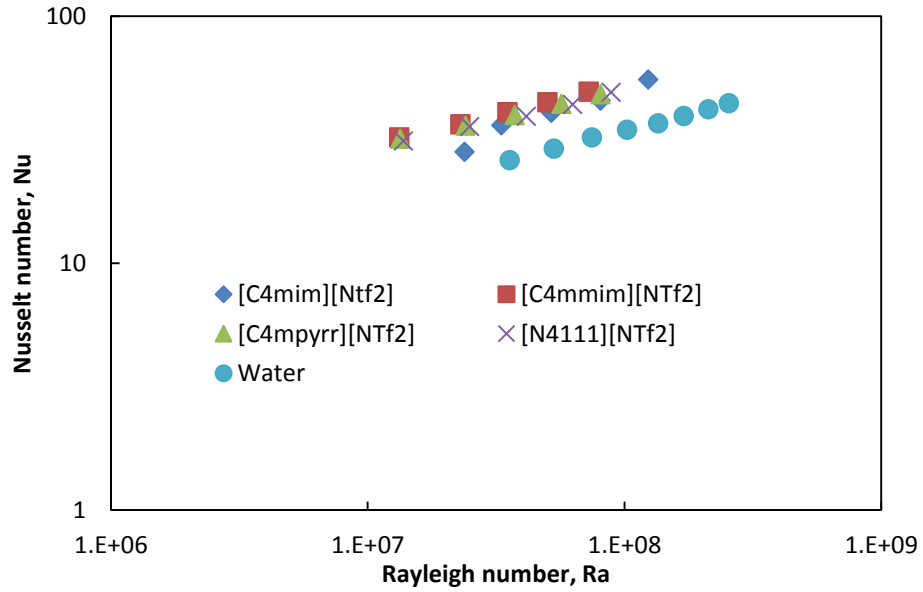

Figure 5.7 Nusselt number as a function of Rayleigh number at AR=1

Table 5.1 Natural convection correlation constant of four ILs within the studied Rayleigh number limit

Ionic liquids		Ra	c'	n'
$[C_4mim][NTf_2]$	AR-1	4.15×10^6-2.41×10^7	0.462	0.239
	AR-1.5	1.32×10^7-7.26×10^7	0.509	0.252
$[C_4mmim][NTf_2]$	AR-1	4.15×10^6-2.41×10^7	0.462	0.239
	AR-1.5	1.32×10^7-7.26×10^7	0.509	0.252
$[C_4mpyrr][NTf_2]$	AR-1	4.13×10^6-2.77×10^7	0.823	0.208
	AR-1.5	1.33×10^7-8.08×10^7	0.721	0.231
$[N_{4111}][NTf_2]$	AR-1	4.0×10^6-2.82×10^7	0.619	0.224
	AR-1.5	1.37×10^7-8.87×10^7	629	0.237

5.4 Experiments with NEILs

The systematic natural convection experiments were performed for NEILs forming $[C_4mim][NTf_2]$ IL with spherical Al_2O_3 and $[C_4mpyrr][NTf_2]$ IL with spherical and whiskers Al_2O_3 nanoparticles of three different concentrations (0.5, 1.0, and 2.5 wt%). Firstly the experimental results of $[C_4mpyrr][NTf_2]$ NEILs are presented. The initial transient heating and cooling surface temperature of base IL and spherical Al_2O_3 NEILs for AR-1 is presented in Fig.5.8. It is clear from the Fig.5.8 that 2.5 wt% NEILs have the highest and base the ILs have the lowest heating surface temperature. Also, it takes a longer time to reach the steady state for 2.5 wt% NEILs. The steady state temperature difference between heating and cooling surface were increased with nanoparticles concentration which results in the systematically decreased heat transfer coefficient. The scenario occurred in both aspect ratios.

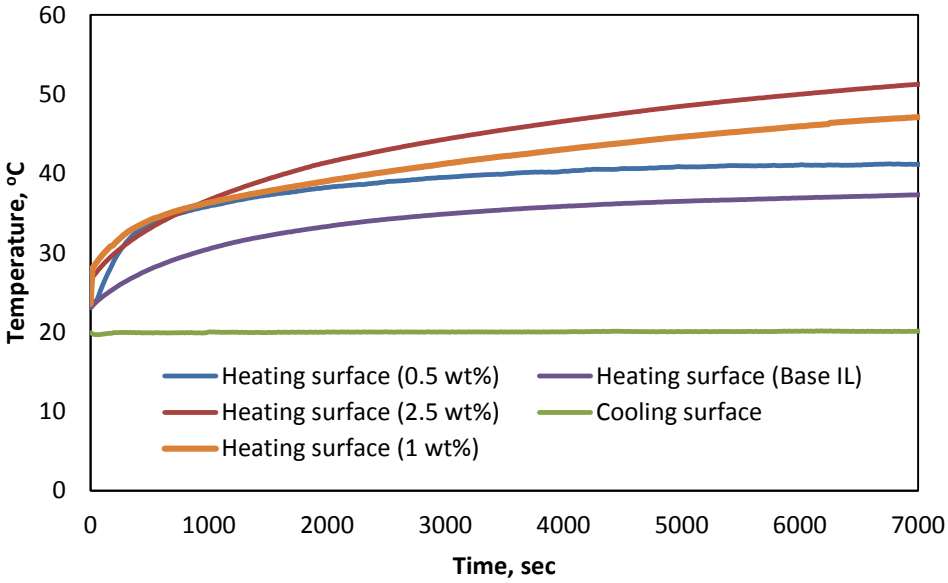

Figure 5.8 The transient temperature profile of heating and cooling surface

The experimental effective Rayleigh number at the same temperature difference of three concentrations of spherical Al_2O_3 NEILs have presented in Fig.5.9, where the Rayleigh number was normalized by effective Rayleigh number of NEILs divided by the Rayleigh number of base IL. The effective Rayleigh number of NEILs was calculated using the corresponding effective thermophysical properties of NEILs. The Fig.5.9 shows that the normalized Rayleigh number decreased with nanoparticle concentration. This means increasing nanoparticles concentration increases the viscous force in the rectangular cavity, which results in the reduction of Rayleigh number as well as natural convection heat transfer coefficient.

The Nusselt number and Rayleigh number (both AR=1 and 1.5) of base IL and the different concentration of spherical and whiskers NEILs are presented in Fig. 5.10(a) and (b) respectively. It is clear from the Fig.5.10 that Nusselt number of both NEILs

shows lower Nusselt number compared to the base IL over the measured Rayleigh number range. Both AR shows at almost the same rate of degradation.

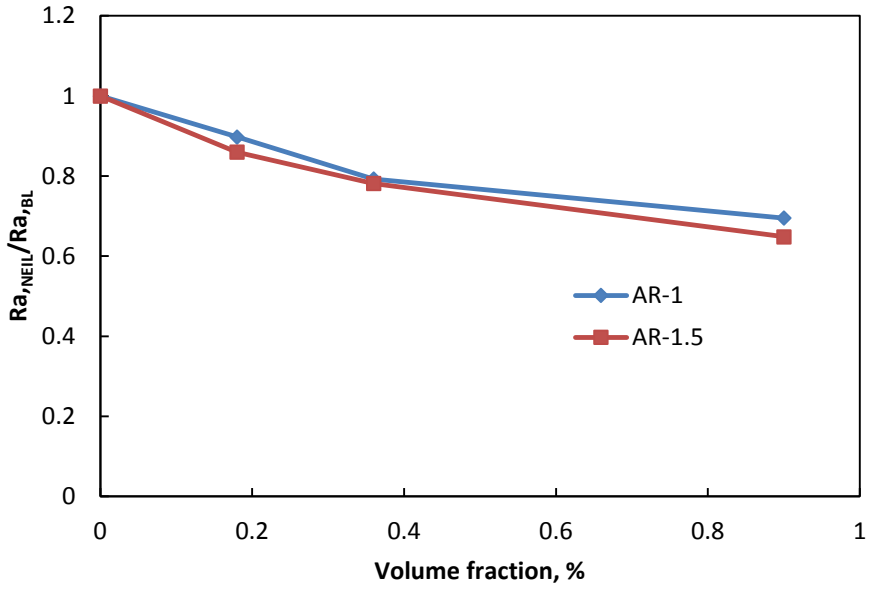

Figure 5.9 Normalized Rayleigh number as a function of nanoparticle volume concentration

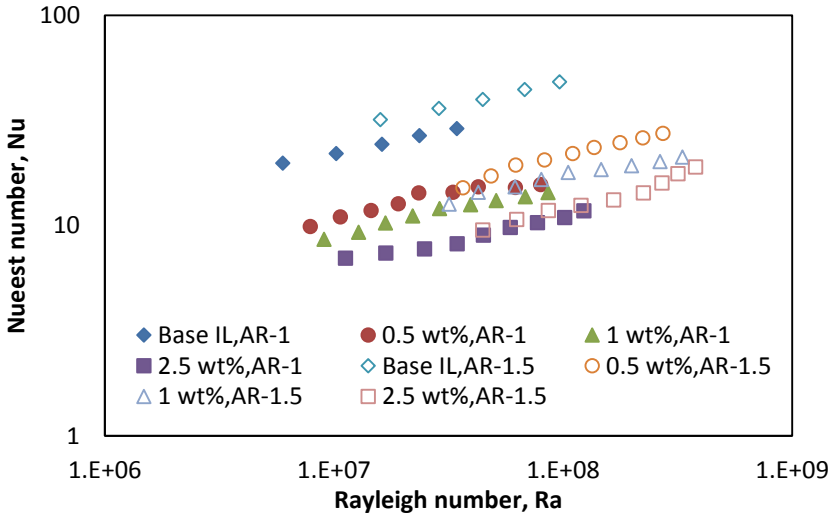

(a)

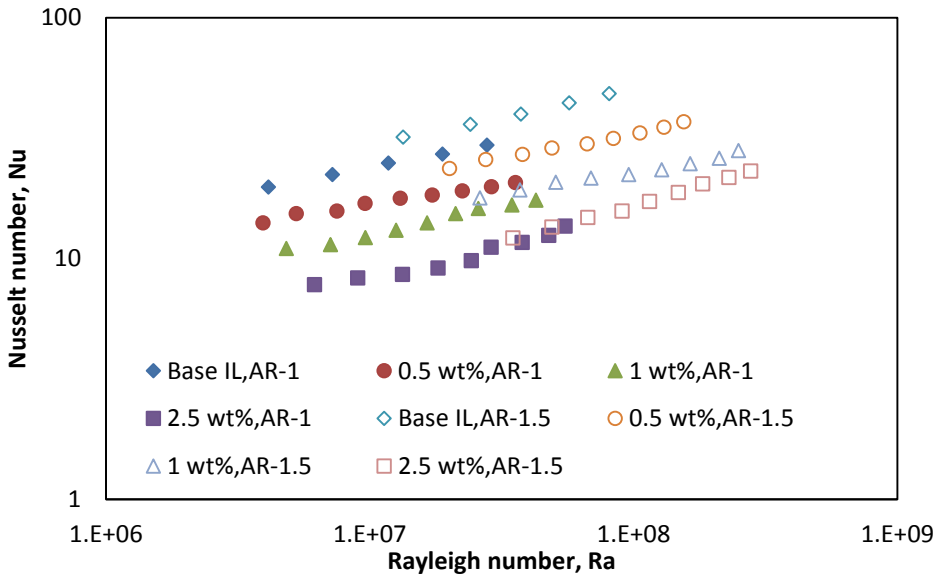

(b)

Figure 5.10 Nusselt number as a function of Rayleigh number of base IL and NEILs of two different enclosures (a) spherical (b) whiskers Al_2O_3

Fig.5.11 (a) and (b) represent the comparison of natural convection heat transfer results of spherical and whiskers Al_2O_3 NEILs for AR 1 and 1.5 respectively. In both aspect ratios it is clear that whiskers Al_2O_3 NEILs shows higher Nusselt number compared to spherical Al_2O_3 NEILs at the same Rayleigh number. The higher heat transfer of whiskers NEILs may be the consequence of the higher effective thermal conductivity and lower effective viscosity of whiskers NEILs compared to the spherical NEILs. The same higher heat transfer performance of cylindrical shaped nanoparticles was found analytically in shell and tube heat exchanger (Elias, Miqdad et al. 2013) and experimentally in the oscillating heat pipe (Ji, Wilson et al. 2011).

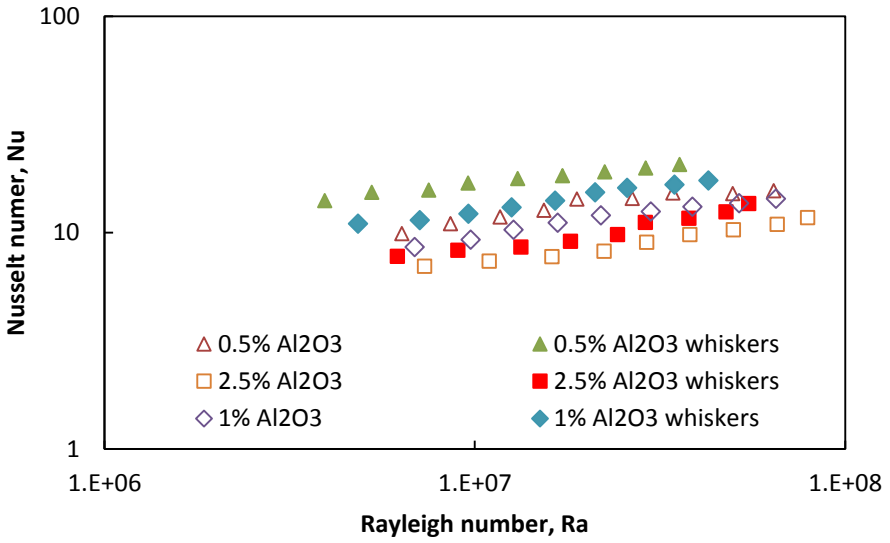

(a)

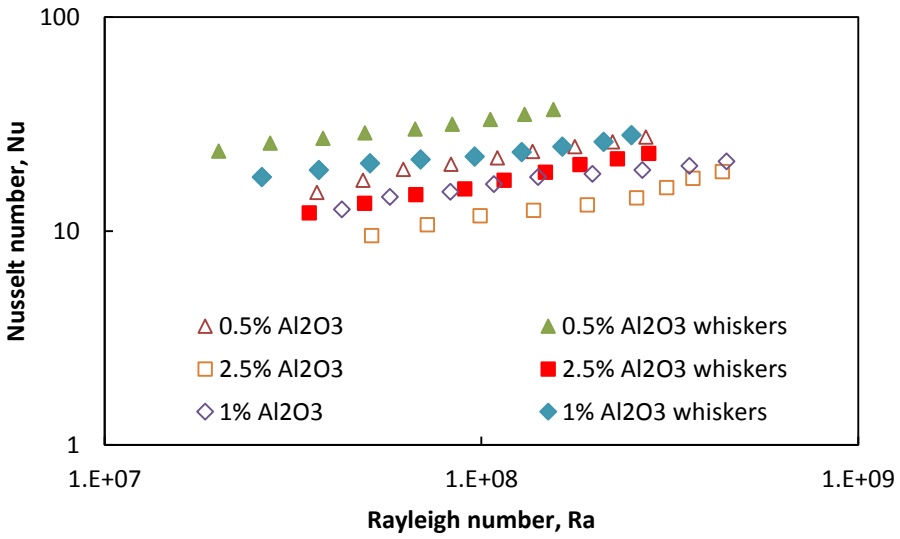

(b)

Figure 5.11 Comparison of spherical and whiskers NEILs with respect to natural convection heat transfer for (a) AR-1 and (b) AR-1.5

It is generally thought that the change of effective thermophysical properties has a great influence on the degradation of the natural convection performance of nanoparticle

enhanced fluids (Hwang, Lee et al. 2007; Nnanna 2007). To understand and quantify the degree with which thermophysical properties effects much, there are also other factors with the thermophysical properties that lead to degradation of natural convection of NEILs. Fig.5.12 was constructed by all of the effective thermophysical properties and effective heat transfer coefficient of spherical NEILs. From the natural convection correlation eq. (13):

$$Nu = cRa^n \tag{5-4}$$

$$\frac{hH}{k_f} = c\left(\frac{g\beta\Delta TH^3C_p\rho^2}{\mu k_f}\right)^n \tag{5-5}$$

From the equ (5-5) normalizing the heat transfer coefficient by dividing the heat transfer coefficient of NEILs to IL we can find the correlation:

$$\frac{h_{NEIL}}{h_{BL}} \sim \left(\frac{\beta_{NEIL}}{\beta_{BL}}\right)^n \left(\frac{\rho_{NEIL}}{\rho_{BL}}\right)^{2n} \left(\frac{C_{p,NEIL}}{C_{p,BL}}\right)^n \left(\frac{\mu_{NEIL}}{\mu_{BL}}\right)^{-n} \left(\frac{k_{NEIL}}{k_{BL}}\right)^{1-n} \tag{5-6}$$

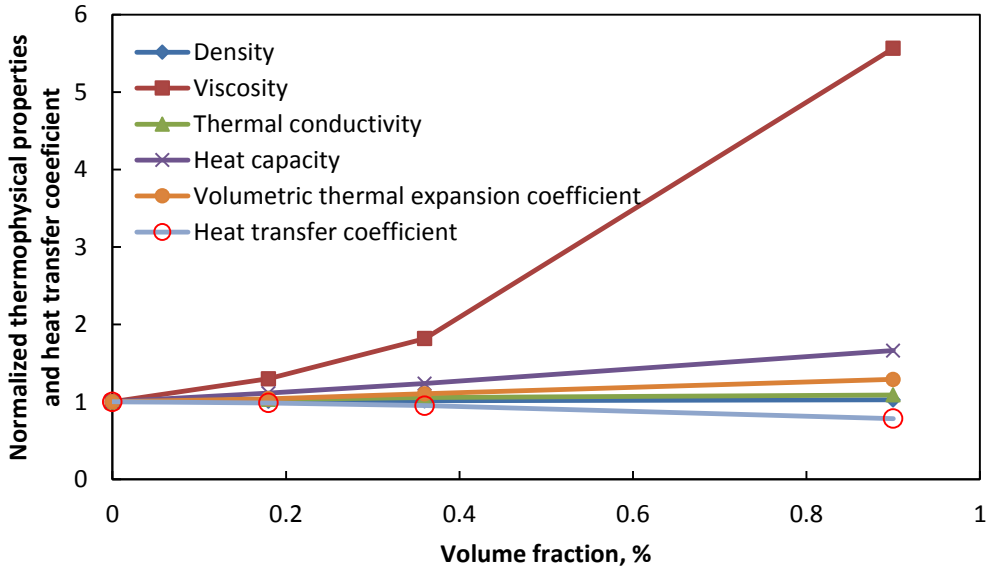

Figure 5.12 Normalized thermophysical properties and heat transfer coefficient as a function of nanoparticle volume fraction.

From the Fig.5.12 and previous thermophysical properties it can be seen that all of the thermophysical properties increase with nanoparticle concentration. In the normalized heat transfer coefficient correlation, all of the thermophysical properties except dynamic viscosity have the positive impact on heat transfer coefficient. In the correlation, inserting a typical natural convection correlation exponent value of $n = {}^{1}/_{3}$, the normalized heat transfer coefficient was calculated and presented in Fig.5.12. Although all properties are enhanced with nanoparticle concentration and have a positive effect except dynamic viscosity, heat transfer coefficient decreases with nanoparticle concentration, and the highest degradation was ~22% for 2.5 wt% NEILs. That means the negative effect of enhanced viscosity surpassed the enhancement of other thermophysical properties. However, experimentally the maximum degradation was ~68% for 2.5 wt% NEILs which indicates the change of thermophysical properties could not fully explain the experimental degradation of natural convection performance of NEILs. The present observations of natural convection behavior of NEILs are consistent with the previous experimental studies of the water based nanofluids (Putra, Roetzel et al. 2003; Wen and Ding 2005; Nnanna 2007; Ho, Liu et al. 2010; Li and Peterson 2010) and opposite to the numerical studies (Khanafer, Vafai et al. 2003; Jou and Tzeng 2006). There are several explanations of the deteriorating behavior of water based nanofluids mentioned by previous researchers. Putra et al. (Putra, Roetzel et al. 2003) emphasizes the role of particle fluid interaction and nanoparticles sedimentation as possible reasons for this deterioration; and along with those Wen et al. (Wen and Ding 2005) included the thermophysical properties influence, convection by concentration difference, influence of P^{H}, and particle-surface interaction. Ho et al. (Ho, Liu et al. 2010) added that particles-

fluids interactions and transport mechanisms as similar to Brownian diffusion at high temperature differences.

In addition to the above mentioned factors, deterioration of natural convection heat transfer of NEILs may have other influences. One of the important things is interaction energies of IL with nanoparticles; Podgorsek et al. (Podgoršek, Pensado et al. 2013) found stronger interactions of ruthenium nanoparticles (RuNPs) with longer alkyl chain ILs by analyzing titration calorimetry and molecular simulation. Carper et al. (Carper, Wahlbeck et al. 2011) also reported interactions of ILs with Al_2O_3 and reveal that ILs makes a protective coating on the nanoparticle surface which helps to better the tribological properties. Pensado et al. (Pensado and Pádua 2011) also performed the molecular dynamic (MD) simulations of 2 nm RuNPs in ILs to see the solvation and stabilization of nanoparticles and found good contact with nanoparticles and anion and cation of ILs with nanoparticles solvated preferentially by the charged group of the IL ions. Those interactions of ILs with the nanoparticles surface may change the surface properties and help to make clusters of nanoparticles. Such clustering is prominent to agglomeration and sedimentation formation which make extra resistance to flowing heat to the NEILs. So the plausible mechanisms of degradation of NEILs are combinations of effect of thermophysical properties, particle-fluid interaction and clustering of nanoparticles which influences the formation of sedimentation. However, extensive theoretical and experimental studies are required to explain the exact cause.

The same natural convection behavior was observed for $[C_4mim][NTf_2]$ and spherical Al_2O_3 NEILs. The experimental results of the Rayleigh number and Nusselt number are presented in Fig. 5.13 (a) and (b) for AR=1 and 1.5 respectively.

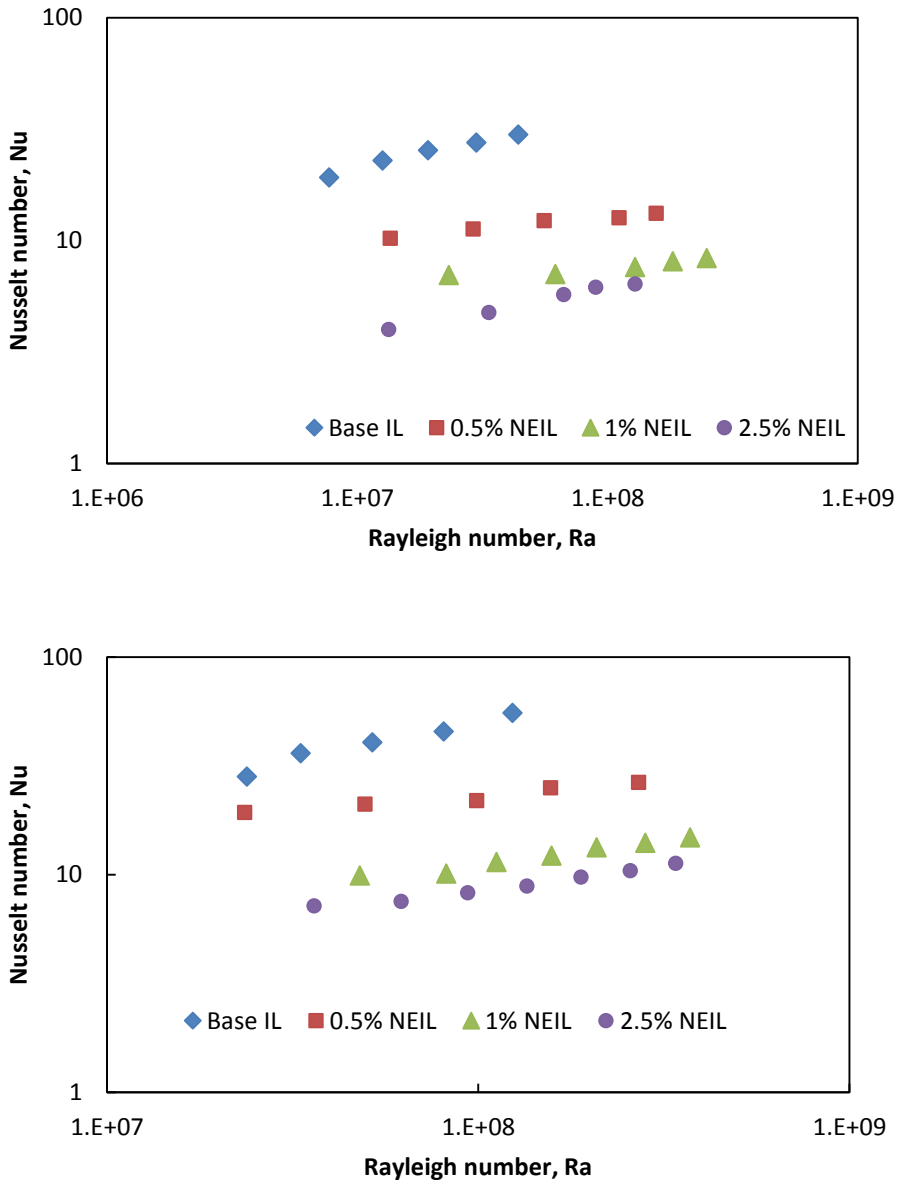

Figure 5.13 Natural convection results of [C_4mim][NTf_2] NEILs (a) AR=1 and (b) AR=1.5

5.5 Summary

The interest of ionic liquids and nanoparticle enhanced ionic liquids (NEILs) has been increasing in recent years due to increased needs for new heat transfer fluids. Natural convection heat transfer behavior is an important finding for any heat transfer fluids. Here, the natural convection study of four ILs and two NEILs has been performed

in a rectangular cavity heated from below at two different aspect ratios. The following conclusions can be drawn:

-The convective heat transfer coefficient of IL is lower than DI-water for the same heat input due to the higher viscous force of IL than DI-water and lower thermal conductivity. Nusselt number of IL is higher than DI-water at same experimental condition, which is also due to the lower thermal conductivity of IL. At the same condition, high aspect ratio has higher natural convection heat transfer compared to low aspect ratio.

-New correlation for Nusselt Number as a function of Rayleigh Number is proposed for ILs.

-The findings from this study will help to consider this natural convection behavior of ionic liquids for the design of passive solar collector storage tank where one would need to account for the natural convection heat transfer.

-The systematic degradation of natural convection heat transfer of both spherical and whiskers NEILs was observed for both aspect ratios. The whiskers NEILs had slightly higher heat transfer coefficient compared to the spherical NEILs. The relative change of effective thermophysical properties are not fully responsible for the degradation of the natural convection of NEILs. In addition to thermophysical properties, particle-fluid interaction and clustering of nanoparticles also play a role to degrade the natural convection heat transfer.

CHAPTER 6

FORCED CONVECTION OF ILS AND NEILS

6.1 Introduction

Ionic liquids and nanoparticle enhanced ionic liquids (NEILs) are considered as a heat transfer fluid (HTF) for the potential application in solar thermal collector. Forced convection is an important study to get the thermal performance of any HTF. ILs are being investigated by a number of researchers to explore different perspectives of the liquid; most of these researchers have concentrated on the thermophysical properties study; among those only a few studies were concentrated on thermal and transport properties (Jacquemin, Husson et al. 2006; Tokuda, Tsuzuki et al. 2006; Jacquemin, Husson et al. 2007; Kilaru, Baker et al. 2007; Wandschneider, Lehmann et al. 2008; Liu, Maginn et al. 2012). No study has been reported yet on high temperature and turbulent heat transfer performance of these ILs. To assess effectiveness of ILs in CSP plant, conjugate study of thermophysical properties and high temperature heat transfer performance is necessary.

In the present study, forced convection experiment of different ILs and NEILs at high temperatures were performed. Here, the forced convection study of $[C_4mim][NTf_2]$ and $[N_{4111}][NTf_2]$ ILs and NEILs forming $[C_4mim][NTf_2]$ IL and spherical Al_2O_3 nanoparticles in different concentration (0.5, 1.0, and 2.5 wt%) are presented.

6.2 Convective Heat transfer Coefficient of DI-Water

Before doing experiments with IL, the experimental system was tested with DI-water to evaluate the reliability of measurements. Fig.6.1 (a) and (b) shows the heat transfer behavior of DI-water with the axial distance at laminar $(Re < 2300)$ and turbulent $(Re > 2300)$ flow region. The experimental results were compared with the well-known Shah's correlation for laminar flows (Shah 1975) and Gnielinski equation for turbulent flow (Gnielinski 1975) at the constant heat flux boundary conditions:

Shah's equation for laminar flow:

$$Nu(x) = \begin{cases} 1.953\left(RePr\frac{D}{x}\right)^{\frac{1}{3}} & (RePr\frac{D}{x}) \geq 33.3 \\ 4.364 + 0.0722RePr\frac{D}{x} & (RePr\frac{D}{x}) < 33.3 \end{cases} \quad (6\text{-}1)$$

Gnielinski equation (Gnielinski 1975) for turbulent flow at a range of $<0.5 < Pr < 10^6$ and $2300 < Re < 5 \times 10^6$:

$$Nu = \frac{\left(\frac{f'}{8}\right)(Re-1000)Pr}{1.07+12.7\sqrt{\frac{f'}{8}}(Pr^{\frac{2}{3}}-1)} \quad (6\text{-}2)$$

where $Nu(x)$, Re, Pr are the Nusselt, Reynolds, and Prandtl number respectively which were defined as:

$$Nu(x) = \frac{h(x)D}{k_f}, \qquad Re = \frac{\rho u D}{\mu}, \quad Pr = \frac{\nu_f}{\alpha} \quad (6\text{-}3)$$

where $h(x)$ is the local heat transfer coefficient, D is the inner diameter of test section, k_f is the thermal conductivity of fluid, ρ is the fluid density, μ is the fluid viscosity, u is

the velocity of fluid, $\nu_f (= \frac{\mu}{\rho})$is the kinematic viscosity, $\alpha (= \frac{k_f}{\rho C_p})$ is the thermal diffusivity, and f is the friction factor which is given by:

$$f' = \frac{1}{\{1.82 log_{10}(Re) - 1.64\}^2} \tag{6-4}$$

All the fluid properties were evaluated at the average ($T_{av} = \frac{T_{in} + T_{out}}{2}$) of the inlet and outlet fluid temperature of the test section. It was clear from Fig.6.1(a) and 6.1(b) that there are reasonably good agreements between predicted and measured Nusselt number of DI-water over the Reynolds number range studied for laminar and turbulent flow region.

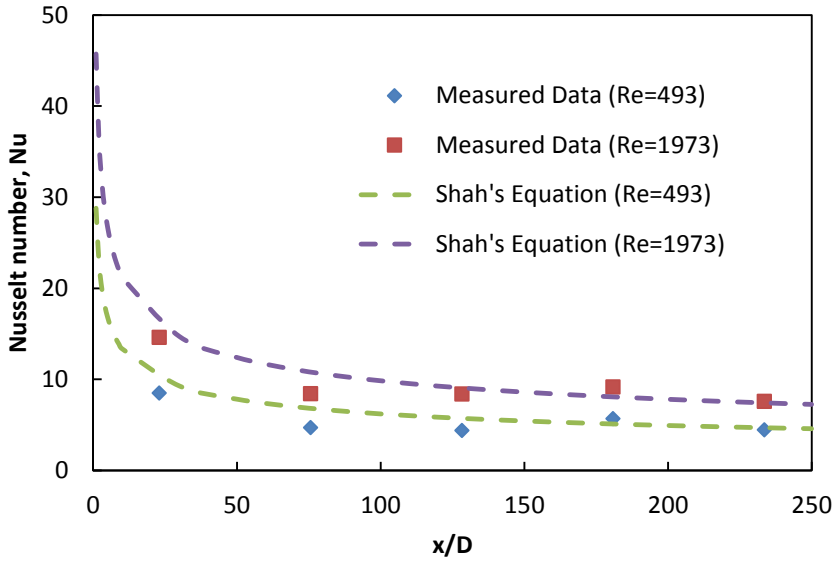

(a)

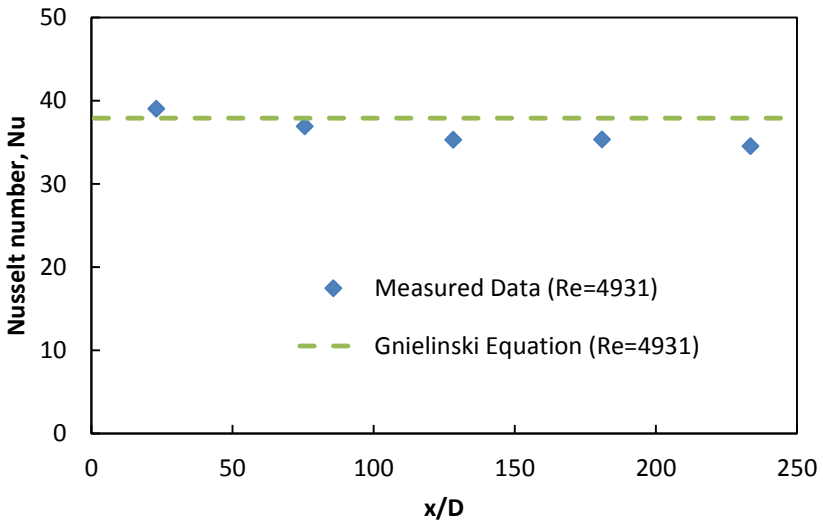

(b)

Figure 6.1 Comparison of the measurements with the (a) Shah's equation for laminar flow and (b) Gnielinski's equation for turbulent flow of DI water

6.3 Convective Heat Transfer of ILs

After gaining confidence with the experimental setup with DI-water, forced convection experiments were performed for $[C_4mim][NTf_2]$ and $[N_{4111}][NTf_2]$ ILs under laminar and turbulent flow conditions. First the forced convection results of $[N_{4111}][NTf_2]$ ILs are presented. Fig.6.2 is the typical surface and fluid temperature profile along the axial distance at two different Reynolds numbers. In the present study the fluid temperature was within 95-135^{o}C, which was also clear from the Fig.6.2 and temperature increases linearly along the axial distance due to constant heat flux condition. From Fig.6.2 it was also clear that turbulent flow temperature profile for surface and fluid has almost a constant rate increment from the beginning which was expected because in turbulent flow the entrance length is very small ($hydrodynamicentrylength = x_h \approx thermalentrylength = x_t \approx 10D$), whereas in the laminar flow the hydrodynamic

entrance length is $x_h = 0.05Re.D$ and thermal entrance length is $x_t = 0.05Re.Pr.D$ (Bejan and Kraus 2003); these behaviors are also discussed in the following sections. The schematic of development of flow through the pipe in laminar flow regime was shown in Fig. 6.3.

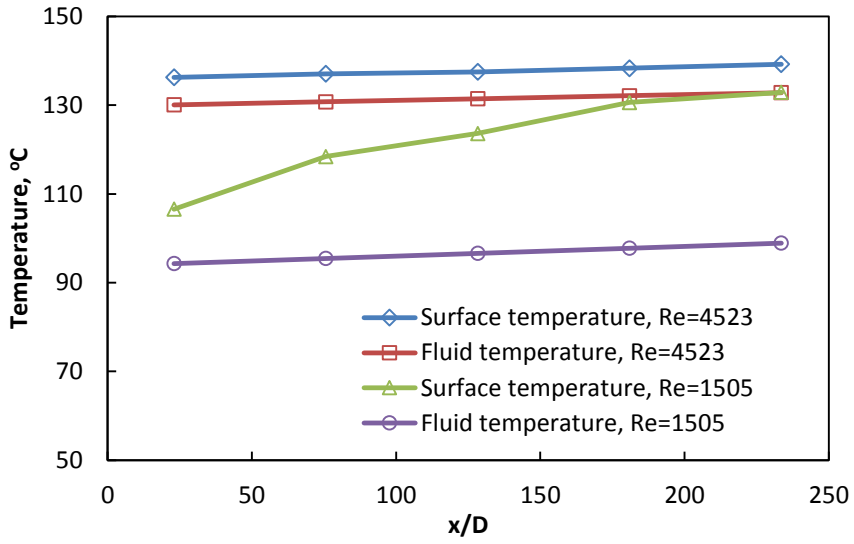

Figure 6.2 Typical temperature profile along the test section

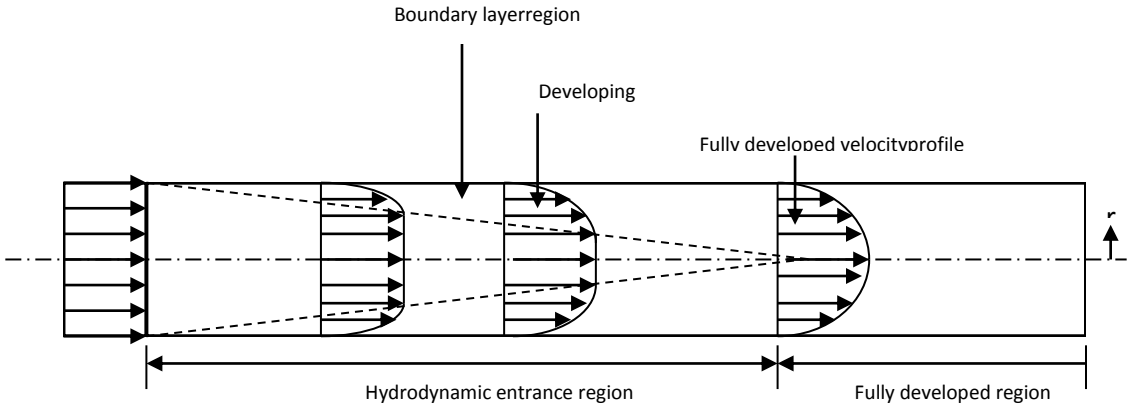

Figure 6.3 Schematic of development of boundary layer in a pipe flow in laminar flow regime

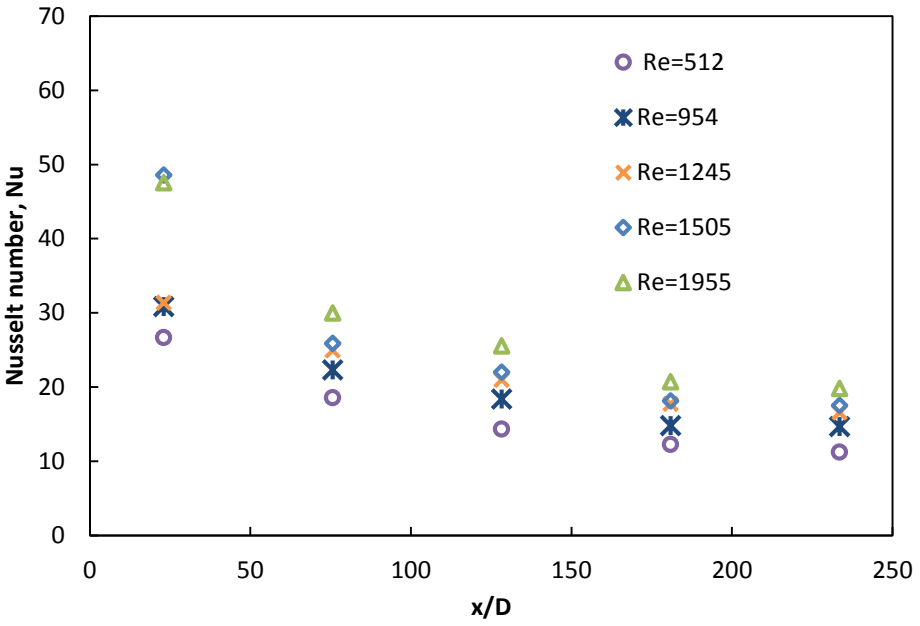

(a)

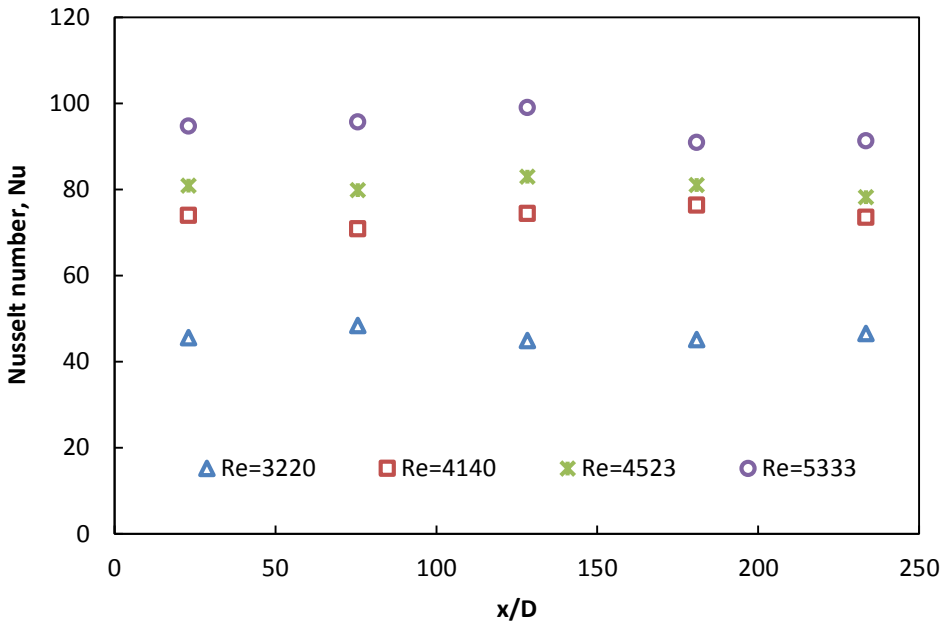

(b)

Figure 6.4 Heat transfer behavior of $[N_{4111}][NTf_2]$ (a) laminar (b) turbulent flow condition

Fig.6.4 (a) and (b) show the heat transfer behavior of $[N_{4111}][NTf_2]$ IL for different Reynolds number at laminar and turbulent flow region respectively. In laminar flow (Fig.6.4 (a)) for a certain Reynolds number, Nusselt number decreases along the axial distance due to entrance effect. Initially the thermal boundary layer thickness remains thin, then gradually increases the thickness up to hydrodynamically full development. Whereas in turbulent flow (Fig. 6.4 (b)) for a certain Reynolds number, Nusselt number remains almost constant along the axial distance since for turbulent flow the entrance effect is very low compared to laminar flow. The studied laminar Reynolds number ranges the hydrodynamic entrance length in terms of diameter varies from $x = 25D - 113D$. But the thermal entrance length in terms of diameter varies from $x = 3000D - 13560D$ which means the experiment was hydrodynamic developing and not thermally developing; this was clear from the Fig. 6.4(a).

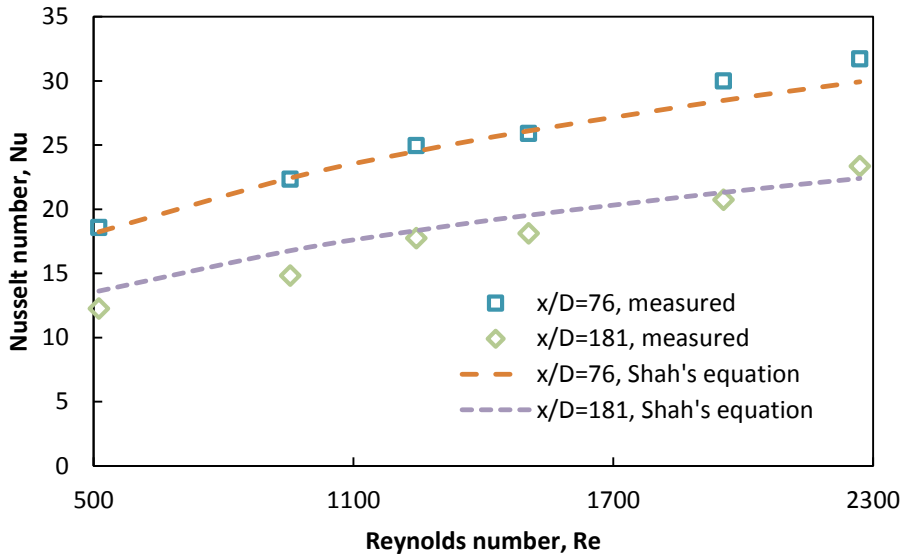

(a)

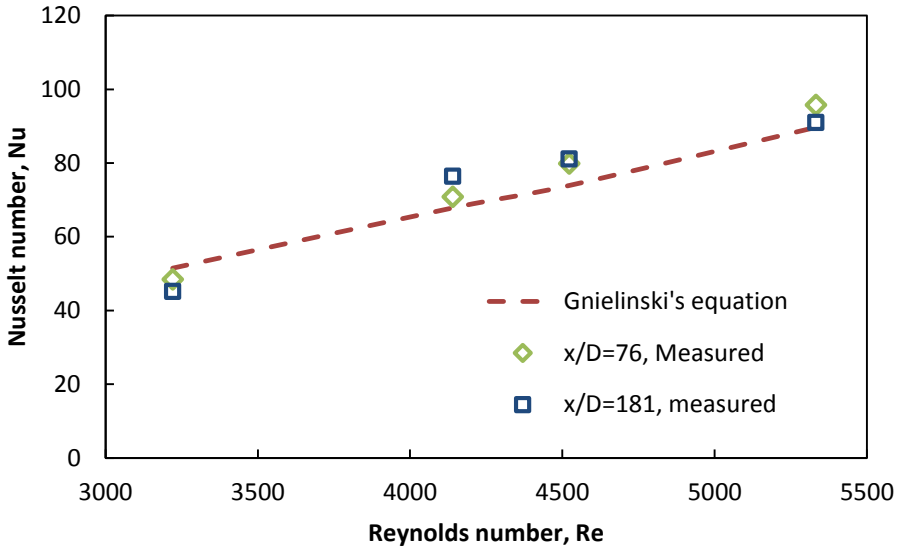

(b)

Figure 6.5 Experimental results and comparison with Shah's equation and Gnielinski equation for (a) laminar and (b) turbulent flow region respectively

At a certain point both for laminar and turbulent flow conditions Nusselt number increases with Reynolds number which was clear from Fig.6.5(a) and Fig.6.5(b). This is because as a result of the higher Reynolds number the boundary layer thickness becomes thinner, which increases the heat transfer coefficient. The experimental results were also compared with the predicted Shah's (Shah 1975) equation for laminar flow and Gnielinski's(Gnielinski 1975) equation for turbulent flow in Fig.6.5(a) and Fig.6.5(b) respectively. It can be seen that the experimental results were well predicted by the well-established equations for laminar and turbulent flow conditions, which is an important finding for ILs so that the well-established equations could be used to predict the heat transfer behavior of ILs at high temperature condition for solar thermal applications.

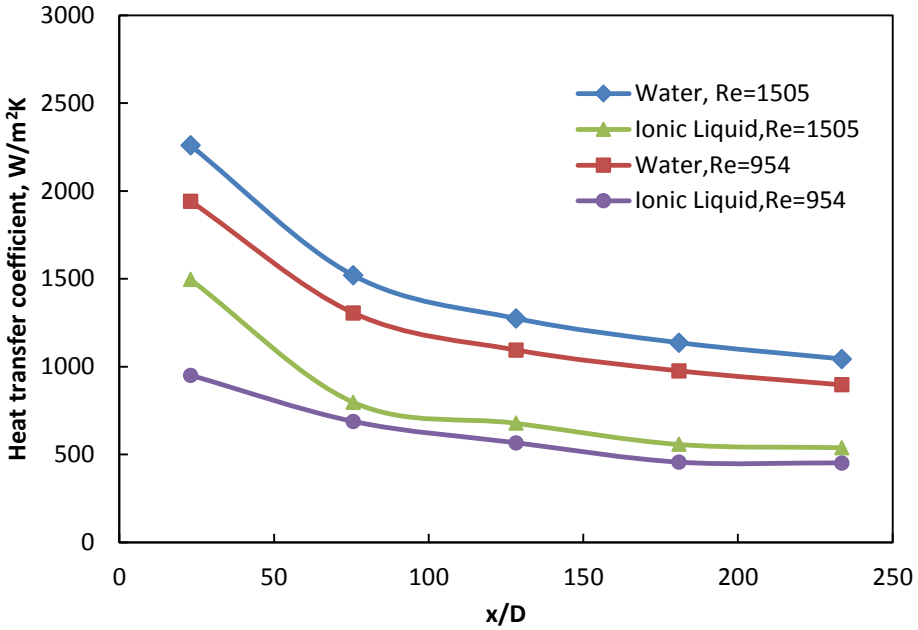

(a)

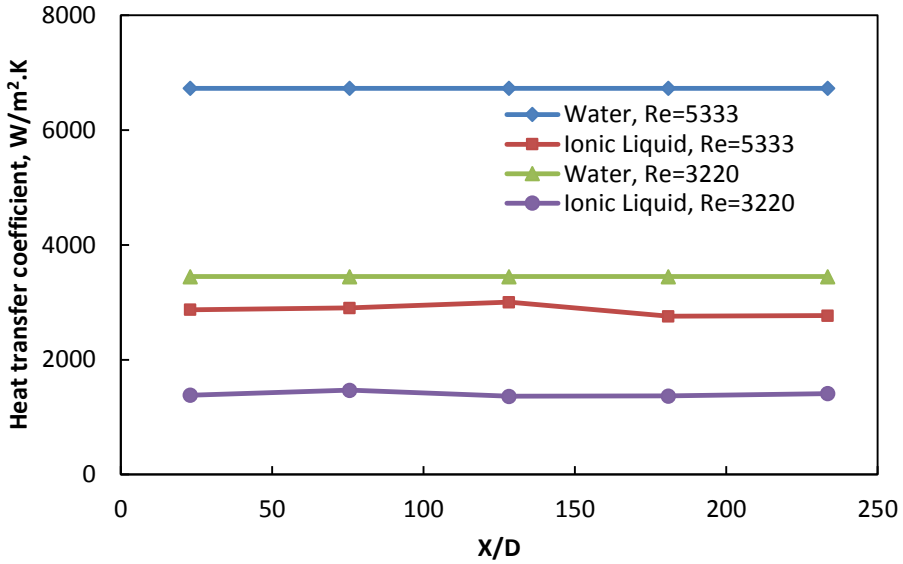

(b)

Figure 6.6 Heat transfer coefficient of ionic liquid and water as a function of axial distance; (a) laminar flow, (b) turbulent flow

Fig.6.6(a) and Fig.6.6(b) show the comparison of heat transfer coefficient of IL and DI-water for laminar and turbulent flow conditions respectively. It was clear that the

heat transfer coefficient of IL is much lower than the DI-water; this may be because of the lower thermal conductivity and higher viscosity of IL. The same lower heat transfer coefficient IL was observed by previous forced (Chen, He et al. 2008) and natural (Paul, Morshed et al. 2014) convection study of 1-butyl-3-methylimidazolium bis{(trifluoromethyl)sulfonyl}imide, $[C_4mim][NTf_2]$ IL. They studied the forced convection in laminar flow region at maximum Reynolds number 120 and lower operating temperature. In the solar thermal collector, the operating temperature of the fluid is high and the flow is in turbulent region. However, the Fig.6.7 shows that the Nusselt number of IL was much higher than the DI-water because thermal conductivity ratio of water to IL is approximately 5.62 (0.68/0.121) and the heat transfer coefficient ratio of water to IL in the middle of the test section (x/D=128) was approximately 1.88 (1278/678). That means by the Nusselt number of IL should be approximately 2.98 (5.62/1.88) times higher than DI-water, which was clear in Fig.6.7 where the Nusselt number of IL was 2.72 (22/8.09) times higher than the DI-water.

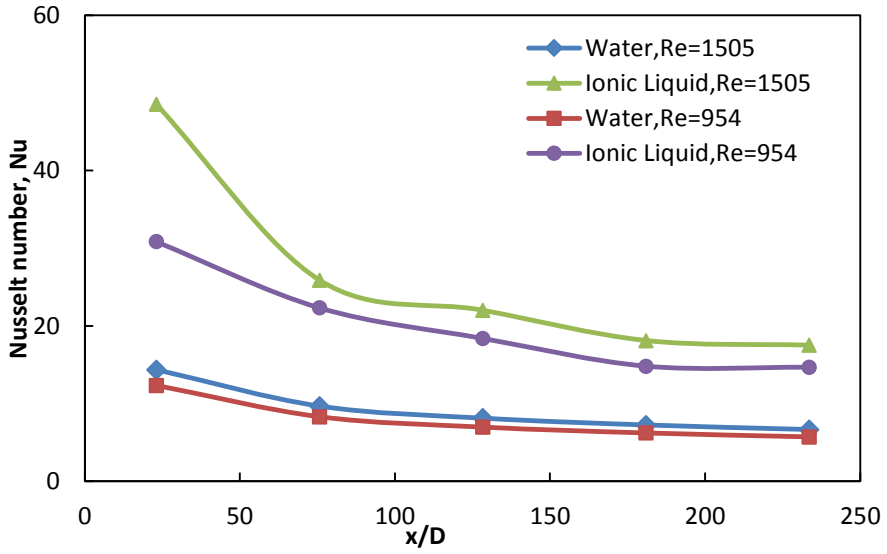

(a)

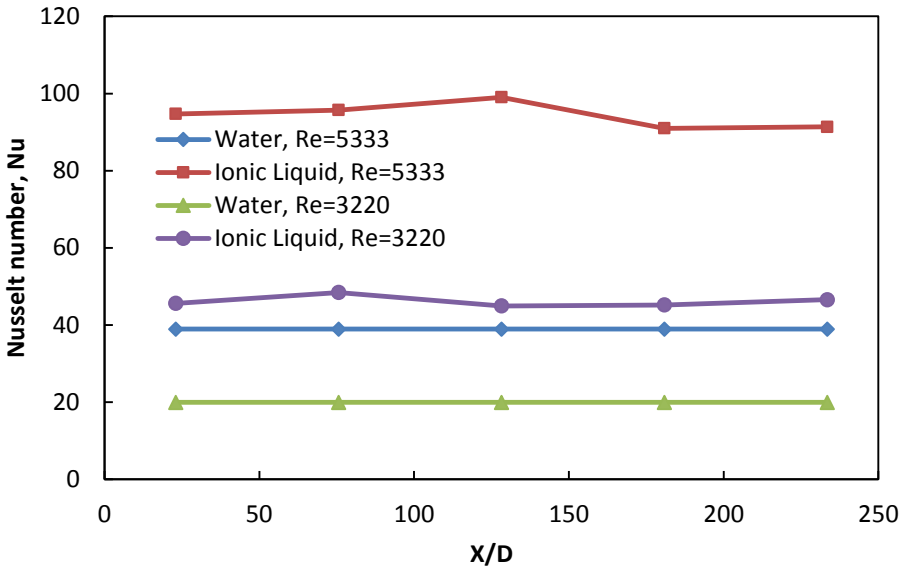

(b)

Figure 6.7 Nusselt number of ionic liquid and water as a function of axial distance (a) laminar (b) turbulent flow condition

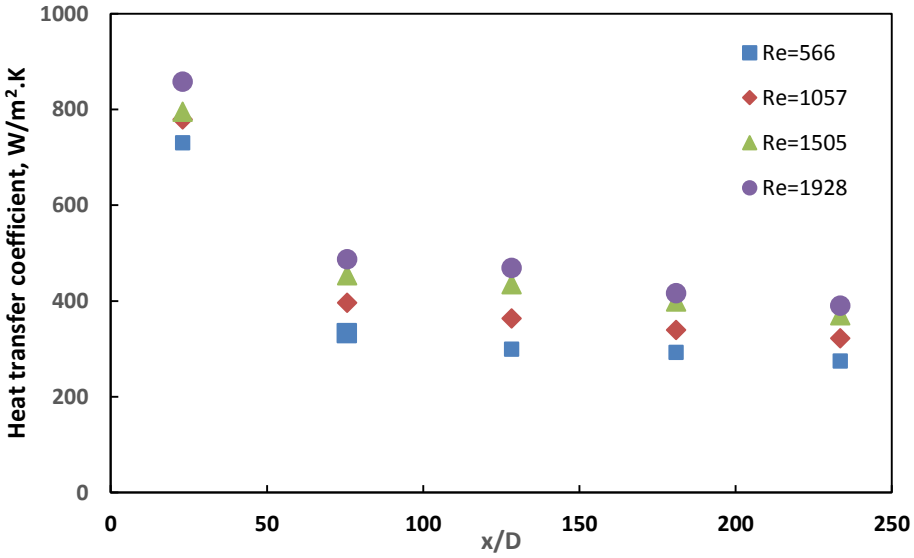

(a)

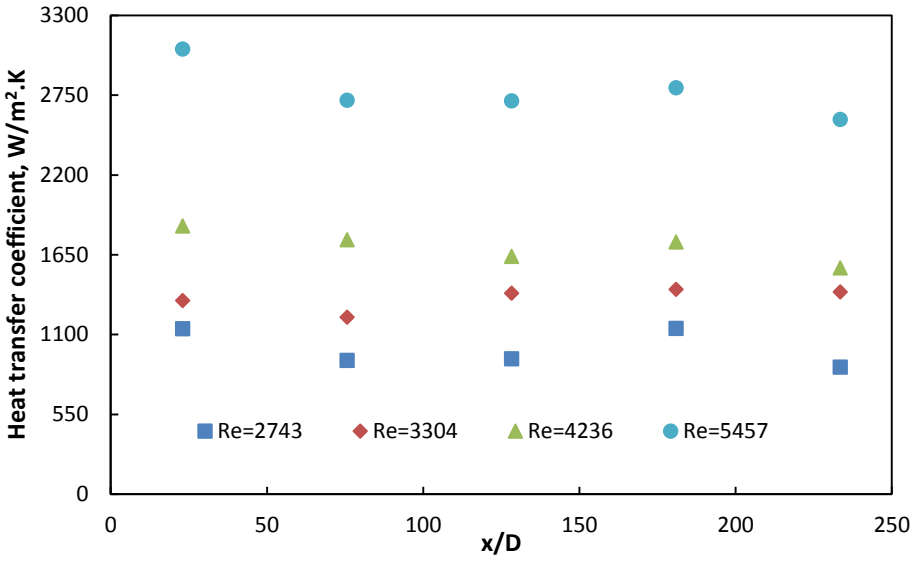

(b)

Figure 6.8 Heat transfer coefficient of [C_4mim][NTf_2] (a) laminar (b) turbulent flow condition

The same force convection behavior was observed for [C_4mim][NTf_2] IL. Fig.6.8 shows the heat transfer coefficient of [C_4mim][NTf_2] IL as a function of axial distance. It is clear that the heat transfer coefficient increases with Reynolds number. In laminar flow condition in Fig.6.7(a), heat transfer coefficient decreases along the axial distance and in turbulent flow condition in Fig.6.7(b), the heat transfer coefficient was almost the same along the axial distance.

6.4 Convective Heat Transfer of NEILs

Forced convection experiments were performed for base [C_4mim][NTf_2] IL and spherical Al_2O_3 NEILs in laminar and turbulent flow condition. Fig.6.9 presents the typical temperature profile of the fluid and tube surface of the test section along the axial

distance and it shows increasing fluid temperature with axial distance because of constant wall heat flux condition.

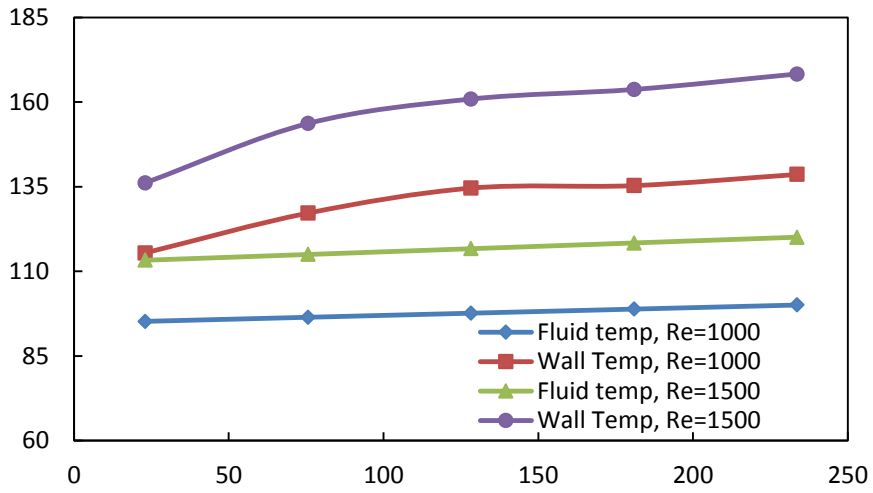

Figure 6.9 Temperature profile along the test section of 1 wt% NEIL

The local heat transfer coefficient as a function of axial distance of base IL and NEILs at laminar ($Re = 1500 \pm 50$) and turbulent ($Re = 4500 \pm 50$) flow regimes are presented in Fig.6.10(a) and (b). Due to the viscosity variation of base IL and NEILs the maximum variation in Reynolds number was ±50. Because of the much higher shear viscosity of 2.5 wt% NEIL, turbulent flow could not be achieved. It is clear from Fig. 6.10(a) and (b) that the NEILs has significantly higher heat transfer coefficient than base IL and higher concentration NEILs has more enhancement. As of Fig.6.10(a) at point 2 (x/D=75.65) the enhancement of heat transfer coefficients are ~15%, 28%, and 31% for 0.5, 1, and 2.5 wt% NEILs respectively. For turbulent flow in Fig.6.10(b) at point 2 (x/D=75.65) the enhancement of heat transfer coefficients are ~26% and 29% for 0.5 and 1 wt% NEILs respectively. In the laminar flow regime at a certain concentration of NEIL the enhancement of heat transfer coefficient is more in the entrance region; for example,

1 wt% NEIL the enhancement of heat transfer coefficient is varied from 27.5% (x/D=23.02) to 16.4% (x/D=233.55). But in the turbulent regime the enhancement of heat transfer coefficient does not follow any imperative rule with the axial distance. The higher enhancement is observed in the turbulent flow regime compared to the laminar flow regime. For example, at $Re = 4500$ the average heat transfer enhancement of 1 wt% NEIL is ~31% and at $Re = 1500$ the average heat transfer enhancement of same concentration NEIL is ~19%. The heat transfer enhancement rate is not linear with the concentration of nanoparticles. The enhancement of 0.5 wt% and 1 wt% NEILs shows almost the same rate of enhancement, but at 2.5 wt% NEILs it does not enhance too much compared to the 0.5 and 1 wt% NEILs. At a certain concentration and Reynolds number in the laminar regime, the heat transfer coefficient decreases with the axial distance which is clear in Fig.6.10(a). This is because of the entrance effect; initially the boundary layer thickness is lower and after the fully developed boundary layer the heat transfer coefficient become constant.

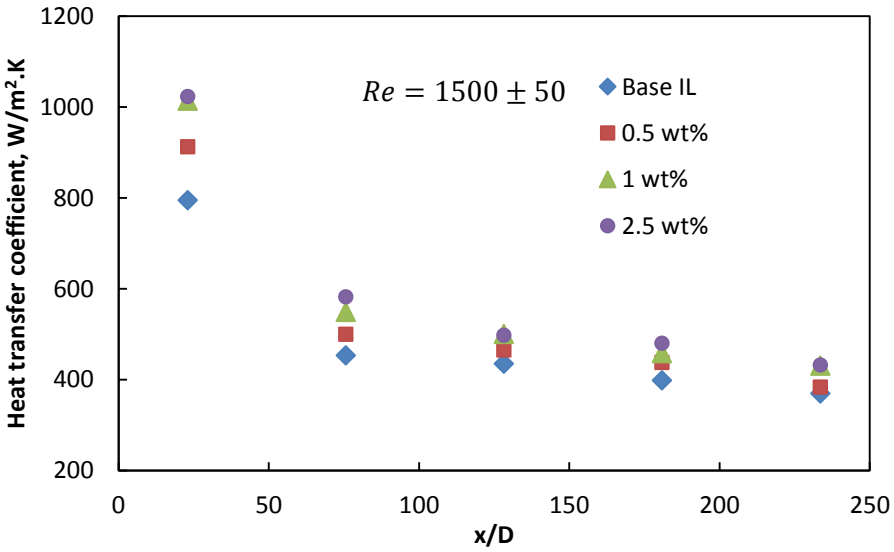

(a)

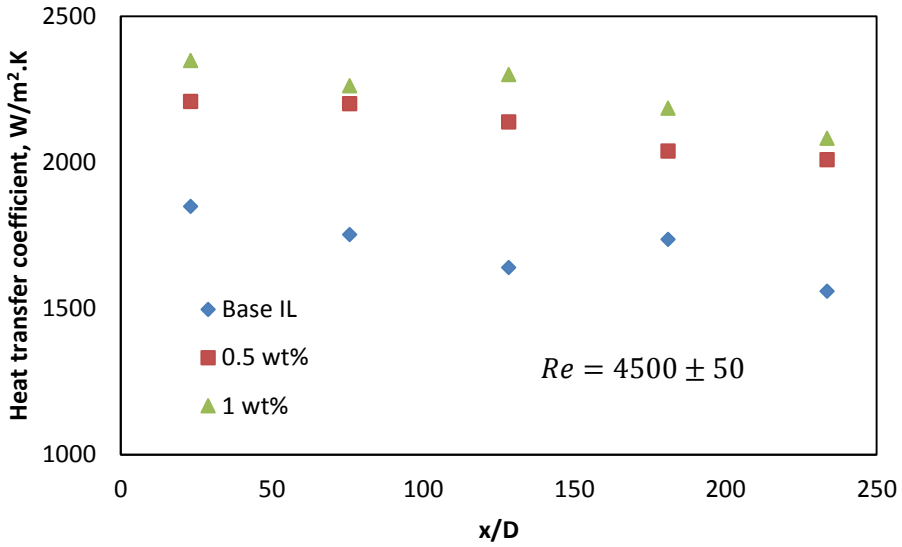

(b)

Figure 6.10 Heat transfer coefficient of base IL and NEILs as a function of axial distance (a) laminar flow and (b) turbulent flow

The enhancement of heat transfer coefficient similar behavior was also reported by other researchers, where forced convection experiments were carried out for Al_2O_3-water nanofluids at laminar (Wen and Ding 2004; Zeinali Heris, Nasr Esfahany et al. 2007; Lai, Phelan et al. 2008) and turbulent (Torii 2010) flow regimes. Wen et al. (Wen and Ding 2004) reported up to ~47% enhanced heat transfer of 1.6 vol% Al_2O_3-water nanofluids. Lai et al. (Lai, Phelan et al. 2008) investigated forced convection of Al_2O_3-water nanofluids in a 1.02mm diameter tube and reported enhanced heat transfer coefficient of nanofluids. Heris et al. (Zeinali Heris, Nasr Esfahany et al. 2007) reported enhanced heat transfer coefficient of Al_2O_3-water nanofluids performing forced convection in a circular tube with the constant temperature boundary condition. Torii (Torii 2010) studied the forced convection of diamond, CuO, and Al_2O_3 nanofluids in the turbulent flow regime and reported 9.8%, 6.6%, and 5.4% enhancement of Nusselt number respectively for 1vol% nanofluids at $Re = 6000 \pm 100$.

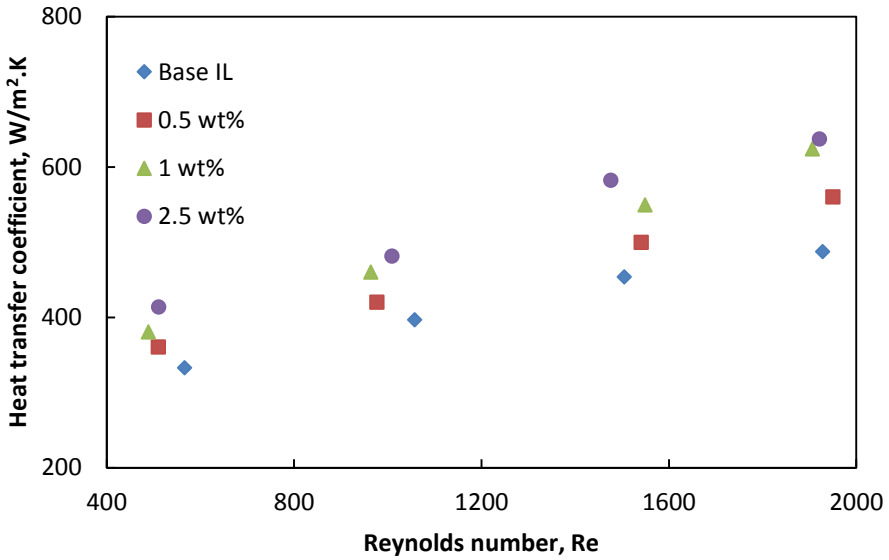

(a)

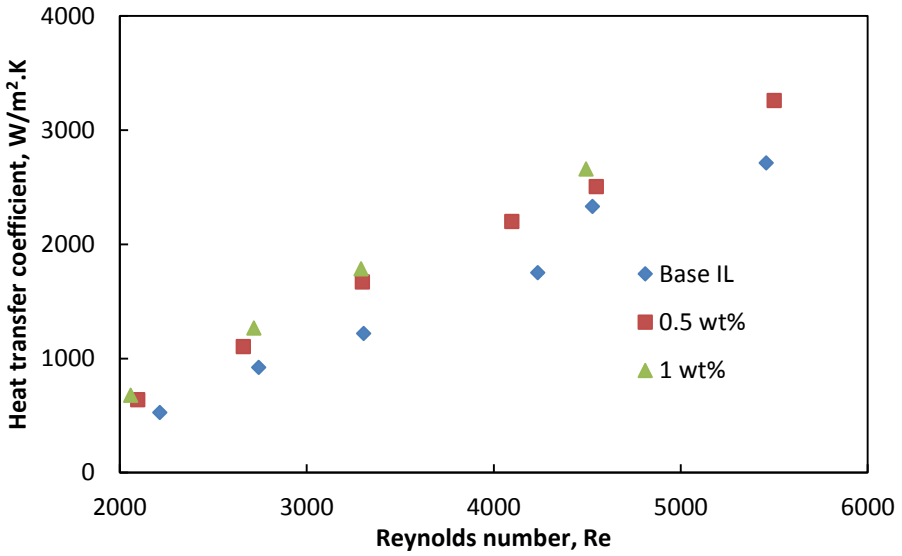

(b)

Figure 6.11 Convective heat transfer coefficient of different concentration NEILs as a function of Reynolds number ($x/D = 75.65$), (a) Laminar flows and (b) Turbulent flows.

The above enhancements of convective heat transfer coefficient depending on the nanoparticle concentration, Reynolds number, and axial distance are not fully dependent

on the thermal conductivity enhancement. In an example the maximum thermal conductivity enhancement of 2.5 wt% NEIL was found ~11% which is much less than the convective heat transfer enhancement at the same concentration. The local convective heat transfer coefficient h can be defined approximately k_{NEIL}/δ_t, where δ_t is the thermal boundary layer thickness (Incropera, Lavine et al. 2011). It is clear from the correlation of heat transfer coefficient that the enhanced heat transfer coefficient of NEILs depends on either the thermal conductivity enhancement or the decrease in thermal boundary layers. One of the reasons may be the dynamic effect of the thermal conductivity. The experimental local heat transfer coefficients are measured based on the static thermal conductivity measurements. But in the flow condition through a circular pipe, significant shear exists in the NEILs. NEILs also shows shear thinning behavior which may be the result of higher effective thermal conductivity of NEILs at flow conditions compared to the static conditions. The enhanced thermal conductivity at dynamic conditions were observed by Ahuja (Ahuja 1975; Ahuja 1975) for saline/polystyrene latex suspension who reported that enhancement of thermal conduction was followed by the particle rotation. Shin et al. (Shin and Lee 2000) also measured the effective thermal conductivity of micro-particles suspended at rotating couette flow conditions and found enhanced thermal conductivity.

In the circular pipe flow, the flow became hydrodynamically and thermally fully developed at $(x/D)_h \geq (0.05.Re)$ and $(x/D)_t \geq (0.05.Re.\mathrm{Pr})$ respectively (Bejan and Kraus 2003). In the present experiment, the flow is not thermally fully developed because of high Prandtl number of ILs and NEILs. The inclusion of nanoparticles affects the boundary layer development as well as the heat transfer coefficient. NEILs has greater

thermal developing length compared to base IL and it increases with the nanoparticles concentration which is clear in Fig.6.10(a). The higher thermal developing length of NEILs means smaller thermal boundary layer thickness at a certain location, which may lead to the enhanced heat transfer coefficient of NEILs. Particle migration, viscosity, and shear rate gradient also may have an effect on the boundary layer development (Ding and Wen 2005; Wen and Ding 2005;Ding, Chen et al. 2010). In this mechanism, particles have the tendency to concentrate in the center of the pipe, which leads to the decrease in viscosity near the wall as well as lower boundary layer thickness. Ding et al. (Ding and Wen 2005) and Wen et al. (Wen and Ding 2005) formulated a theoretical model to observe the particle migration flowing through the circular pipe and minichannels respectively and reported non-uniformity particle concentration, which has consequence in higher heat transfer. Based on the shear thinning behavior of NEILs as shown, the enhanced heat transfer coefficient of NEILs also may be the result of particle migration in flow conditions. Aggregation of nanoparticles in base liquid is a common phenomenon which increases the effective thermal conductivity (Keblinski, Phillpot et al. 2002) and leads to the enhancement of heat transfer coefficient. The TEM image of NEIL shows aggregation of primary particles which also is promising to higher heat transfer.

The previous studies of flow and possible mechanism of the enhancements are based on the studies of traditional nanofluids. But the exact mechanism for enhanced heat transfer coefficient of NEILs is unclear. Pensado et al. (Pensado and Pádua 2011) performed molecular dynamic simulations for salvation and stabilization of nanofluids containing ruthenium nanoparticle in ILs and reported that nanoparticles are in contact with the anion and cation of ILs. Carper et al. (Carper, Wahlbeck et al. 2011)

theoretically modeled IL and Al_2O_3 surfaces and reported complex interaction formation of IL with Al–O surface. The high-quality contact of the IL with nanoparticles may be another plausible reason for the thermal conductivity and heat transfer coefficient enhancement in flow condition (Keblinski, Eastman et al. 2005).

Fig.6.11(a) and (b) show the heat transfer coefficient base IL and NEILs as a function of Reynolds number at laminar and turbulent flow regime respectively at x/D=75.65. In both cases the heat transfer coefficient increases with the Reynolds number. This observation could be explained by the boundary layer thickness. At high Reynolds number boundary layer becomes thinner and shear stress increases within the boundary layer. This alters the migration behavior of the nanoparticles, which in turn increases the heat transfer coefficient. The higher enhancement of high concentration NEILs is also clear from the Fig.6.11(a) and (b).

6.5 Nusselt Number Correlation for NEILs

The forced convection behavior of NEILs under laminar flow region could not be expressed by the conventional equation. From the experimental results it is clear that the thermal performance of NEILs are functions of Reynolds number, Prandtl number, axial distance, and nanoparticle concentration. In general the Nusselt number can be expressed as (Asirvatham 2009):

$$Nu_{NEIL} = f\left(Re, Pr, \frac{k_{NEIL}}{k_{BL}}, \frac{(\rho c_p)_{NEIL}}{(\rho c_p)_{BL}}, \varphi, dimensions\ and\ shape\ of\ particles\right) \qquad (6\text{-}5)$$

For the present data a multi variable linear regression analysis was applied to find the Nusselt number correlation. The Nusselt number correlation was expressed as:

$$Nu_{NEIL} = c_1 \varphi^a Re^b Pr^c (\frac{D}{x})^d \quad (6\text{-}6)$$

where c_1, a, b, c, and d are the unknown constants. Taking the natural logarithm in the both side of equation (6-6)

$$\ln(Nu_{NEIL}) = \ln c_1 + a \ln(\varphi) + b \ln(Re) + c \ln(\mathrm{Pr}) + d \ln(\frac{D}{x}) \quad (6\text{-}7)$$

$$P = Q + a\,R + b\,S + c\,T + d\,U \quad (6\text{-}8)$$

where $P = \ln(Nu_{NEIL})$, $Q = \ln c_1$, $R = \ln(\varphi)$, $S = \ln(Re)$, $T = \ln(Pr)$, $U = \ln(\frac{D}{x})$

The Nusselt number values of corresponding volume concentration, Reynolds number, Prandtl number, and axial distance were converted to logarithm and inserted in equation deviation equation (6-9) and solve for the constants.

$$E = (P_1 - Q - aR_1 - bS_1 - cT_1 - dU_1)^2 + (P_2 - Q - aR_2 - bS_2 - cT_2 - dU_2)^2 + \cdots (P_n - Q - aR_n - bS_n - cT_n - dU_n)^2 \quad (6\text{-}9)$$

The constants are determined by the partial derivation of equation (6-9) with respect to Q, c_1, a, b, c, and d:

$$\frac{\partial E}{\partial Q} = 0 \qquad \frac{\partial E}{\partial a} = 0 \qquad \frac{\partial E}{\partial b} = 0 \qquad \frac{\partial E}{\partial c} = 0 \qquad \frac{\partial E}{\partial d} = 0 \quad (6\text{-}10)$$

Finally, the constants are $c_1 = 30.768$, $a = 0.1135$, $b = 0.3378$, $c = -0.136$, and $d = 0.3713$ and the equation (6-6) can be represented as:

$$Nu_{NEIL} = 30.768 \varphi^{0.1135} Re^{0.3378} Pr^{-0.136} (\frac{D}{x})^{0.3713} \quad (6\text{-}11)$$

This equation is valid for laminar flow condition $Re < 2300$ and nanoparticle concentration up to 2.5 wt%. Fig.6.12(a-c) shows that the comparison of the experimental and predicted results for 0.5, 1.0, and 2.5 wt% NEILs at $Re = 1950$ and it is clear that the experimental results were predicted well by the above correlation. Also the R^2 value for the expression with respect to the experimental measurements is 0.948.

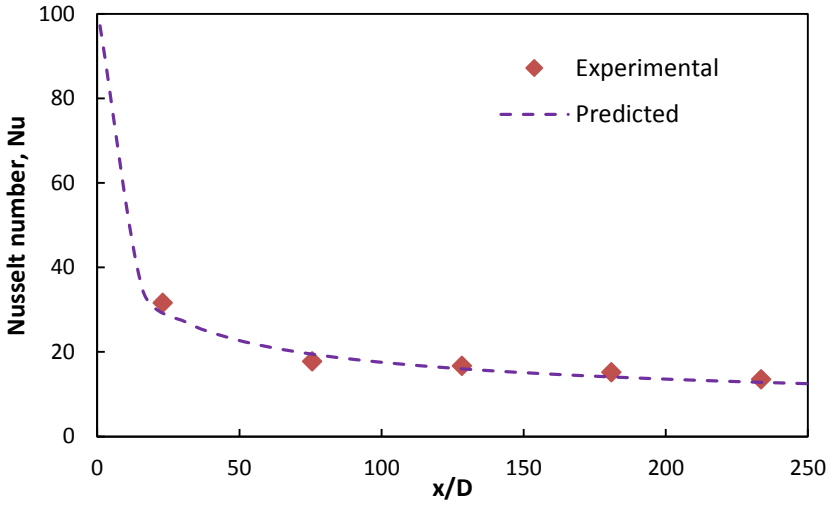

(a)

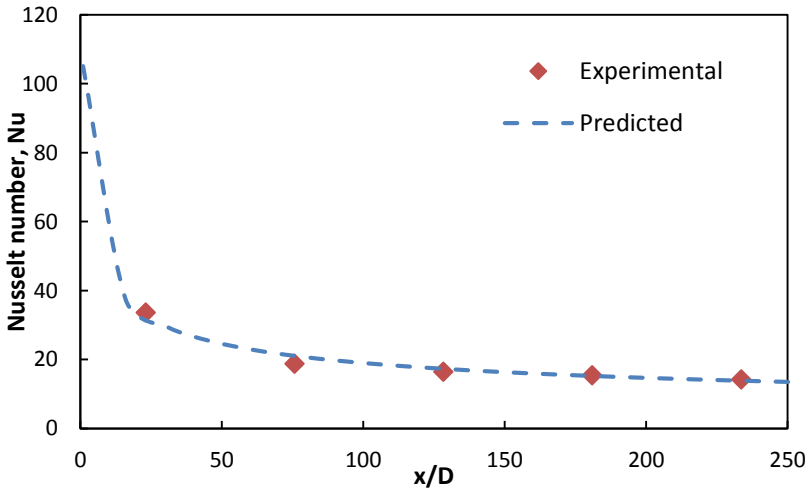

(b)

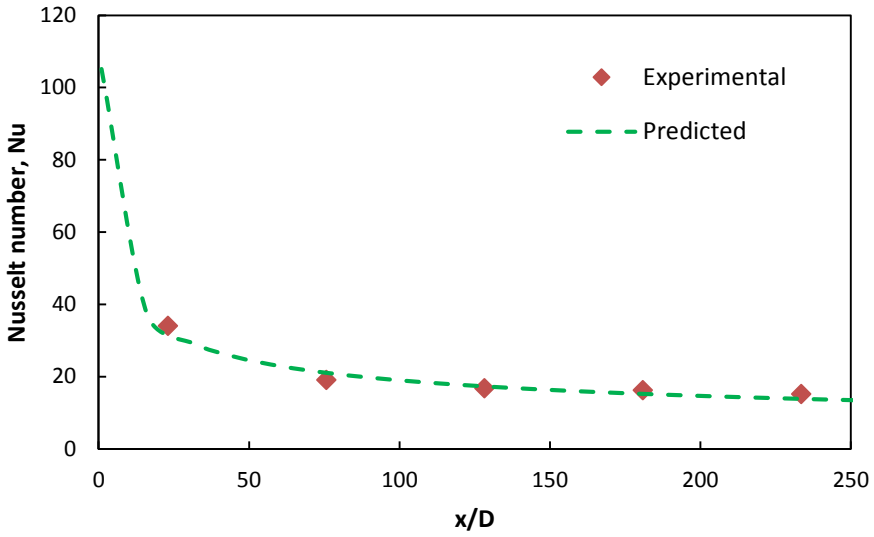

(c)

Figure 6.12 Nusselt number as a function of axial distance at Re=1950 for (a) 0.5 wt%, (b) 1.0 wt%, and (c) 2.5 wt% NEILs

6.6 Summary

Forced convection experiments were performed with $[N_{4111}][NTf_2]$ and $[C_4mim][NTf_2]$ ionic liquids and $[C_4mim][NTf_2]$ NEILs under laminar and turbulent flow conditions. From the experimental results the following conclusions can be drawn:

-Laminar convection behavior shows that the flow is hydrodynamically developed, but not thermally developed, due to high viscosity and low thermal conductivity of ionic liquid. In turbulent condition the flow was fully developed because there was no entrance effect observed. Heat transfer behavior well correlates with the Shah's and Gnielinski's equations for laminar and turbulent flow conditions respectively. The finding of this experiment is useful for the assessment of ionic liquid in solar thermal collector for high

temperature applications and heat transfer behavior could be predicted by the well-established equations.

-Heat transfer coefficient is higher for the NEILs compared to the base IL. The enhancement of heat transfer coefficient is much higher than the thermal conductivity enhancement depending on the nanoparticle concentration. In a particular concentration and Reynolds number, enhancement of convective heat transfer is more in the entrance region. Also turbulent flow regime shows higher enhancement compared to the laminar flow. The enhancement in heat transfer coefficient may be due to the enhanced thermal conductivity and particle migration behavior in the boundary layer.

-The experimental results of this study will assist to understand the flow behavior and thermal performance of NEILs. The enhanced thermal performance of NEILs will help to develop energy efficient HTF for the next generation CSP system. However, the more specific mechanism of the heat transfer enhancement of NEILs and nanoparticles size and shape effect needs to be explored. The future research would look at the effect of particle morphology on thermal performance of NEILs and find a specific particle size and shape for maximum enhancement.

CHAPTER 7

NUMERICAL ANALYSIS OF ILS AND NEILS

7.1 Introduction

Nowadays numerical simulation has become an important way for many engineering analyses to predict the experimental results and extend the prediction with varying different parameters. This subsequently reduces the number of complex experiments as well as cost of experiments. There are a lot of numerical studies of natural and forced convection of conventional water or ethylene glycol based nanofluids. Khanafer et al. (Khanafer, Vafai et al. 2003) at first studied numerically the natural convection of nanofluids in a two dimensional enclosure and reported enhanced heat transfer of nanofluids compare to base fluid. Hwang et al. (Hwang, Lee et al. 2007) numerically studied the natural convection of Al_2O_3 nanofluids and reported decreased Rayleigh number with increasing nanoparticle volume fraction. Choi et al. (Choi, Kim et al. 2014) reported the deterioration of natural convection of CuO-water nanofluids which correlates well with the experimental results. Rashmi et al. (Rashmi, Ismail et al. 2011) studied numerically the natural convection heat transfer of Al_2O_3-water nanofluids in a cavity heated by side wall which was found consistent with the experimental results of Putra et al. (Putra, Roetzel et al. 2003). Numerical and experimental studies of nanofluids natural convection are still paradoxical. But the forced convection numerical studies of nanofluids are consistent with the experimental studies. All of the literatures found

enhanced heat transfer coefficient of nanofluids compared to base fluid and heat transfer increases with nanoparticle concentration. Bianco et al. (Bianco, Chiacchio et al. 2009; Bianco, Manca et al. 2010; Rashmi, Khalid et al. 2013) numerically studied the forced convection of water-Al_2O_3 in a circular tube with single and two phase method and found higher enhancement of heat transfer coefficient in the temperature dependent model. Namburu et al. (Namburu, Das et al. 2009) numerically investigated the turbulent flow behavior of nanofluids containing CuO, Al_2O_3 and SiO_2 nanoparticles and ethylene glycol-water mixture. They reported maximum 35% enhancement of heat transfer coefficient of 6 vol% CuO nanofluids and their numerical results well correlate with the established equation. Davarnejad et al. (Davarnejad, Barati et al. 2013) performed the CFD analysis of Al_2O_3-water nanofluids in a circular tube in laminar flow region with two different particle shapes and found the highest heat transfer enhancement for 2.5 vol% nanofluids with smaller particle size.

In the present chapter of the dissertation, two-dimensional numerical analysis of natural and forced convection heat transfer of ionic liquids (ILs) and nanoparticle enhanced ionic liquids (NEILs) by using commercially available Computational Fluid Dynamics (CFD) package, FLUENT, are presented. For natural convection analysis N-butyl-N-methylpyrrolidiniumbis{trifluoromethyl)sulfonyl} imide ($[C_4mpyrr][NTf_2]$) IL and for forced convection 1-butyl-3-methylimidazolium bis{(trifluoromethyl)sulfonyl} imide ($[C_4mim][NTf_2]$) IL was considered. The thermophysical properties of ILs and NEILs were used from the experimental results presented in chapter 4. Numerical results of natural and forced convection were compared with the experimental results presented

in chapter 5 and chapter 6 respectively. There were some parametric studies also performed using the natural and forced convection model.

7.2 Geometry of Natural Convection

Numerical simulations of natural convection study of ILs and NEILs are straight forward in laminar region. The numerical simulation was performed in three enclosures with different aspect ratios (AR-0.5, 1.0, and 1.5) and the dimension of the enclosures are 50×50×25 mm, 50×50×50 mm, and 50×50×75 mm (length×width×height) which are the same as the experimental geometrical configuration. The geometry of the natural convection numerical enclosure is shown in Fig.7.1. The natural convection enclosure geometry was generated in GAMBIT 2.4.6 (Gambit 2007) and there were 12500 (500×250), 250000 (500×500), and 375000 (500×750) mesh elements for AR-0.5, 1.0, and 1.5 respectively.

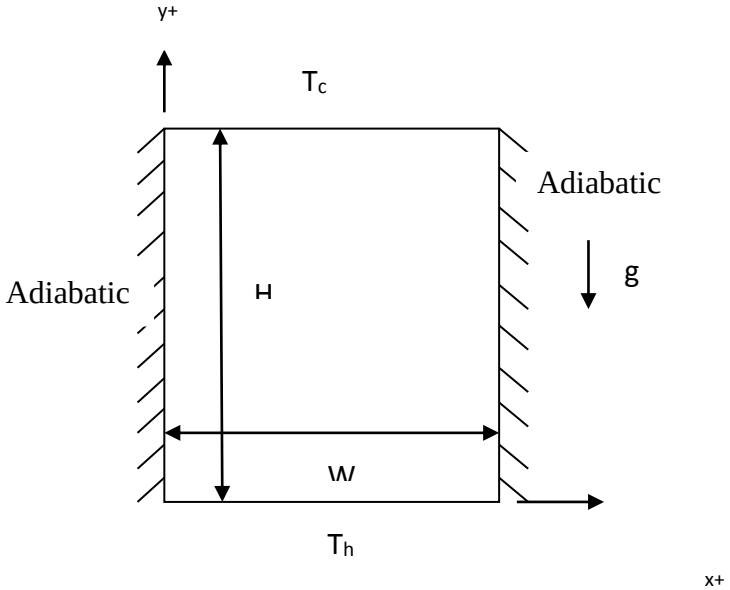

(a)

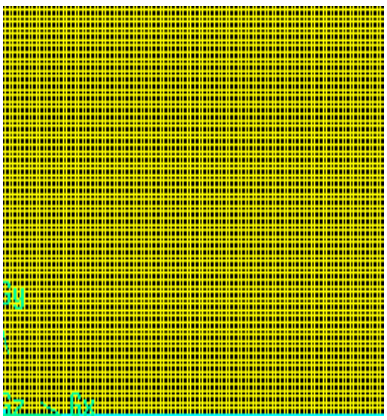

(b)

Figure 7.1(a) Schematic and coordination of system of natural convection configuration (b) The uniform grid of the natural convection enclosure

7.3 Boundary Condition of Natural Convection

The boundary conditions of the numerical simulation are simple bottom wall as hot surface with constant temperature, top wall as cold surface with constant temperature, and other walls (left and right) are at adiabatic condition. Also the no slip boundary condition of the all wall was considered. The enclosures are filled with base ILs and NEILs, and NEILs is considered as single fluid with temperature dependent thermophysical properties.

7.4 Simulation Methodology of Natural Convection

The numerical problem was solved by using two-dimensional ANSYS Fluent CFD program (Fluent 2011). NEILs is the combination of ILs and nanoparticles, and here the NEILs was considered as a single fluid with thermal equilibrium of nanoparticles and ILs. Also no relative velocity between nanoparticles and ILs was considered. The governing equations with single phase approximation are as follows:

Continuity equation:

$$\frac{\partial \rho}{\partial t} + \nabla.\left(\rho \vec{V}\right) = 0 \tag{7-1}$$

Momentum equation:

$$\frac{\partial \rho V}{\partial t} + \nabla.\left(\vec{V}.\vec{V}\right) = -\nabla P + \mu \nabla^2 V - \rho g \beta (T - T_c) \tag{7-2}$$

Energy equation:

$$\frac{\partial T}{\partial t} + V.\nabla \mathrm{T} = \frac{\partial}{\partial \mathrm{x}}\left(\frac{k}{\rho C_p}\frac{\partial T}{\partial t}\right) + \frac{\partial}{\partial \mathrm{y}}\left(\frac{k}{\rho C_p}\frac{\partial T}{\partial t}\right) \tag{7-3}$$

The CFD program solves the governing equations by converting those into algebraic equations with control volume theory technique. The laminar viscous model was used with SIMPLE scheme, Green-Gauss Cell Based gradient, and the convergence criteria of the residuals of governing equation variables are 1×10^{-6}. In the pressure and velocity coupling PRESTO was selected as pressure. For momentum and energy equation Second Order Upwind was selected for higher accuracy. All of the temperature dependent thermophysical properties were provided in the materials section. From the applied heat in the bottom wall the total surface wall heat flux was computed by using area-weighted average surface integrals. The natural convection heat transfer coefficient was calculated by using heat flux and temperature difference between hot and cold walls:

$$h = \frac{q^{"}}{(T_h - T_c)} \tag{7-4}$$

where h is the heat transfer coefficient, $q^{"}$ is the heat flux computed from the simulation, T_h and T_c are the temperature of the hot and cold surface respectively. The dimensionless

Nusselt (Nu), Prandtl (Pr), Grashof (Gr), and Rayleigh (Ra) number are calculated from the following equations:

$$Nu = \frac{hH}{k_f}; \qquad Pr = \frac{\nu_f}{\alpha}; \quad Gr = \frac{g\beta\Delta T H^3}{\nu_f^2} \tag{7-5}$$

$$Ra = Gr.Pr \tag{7-6}$$

where H is the height of the enclosure, k_f is the thermal conductivity, ν_f is the kinematic viscosity, $\alpha(=\frac{k_f}{\rho C_p})$ is the thermal diffusivity, β is the volume expansion coefficient, ρ is the density, C_p is the heat capacity of fluid, ΔT is the temperature difference between hot and cold surface fluid, g is the gravitational acceleration. All the fluid properties were evaluated at the average ($T_{av} = \frac{T_c+T_h}{2}$) of the heated and the cooled surface temperature.

7.5 Results and Discussion of Natural Convection

Before performingsimulations with ILs and NEILs, a grid independence study was carried out with different grid sizes using water thermophysical properties. For each aspect ratio four different grid size simulations were performed and summarized in Table 7.1. It is clear from the Table 7.1 that the Nusselt number variation is less than 1% of the final grid size with the previous grid size. Finally, with the selected grid size the simulation results were compared with the experimental results of chapter 5. The Fig.7.2 shows the simulation results match well with the experimental results of enclosures with aspect ratio 1 and 1.5 and there is no experimental data for aspect ratio 0.5 which is performed for the parametric study to see the natural convection behavior at aspect ratio less 1.

Table 7.1 Grid independent test of different shape enclosure

Enclosures	Grid size	Nu
AR-0.5 $Ra = 2 \times 10^6$	240×120	6.085
	300×150	6.383
	400×200	6.506
	500×250	6.600
AR-1 $Ra = 1 \times 10^7$	240×240	13.944
	300×300	14.508
	400×400	14.620
	500×500	14.684
AR-1.5 $Ra = 1 \times 10^8$	240×360	30.623
	300×4500	30.693
	400×600	30.769
	500×750	30.795

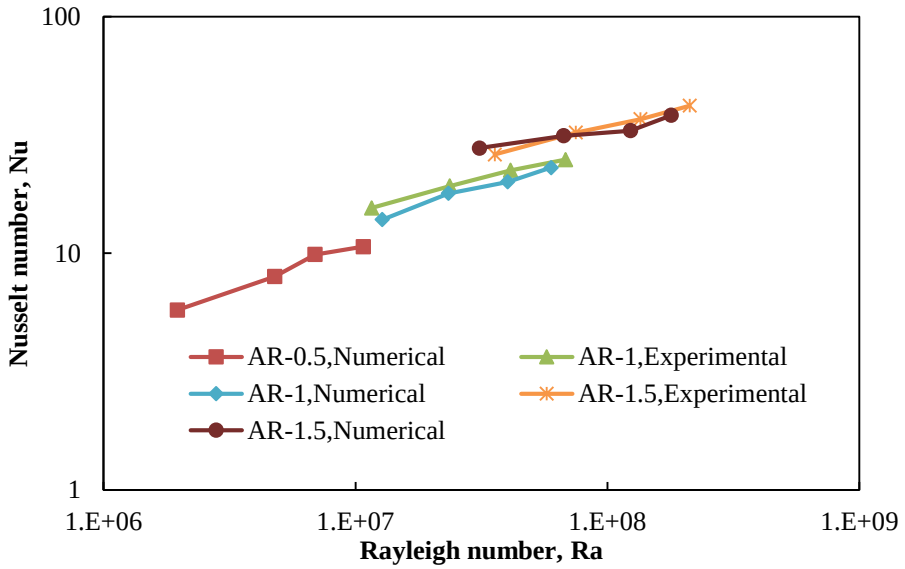

Figure 7.2 Comparison of numerical and experimental data of natural convection of water

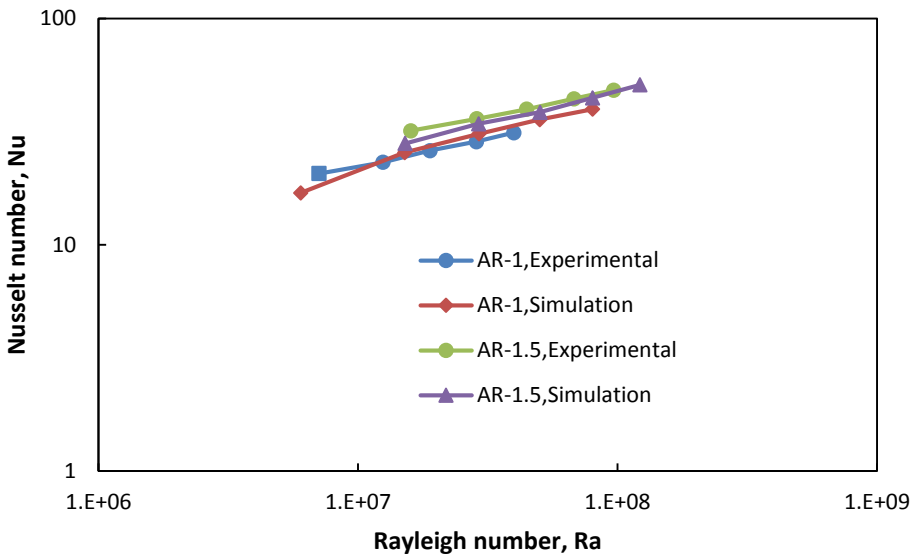

Figure 7.3 Comparison of numerical and experimental data of natural convection of IL

After being confident with the simulation of water, numerical simulation was performed for [C_4mim][NTf_2] IL and different concentration (0.5, 1.0, and 2.5 wt%) of Al_2O_3 NEILs. The numerical results of IL were compared with the experimental results and presented in Fig.7.3. It is clear that the numerical results predict well the experimental results within the studied Rayleigh number range. Fig.7.4 (a-c) represents the natural convection heat transfer behavior of NEILs and compared with the base IL. It is clear from the Fig.7.4 that at a certain Rayleigh number NEILs shows lower Nusselt number compared to the base IL which are consisten with the experimental results presented in chapter 5. But the percentage of degradation is much less in the numerical results compared to the experimental. As mentioned in chapter5 the Nusselt number and Rayleigh number are presented in the form of:

$$Nu = cRa^n \tag{7-7}$$

$$\frac{hH}{k_f} = c\left(\frac{g\beta\Delta TH^3 C_p\rho^2}{\mu k_f}\right)^n \quad (7\text{-}8)$$

From the equ.(7-8) normalizing the heat transfer coefficient by dividing the heat transfer coefficient of NEILs to IL, the following correlation was found:

$$\frac{h_{NEIL}}{h_{BL}} \sim \left(\frac{\beta_{NEIL}}{\beta_{BL}}\right)^n \left(\frac{\rho_{NEIL}}{\rho_{BL}}\right)^{2n} \left(\frac{C_{p,NEIL}}{C_{p,BL}}\right)^n \left(\frac{\mu_{NEIL}}{\mu_{BL}}\right)^{-n} \left(\frac{k_{NEIL}}{k_{BL}}\right)^{1-n} \quad (7\text{-}9)$$

In the normalized heat transfer coefficient correlation, all of the thermophysical properties except dynamic viscosity have the negative impact on heat transfer coefficient. In the correlation, inserting a typical natural convection correlation exponent value of $n = {}^1/_3$, the normalized heat transfer coefficient was calculated. The numerical results of natural convection heat transfer matches well with the theoretical equ.(7-9) where the theoretical calculation maximum 22% degradation was observed for 2.5 wt% NEILs. The

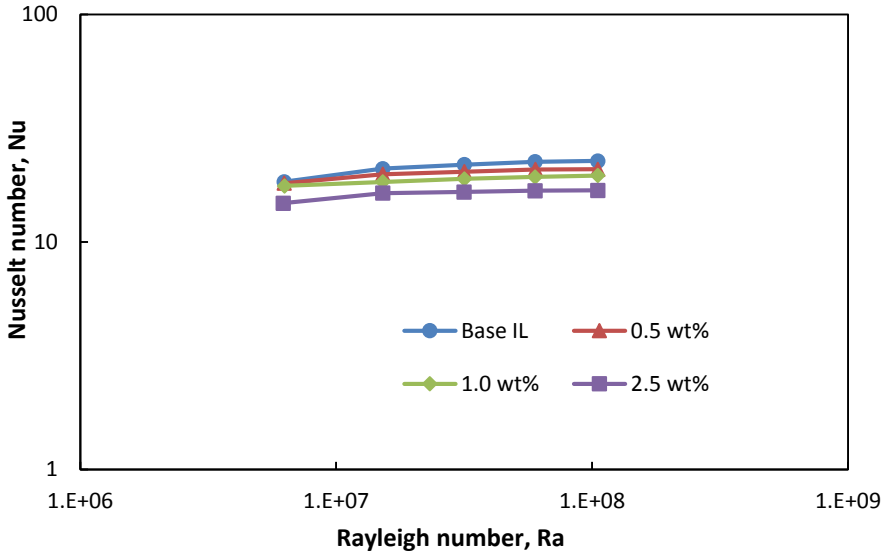

(a)

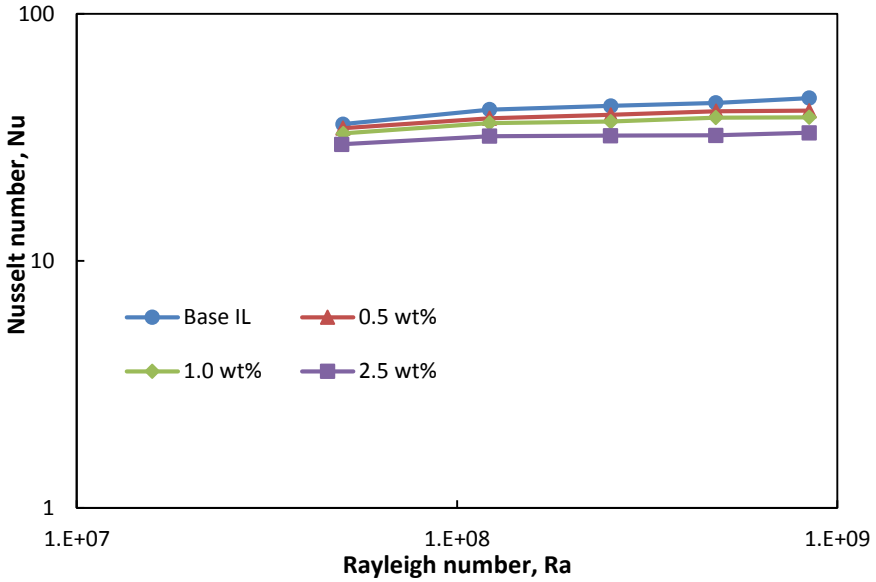

(b)

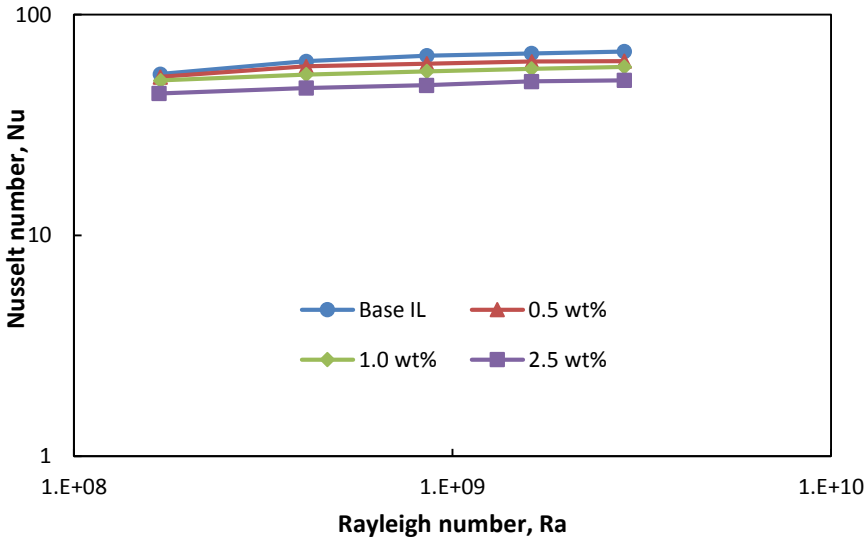

(c)

Figure 7.4 Natural convection heat transfer of base IL and NEILs in different enclosures (a) AR-0.5, (b) AR-1, (c) AR-1.5

numerical simulation degradation was found at a maximum of 27% for 2.5 wt% NEILs in the studied Rayleigh number range which is clear in Fig.7.5. Fig.7.5 represents the normalized Nusselt number (Nusselt number of NEILs divided by the Nusselt number of base IL) at same Rayleigh number as the function of nanoparticle concentration. It is clear from Fig.7.5 that the Nusselt number decreases with the increasing nanoparticle concentration of NEILs and maximum degradation occurs in enclosure at aspect ratio-0.5 with 2.5 wt% NEILs. This may happen because at a certain Rayleigh number the temperature difference as well as the average temperature is higher in the lower aspect ratio enclosure than the higher aspect ratio. It is clear from the Fig.7.6 that the normalized heat transfer coefficient decreases with the increase of the average temperature. The reason for the average temperature effect may be the dominance of viscosity enhancement of NEILs compared to other thermophysical properties.

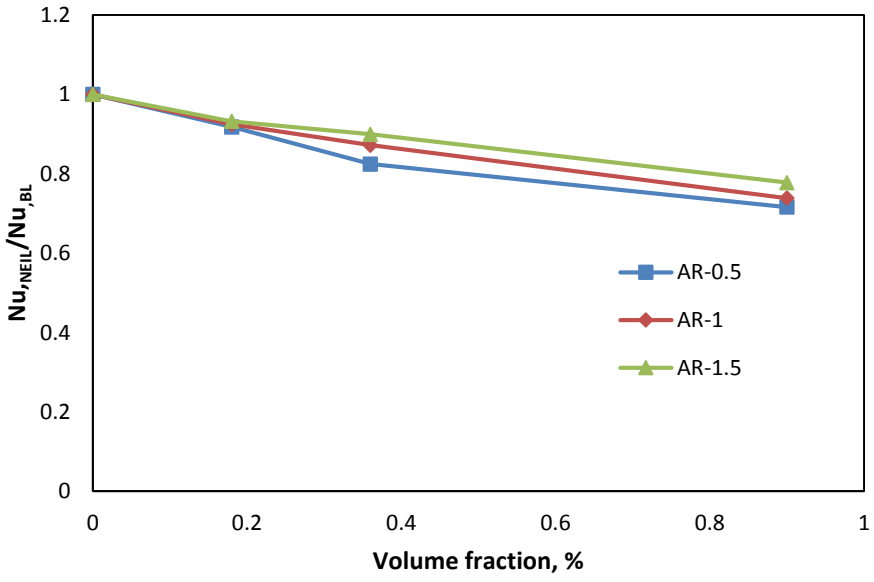

Figure 7.5 Normalized Nusselt number as a function of nanoparticle volume concentration ($Ra = 1.37 \times 10^8$)

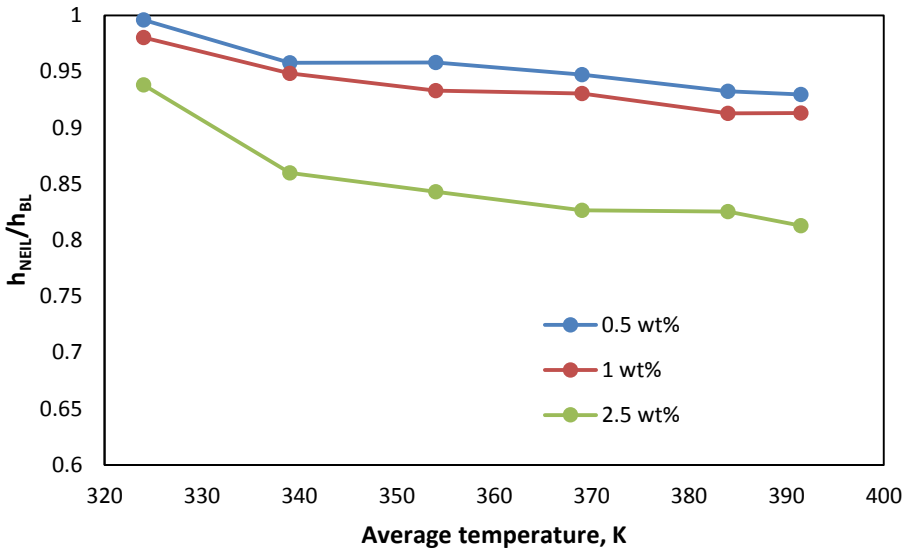

Figure 7.6 Heat transfer coefficient ratio as a function of average temperature (AR-1)

The numerical results can explain the huge degradation of the experimental results in chapter 5. Since the numerical results match well with the theoretical calculation of heat transfer coefficient, that means in experimental results the extra degradation may occur for the particle-fluid interaction, clustering and sedimentation of nanoparticles. The present numerical results contradict with most of the previous studies (Khanafer, Vafai et al. 2003; Ho, Chen et al. 2008;Oztop and Abu-Nada 2008); they reported natural convection heat transfer enhancement of nanofluids compared to base fluids. This is because in their study they calculate the Nusselt number of nanofluids by using the thermal conductivity of base fluids instead of nanofluids. Some literature (Rashmi, Ismail et al. 2011; Abouali and Ahmadi 2012; Choi, Kim et al. 2014) corrected the Nusselt number correlation with the thermal conductivity of nanofluids and reported degradation of heat transfer of nanofluids. The present numerical study also observed the degradation of heat transfer of NEILs compared to base IL.

7.6 Geometry of Forced Convection

The forced convection numerical study was performed in a circular tube having diameter 3.86 mm and 1000 mm in length and the schematic of the geometry is presented in Fig.7.7(a) which is same as the experimental geometrical configuration. The two-dimensional tube geometry was generated in GAMBIT 2.4.6 (Gambit 2007) and there are 800000 (20000×40) uniform mesh elements. Fig.7.7(b) shows the uniform mesh elements of the forced convection problem.

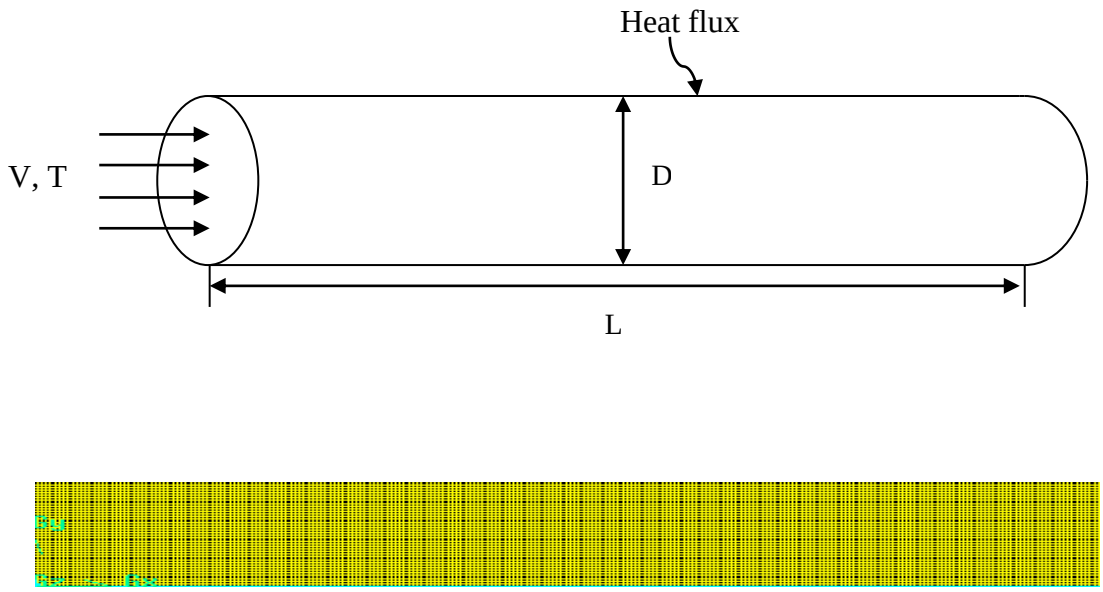

Figure 7.7(a) Schematic of forced convection configuration (b) The uniform grid of the forced convection circular tube

7.7 Boundary Condition of Forced Convection

The boundary conditions of the forced convection problem are uniform inlet axial velocity and temperature profile. Half of the tube is considered for analysis because of the symmetrical velocity and temperature field along the vertical plane passing through the tube main axis. No slip boundary condition and uniform heat flux is applied to the

wall. Experimentally measured thermophysical properties are used in the numerical simulation.

7.8 Simulation Methodology of Forced Convection

The forced convection numerical problem was solved by using two-dimensional ANSYS Fluent CFD program (Fluent 2011). As mentioned above, in natural convection problem the NEILs was considered as single phase fluid with no relative velocity between particle and fluid. NEILs is considered as an incompressible fluid and thermophysical properties are the function of temperature. The governing equations with single phase approximation are as follows:

Continuity equation:

$$div\left(\rho\vec{V}\right) = 0 \tag{7-10}$$

Momentum equation:

$$div\left(\rho\vec{V}\vec{V}\right) = -gradP + \nabla.\left(\mu\nabla\vec{V}\right) \tag{7-11}$$

Energy equation:

$$div\left(\rho\vec{V}C_pT\right) = div(kgradT) \tag{7-12}$$

The CFD program solves the governing equations by converting them into algebraic equations with control volume theory technique. The laminar viscous model was used with SIMPLE scheme, Least-Square-Cell Based gradient, and the convergence criteria of the residuals of governing equation variables are 1×10^{-6}. In the pressure and standard velocity coupling was selected as pressure. For momentum and energy equation Second

Order Upwind was selected for higher accuracy. All of the temperature dependent thermophysical properties were provided in the materials section. From the applied heat flux in the tube surface the wall surface temperature and bulk fluid temperature along the tube length was computed by using area-weighted average surface integrals. The local heat transfer coefficient $h(x)$, at an axial distance x, along the test section was calculated using the equation:

$$h(x) = \frac{q^{"}}{T_w(x) - T_f(x)} \tag{7-13}$$

where $q^{"}$ is the heat flux, $T_w(x)$ and $T_f(x)$ are the local temperatures of the inner surface and liquid respectively.

Average heat transfer coefficient h_{av} was calculated by using the local heat transfer coefficient:

$$h_{av} = \frac{1}{L}\int_0^L h(x)dx \tag{7-14}$$

Average Nusselt number was calculated by:

$$Nu_{av} = \frac{h_{av}.D}{k_f} \tag{7-15}$$

7.9 Results and Discussion of Forced Convection

Before performing simulation with ILs and NEILs, a grid independence study was carried out with different grid sizes using water thermophysical properties. Simulation was performed for four different grid size 40×20,000, 30×15,000, 20×10,000, and 10×5000 and compared with the well-established Shah's equation (Shah 1975) of laminar flow at the constant heat flux boundary conditions:

$$Nu(x) =$$

$$\begin{cases} 1.953\left(RePr\frac{D}{x}\right)^{\frac{1}{3}} & \left(RePr\frac{D}{x}\right) \geq 33.3 \\ 4.364 + 0.0722RePr\frac{D}{x} & \left(RePr\frac{D}{x}\right) < 33.3 \end{cases} \quad (7\text{-}16)$$

where Nu(x), Re, Pr are the local Nusselt number, Reynolds number, and Prandtl number respectively and defined as

$$Nu(x) = \frac{h(x)D}{k_f}, Re = \frac{\rho u D}{\mu}, Pr = \frac{\nu_f}{\alpha} \quad (7\text{-}17)$$

where D is the inner diameter of test section, k_f is the thermal conductivity of fluid, ρ is the fluid density, μ is the fluid viscosity, u is the velocity of fluid, $\nu_f (= \frac{\mu}{\rho})$ is the kinematic viscosity, and $\alpha (= \frac{k_f}{\rho C_p})$ is the thermal diffusivity. All the fluid properties were evaluated at the average ($T_{av} = \frac{T_{in}+T_{out}}{2}$) of the inlet and outlet fluid temperature of the test section.

It is clear from the Fig.7.8 that the grid element 800000 (40×20,000) predicts well the theoretical results. After getting confidence with simulation models, forced convection simulations were performed for 1-butyl-3-methylimidazolium bis{(trifluoromethyl)sulfonyl}imide ([C_4mim][NTf_2])IL and Al_2O_3 NEILs. The heat transfer coefficient of [C_4mim][NTf_2] IL as a function of axial distance is presented in Fig.7.9 and compared with the experimental results. The numerical simulation was performed with both constant and temperature dependent thermophysical property of IL

and it is clear that the temperature dependent properties predict well the experimental results.

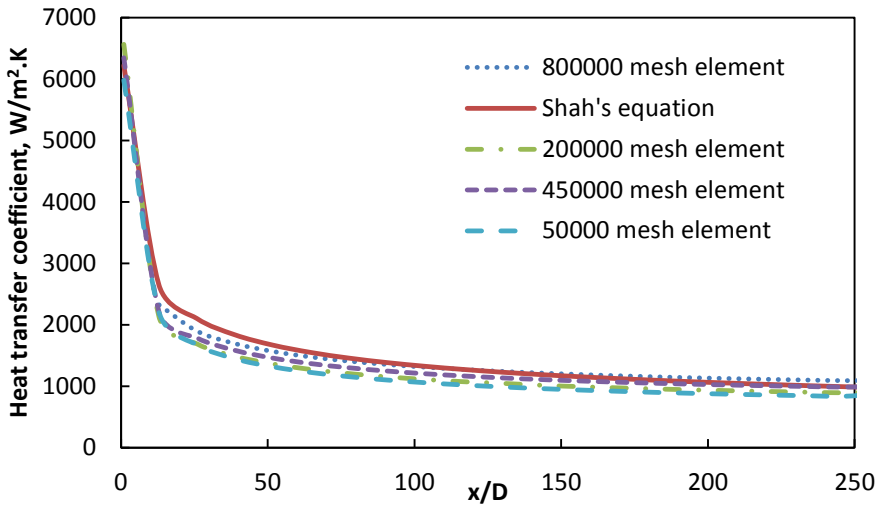

Figure 7.8 Comparison of the simulation with the Shah's equation for laminar ($Re = 1400$) flow of pure water

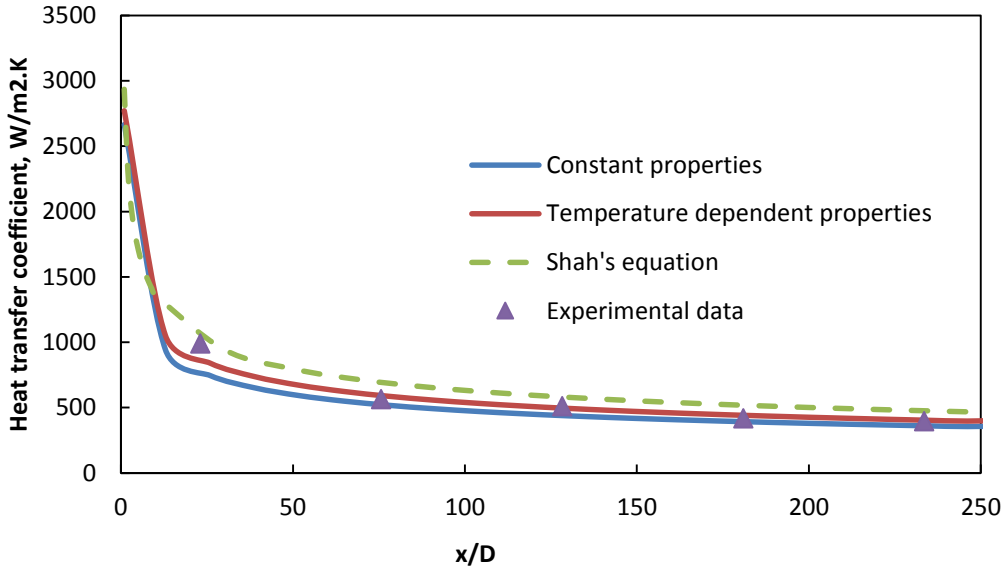

Figure 7.9 Heat transfer coefficient of [C_4mim][NTf_2] IL as a function of axial distance at $Re = 1378$

Since numerical simulation with temperature dependent properties gives the better prediction of experimental results, here in the next section all of the results present the

simulation with temperature dependent properties. Fig.7.10(a) shows the axial velocity profile along tube radius in different locations for 1 wt% NEIL at $Re = 1057$ and it is clear that the flow becomes fully developed at x=0.05m. Fig.7.10(b) shows the axial velocity profile of base IL and NEILs at x=0.1m for $Re = 1057$ and it is clear that the 2.5 wt% NEIL velocity profile is not fully developed at that point, which means the higher concentration of NEILs has larger hydrodynamic entry length. The dimensionless temperature ($T^* = \frac{T-T_w}{T_b-T_w}$) profile along tube radius in different location for base IL and 1 wt% NEIL are presented in Fig.11(a) and Fig.11(b) respectively. Since ILs and NEILs has very high Prandtl number the flow is not thermally developed which is clear from the Fig.11;temperature profile of NEILs is sharper than the base IL which is because of higher Prandtl number of NEILs compared to base IL.

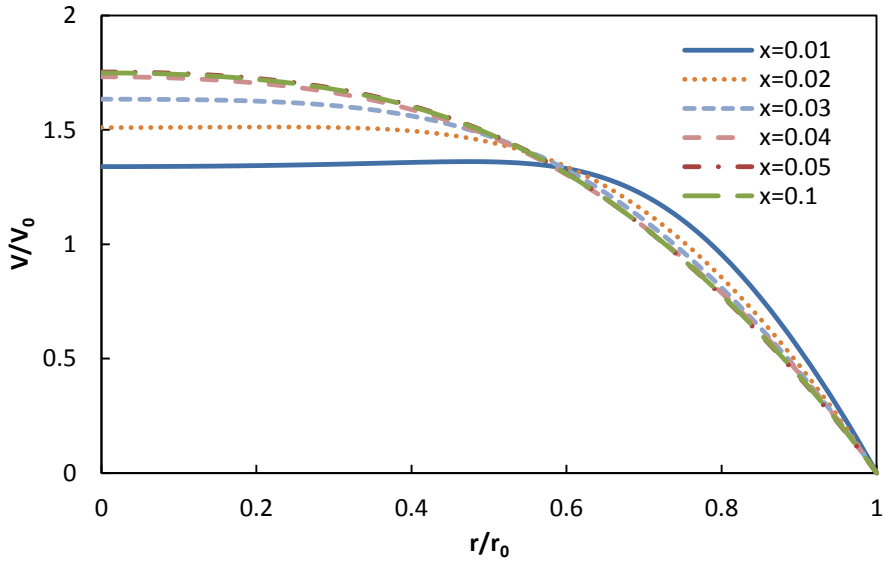

(a)

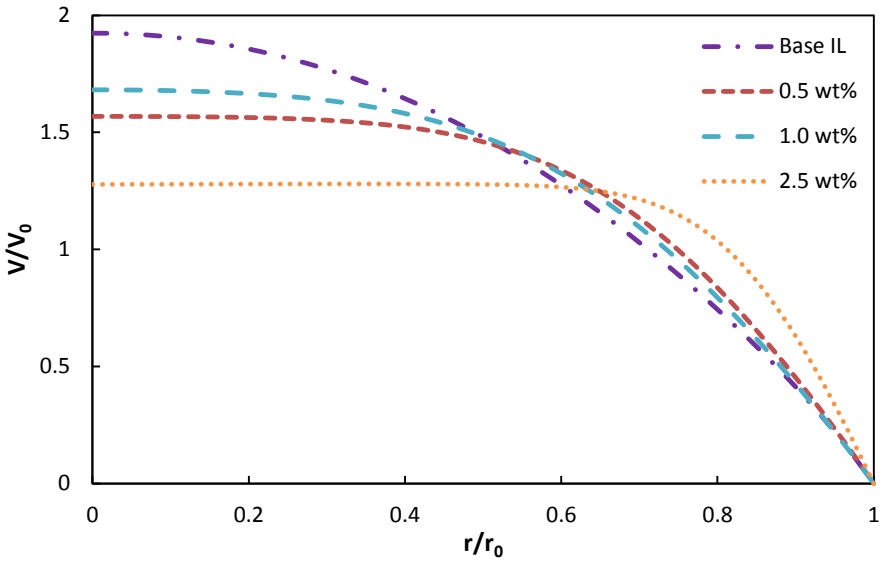

(b)

Figure 7.10(a) Axial velocity profile of 1 wt% NEIL at different location for $Re = 1057$, (b) axial velocity profile of base IL and NEILs at x=0.1m for $Re = 1057$

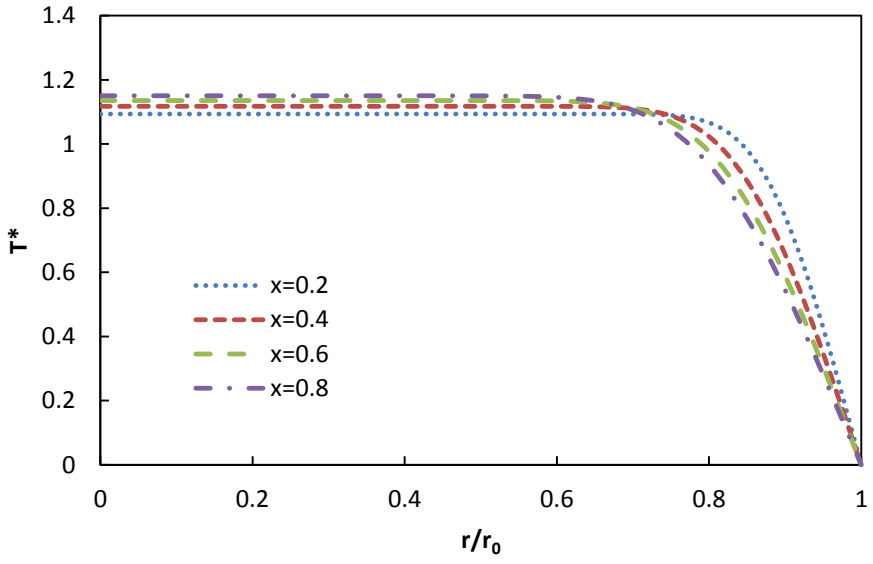

(a)

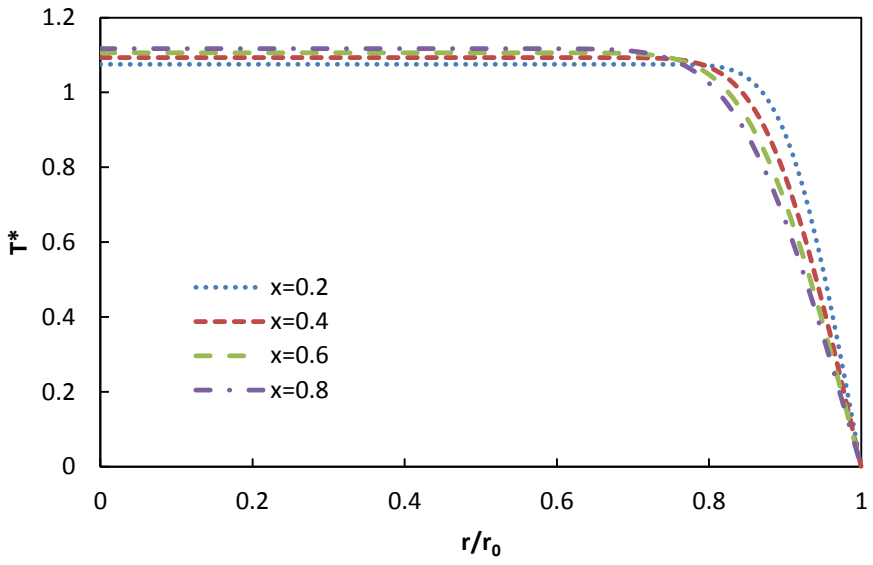

(b)

Figure 7.11 Dimensionless temperature profile of (a) base IL and (b) 1 wt% NEIL for $Re = 1057$ and heat flux 18507 W/m^2

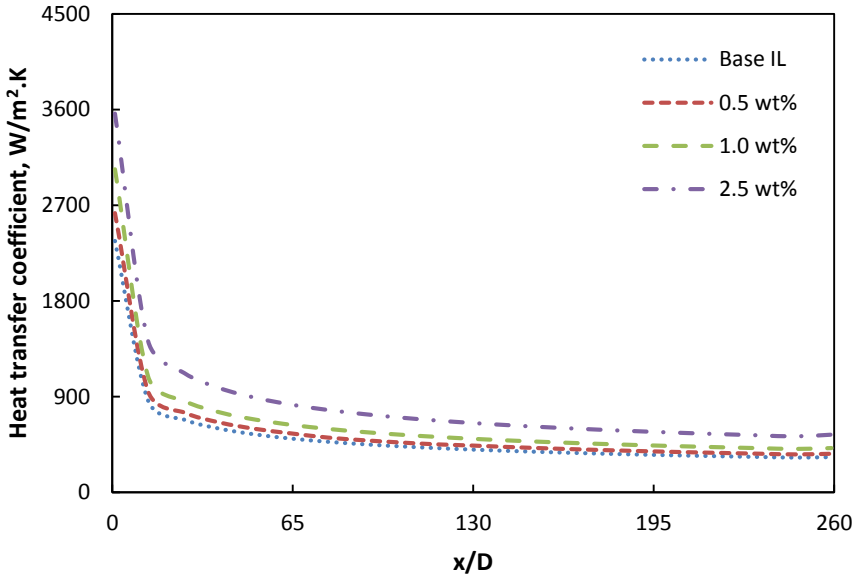

(a)

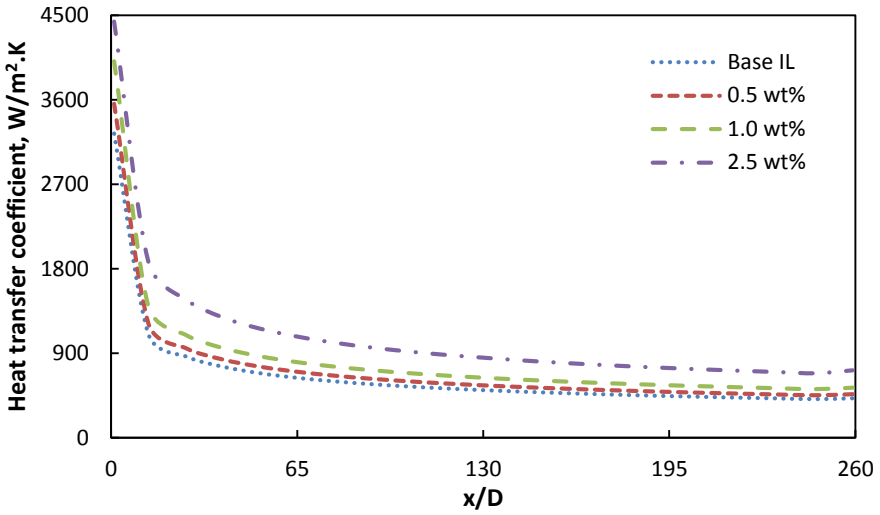

(b)

Figure 7.12 Heat transfer coefficient of base IL and NEILs as a function of axial distance at (a) $Re = 1057$ (b) $Re = 1928$

Fig.7.12 represents the local heat transfer coefficient of base IL and NEILs along the axial distance at heat flux 18507 W/m^2 in two different Reynolds numbers. The NEILs show enhanced heat transfer coefficient along the entire axial distance and heat transfer coefficient decreases with axial distance. Along the axial distance the average heat transfer enhancement is ~10%, 27%, and 63% for 0.5, 1.0, and 2.5 wt% NEILs respectively. The numerical results match well with the experimental results up to 1 wt% NEILs but 2.5 wt% NEILs shows much higher enhancement in numerical studies comapred to the experimental values. Fig.13(a) represents the heat transfer coefficient of 1 wt% NEIL along axial distance at different Reynolds number and heat transfer increases with Reynolds number. The effect of Reynolds number is more clear in Fig.13(b) where the average heat transfer coefficient of base IL and NEILs is presented as a function of Reynolds number and heat transfer coefficient increases with Reynolds

number. At a certain Reynolds number, heat transfer coefficient increases with nanoparticle concentration. This is because of the higher thermal conductivity of NEILs compared to base IL and particle migration. The increment is higher at higher Reynolds number beacause at high Reynolds number the boundary layer becomes thinner and as a results high heat transfer coefficient increases.

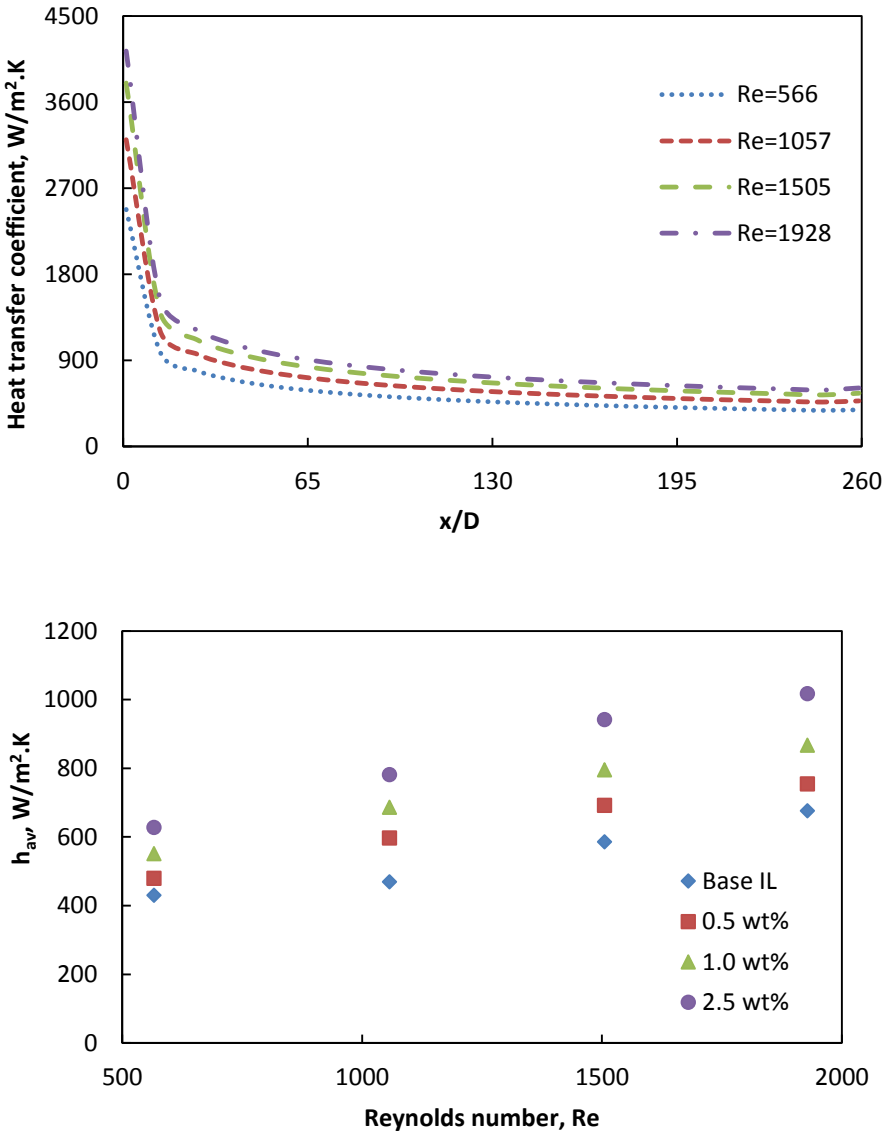

Figure 7.13 (a) Heat transfer coefficient of 1 wt% NEIL, (b) Average heat transfer coefficient of base IL and NEILs for different Reynolds number

7.10 Summary

Natural convection numerical studies of N-butyl-N-methylpyrrolidiniumbis {trifluoromethyl)sulfonyl} imide ([C_4mpyrr][NTf_2]) IL and forced convection numerical studies of 1-butyl-3-methylimidazolium bis{(trifluoromethyl)sulfonyl}imide ([C_4mim][NTf_2]) IL and Al_2O_3 NEILs has been performed and compared with the experimental results.

NEILs shows degradation of natural convection heat transfer compared to base IL and matches well with the predicted model of using thermophysical properties of NEILs. The forced convection of NEILs shows higher heat transfer coefficient compared to base IL. In forced convection numerical simulation the temperature dependent model gives a better prediction of the experimental results. The forced convection is fully hydrodynamically developed but not thermally developed because of high Prandtl number of base IL and NEILs.

CHAPTER 8

CONCLUSIONS AND FUTURE WORK

The interest of ionic liquids as heat transfer fluids (HTFs) has been increasing in recent years because of their thermophysical properties. Enhanced thermophysical properties can be achieved by dispersing small amount of nanoparticles into the base liquid. In the present research, heat transfer behavior under natural and forced convection of ionic liquids (ILs) and nanoparticle enhanced ionic liquids (NEILs) was investigated. For better understanding of the heat transfer behavior, thermophysical properties such as density, viscosity, thermal conductivity, and heat capacity of ILs and NEILs were also experimentally measured and reported. Thermophysical properties of four ILs and Al_2O_3 (spherical and whiskers) NEILs with different concentrations (0.5, 1.0, and 2.5 wt%) were investigated. From the experimental and numerical results the following conclusions can be drawn.

8.1 Thermophysical Properties on ILs and NEILs

The thermophysical properties of ILs were correlated well with previously published literature. NEILs shows enhanced thermophysical properties compare to base ILs. Density of ILs and NEILs decreases with temperature increases within the measured temperature range (10-70^{o}C). ILs shows Newtonian behavior but NEILs shows shear thinning behavior in all measured temperature ranges. Highly temperature dependent shear viscosity was observed both for ILs and NEILs. Whiskers shaped nanoparticle

enhanced NEILs has lower viscosity compared to spherical nanoparticles. The experimental effective viscosity was predicted by considering aggregation of nanoparticles in NEILs. The thermal conductivity of ILs and NEILs shows less temperature dependency. The effective thermal conductivity of NEILs was predicted by considering the nanoparticles interfacial layer on NEILs. The highest enhancement of thermal conductivity was observed for whiskers nanoparticles compared to spherical nanoparticles. The heat capacity of ILs and NEILs increases almost linearly with temperature. Conventional models failed to predict the enormous enhancement of heat capacity of NEILs.

8.2 Natural Convection of ILs and NEILs

The ILs shows much lower heat transfer coefficient compare to De-Ionized (DI) water. However the dimensionless Nusselt number of ILs is higher than DIiwater due to lower thermal conductivity. At the same condition high aspect ratio has higher natural convection heat transfer compared to the low aspect ratio. New correlation of Nusselt Number as a function of Rayleigh Number is proposed for ILs. The systematic degradation of natural convection heat transfer of NEILs was observed. The changes of thermophysical properties could not fully explain the huge degradation of NEILs. The whiskers NEILs had slightly higher heat transfer coefficient compared to the spherical NEILs. In addition to thermophysical properties, particle-fluid interaction and clustering of nanoparticles also play a role to degrade the natural convection heat transfer. The findings from this study will help to consider this natural convection behavior of ILs and NEILs in the design of passive solar collector storage tank where one would need to account the natural convection heat transfer.

8.3 Forced Convection of ILs and NEILs

The laminar forced convection behavior ILs shows hydrodynamically developed, but not thermally developed, flow due to high viscosity and low thermal conductivity of ILs. In turbulent condition the flow was fully developed because there was no entrance effect observed. The heat transfer behavior of ILs well correlates with the Shah's and Gnielinski's equations for laminar and turbulent flow conditions respectively. The enhanced heat transfer coefficient of NEILs was observed. In laminar flow the more enhancement was found in entrance region and turbulent flow shows higher enhancement compared to laminar flow. The clustering of nanoparticles, particle migration, and enhancement of thermal conductivity were the plausible reasons for enhanced heat transfer behavior of NEILs. The finding from this experiment is useful for the assessment of NEILs in solar thermal collector for high temperature applications.

8.4 Numerical Investigation of Natural and Forced Convection of NEILs

The forced convection numerical results also shows the enhanced heat transfer coefficient of NEILs compared to base IL and heat transfer coefficient increases with nanoparticle concentration. The temperature dependent numerical model predicts well the experimental results. Numerical investigation of natural convection shows degradation of heat transfer coefficient of NEILs compared to base IL but the degradation is not as much as in experimental results, which confirms that the experimental huge degradation was not fully for the relative change in thermophysical properties of NEILs. The numerical results also correlate well with the theoretical model calculating heat transfer coefficient by using the relative change of thermophysical properties of NEILs.

8.5 Recommendation for Future Research

The present research was conducted on the thermal performance of the ionic liquids (ILs) and nanoparticle enhanced ionic liquids (NEILs). The experimental results show that NEILs has enhanced thermophysical properties compared to base ILs which makes them a potential heat transfer fluid for solar collector applications. However there is a broad scope to work within on the NEILs to assess the fluids in solar thermal applications.Suggestion for future research are as follows:

1. In the forced convection thermal performance there needs to be more exploration of specific mechanism of heat transfer enhancement of NEILs. Nanoparticle size and shape effect also need to explored. Future research would study the effect of particle morphology on thermal performance of NEILs and find a specific particle size and shape for maximum enhancement.
2. Molecular dynamic simulation can be performed in NEILs to see the nanoparticle and ion interaction which may give insight into the mechanism of the thermophysical properties enhancement.
3. Since numerical simulation by FLUENT predict well the experimental studies, many parametric studies can be performed numerically. Forced convection parametric study could concern: i) change in heat flux, ii) turbulent flow condition. Natural convection parametric study could concern change in heating condition.
4. Levelized cost analysis can be performed by considering a small capacity power plant. The study can give a comparison of NEILs with the currently used heat transfer fluid.

REFERENCES

Abouali, O. and G. Ahmadi (2012). "Computer simulations of natural convection of single phase nanofluids in simple enclosures: A critical review." Applied Thermal Engineering 36: 1-13.

Ahuja, A. S. (1975). "Augmentation of heat transport in laminar flow of polystyrene suspensions. I. Experiments and results." Journal of Applied Physics 46(8): 3408-3416.

Ahuja, A. S. (1975). "Augmentation of heat transport in laminar flow of polystyrene suspensions. II. Analysis of the data." Journal of Applied Physics 46(8): 3417-3425.

Anthony, J. L., J. L. Anderson, et al. (2005). "Anion Effects on Gas Solubility in Ionic Liquids." The Journal of Physical Chemistry B 109(13): 6366-6374.

Asirvatham, L. G., Vishal, N., Gangatharan, S. K., Lal, D. M. (2009). "Experimental Study on Forced Convective Heat Transfer with Low Volume Fraction of CuO/Water Nanofluid" Energies 2, 97-119.

Baogang Wang, X. W., Wenjing Lou and Jingcheng Hao (2011). "Gold-ionic liquid nanofluids with preferably tribological properties and thermal conductivity." Nanoscale Research Letters 6(259).

Baogang Wang, X. W., Wenjing Lou and Jingcheng Hao (2011). "Gold-ionic liquid nanofluids with preferably tribological properties and thermal conductivity." Nanoscale Research Letters 6(259).

Barrer, R. M. (1943). "The viscosity of pure liquids. II. Polymerised ionic melts." Transactions of the Faraday Society 39(0): 59-67.Batchelor, G. K. (1977). "The effect of Brownian motion on the bulk stress in a suspension of spherical particles." Journal of Fluid Mechanics 83(01): 97-117.

Bazito, F. F. C., Y. Kawano, et al. (2007). "Synthesis and characterization of two ionic liquids with emphasis on their chemical stability towards metallic lithium." Electrochimica Acta 52(23): 6427-6437.

Bejan, A. and A. D. Kraus (2003). "Heat transfer handbook."

Bhatt, V. D. and K. Gohil (2013). "Performance evaluation of solar cooker using some [N+ 4444] based ionic liquids as thermal energy storage materials." Advanced Materials Letters 4(4).

Bianco, V., F. Chiacchio, et al. (2009). "Numerical investigation of nanofluids forced convection in circular tubes." Applied Thermal Engineering 29(17): 3632-3642.

Bianco, V., O. Manca, et al. (2010). "Numerical Simulation of Water/A l " Advances in Mechanical Engineering 2010.

Blake, D. M., L. Moens, et al. (2002). New heat transfer and storage fluids for parabolic trough solar thermal electric plants. Proceedings of the 11th SolarPACES International Symposium On concentrating Solar Power and Chemical Energy Technologies.

Bonhôte, P., A.-P. Dias, et al. (1996). "Hydrophobic, Highly Conductive Ambient-Temperature Molten Salts†." Inorganic Chemistry 35(5): 1168-1178.

Bridges, N. J., A. E. Visser, et al. (2011). "Potential of Nanoparticle-Enhanced Ionic Liquids (NEILs) as Advanced Heat-Transfer Fluids." Energy & Fuels 25(10): 4862-4864.

Briefing, U. S. (2013). "International Energy Outlook 2013."

Brinkman, H. C. (1952). "The Viscosity of Concentrated Suspensions and Solutions." The Journal of Chemical Physics 20(4): 571-571.

Bruggeman, V. D. (1935). "Berechnung verschiedener physikalischer Konstanten von heterogenen Substanzen. I. Dielektrizitätskonstanten und Leitfähigkeiten der Mischkörper aus isotropen Substanzen." Annalen der Physik 416(7): 636-664.

Buongiorno, J., L.-W. Hu, et al. (2008). "Nanofluids for enhanced economics and safety of nuclear reactors: An evaluation of the potential features, issues, and research gaps." Nuclear Technology 162(1): 80-91.

Calcagni, B., F. Marsili, et al. (2005). "Natural convective heat transfer in square enclosures heated from below." Applied Thermal Engineering 25(16): 2522-2531.

Carper, W. R., P. G. Wahlbeck, et al. (2011). "Semi-Empirical Molecular Modeling of Ionic Liquid Tribology: Ionic Liquid–Aluminum Oxide Surface Interactions." Tribology Letters 43(2): 163-168.

Carvalho, P. J., C. M. S. S. Neves, et al. (2010). "Surface Tensions of Bis(trifluoromethylsulfonyl)imide Anion-Based Ionic Liquids." Journal of Chemical & Engineering Data 55(9): 3807-3812.

Chemfiles. (2006). "Enabling Technologies Ionic Liquids." Retrieved May 29, 2014, from http://www.sigmaaldrich.com/content/dam/sigma-aldrich/docs/Aldrich/Brochure/al_chemfile_v5_n6.pdf.

Chen, B., F. Mikami, et al. (2005). "Experimental studies on transient features of natural convection in particles suspensions." International Journal of Heat and Mass Transfer 48(14): 2933-2942.

Chen, H., Y. Ding, et al. (2007). "Rheological behaviour of ethylene glycol based titania nanofluids." Chemical Physics Letters 444(4–6): 333-337.

Chen, H., Y. He, et al. (2008). "Rheological and heat transfer behaviour of the ionic liquid, [C4mim][NTf2]." International Journal of Heat and Fluid Flow 29(1): 149-155.

Chen, H., W. Yang, et al. (2008). "Heat transfer and flow behaviour of aqueous suspensions of titanate nanotubes (nanofluids)." Powder Technology 183(1): 63-72.

Chen, J., D. L. Officer, et al. (2005). "Photoelectrochemical solar cells based on polyterthiophenes containing porphyrins using ionic liquid electrolyte." Electrochemical and Solid-State Letters 8(10): A528-A530.

Choi, S.-K., S.-O. Kim, et al. (2014). "Computation of the Natural Convection of Nanofluid in a Square Cavity with Homogeneous and Nonhomogeneous Models." Numerical Heat Transfer, Part A: Applications 65(4): 287-301.

Choi, S. U. and J. Eastman (1995). Enhancing thermal conductivity of fluids with nanoparticles, Argonne National Lab., IL (United States).

Choi, S. U. S. and J. A. Eastman (1995). Enhancing thermal conductivity of fluids with nanoparticles.

Chopkar, M., P. K. Das, et al. (2006). "Synthesis and characterization of nanofluid for advanced heat transfer applications." Scripta Materialia 55(6): 549-552.

Chu, Y. (2011). "Review and Comparison of Different Solar Energy Technologies." Research Associate, Global Energy Network Institute (GENI)(619): 595-0139.

Chum, H. L., V. R. Koch, et al. (1975). "Electrochemical scrutiny of organometallic iron complexes and hexamethylbenzene in a room temperature molten salt." Journal of the American Chemical Society 97(11): 3264-3265.

Coggin, S. P. a. J. D. P. (2013). "Fulfilling the Promise ofConcentrating Solar Power: Low-Cost Incentives Can SpurInnovation in the Solar Market." Retrieved May

29, 2014, from http://www.americanprogress.org/wp-content/uploads/2013/06/PoolSolarPower-report-3.pdf.

Crosthwaite, J. M., M. J. Muldoon, et al. (2005). "Phase transition and decomposition temperatures, heat capacities and viscosities of pyridinium ionic liquids." The Journal of Chemical Thermodynamics 37(6): 559-568.

Dalal, A. and M. K. Das (2006). "Natural Convection in a Rectangular Cavity Heated from Below and Uniformly Cooled from the Top and Both Sides." Numerical Heat Transfer, Part A: Applications 49(3): 301-322.

Das, S. K., N. Putra, et al. (2003). "Temperature Dependence of Thermal Conductivity Enhancement for Nanofluids." Journal of Heat Transfer 125(4): 567-574.

Davarnejad, R., S. Barati, et al. (2013). "CFD simulation of the effect of particle size on the nanofluids convective heat transfer in the developed region in a circular tube." SpringerPlus 2(1): 1-6.

Diedrichs, A. and J. Gmehling (2006). "Measurement of heat capacities of ionic liquids by differential scanning calorimetry." Fluid Phase Equilibria 244(1): 68-77.

Ding, Y., H. Alias, et al. (2006). "Heat transfer of aqueous suspensions of carbon nanotubes (CNT nanofluids)." International Journal of Heat and Mass Transfer 49(1–2): 240-250.

Ding, Y., H. Chen, et al. (2010). "Relationship between the thermal conductivity and shear viscosity of nanofluids." Physica Scripta 2010(T139): 014078.

Ding, Y. and D. Wen (2005). "Particle migration in a flow of nanoparticle suspensions." Powder Technology 149(2–3): 84-92.

Dong, Q., C. D. Muzny, et al. (2007). "ILThermo: A Free-Access Web Database for Thermodynamic Properties of Ionic Liquids†." Journal of Chemical & Engineering Data 52(4): 1151-1159.

Einstein, A. (1906). "Eine neue Bestimmung der Moleküldimensionen." Annalen der Physik 324(2): 289-306.

Elias, M. M., M. Miqdad, et al. (2013). "Effect of nanoparticle shape on the heat transfer and thermodynamic performance of a shell and tube heat exchanger." International Communications in Heat and Mass Transfer 44(0): 93-99.

Endres, F. and S. Zein El Abedin (2006). "Air and water stable ionic liquids in physical chemistry." Physical Chemistry Chemical Physics 8(18): 2101-2116.

Fluent, A. (2011). "ANSYS Fluent 13.0.0, User Manual, Fluent Incorporated."

Fox, E. B., A. E. Visser, et al. (2013). "Thermophysical Properties of Nanoparticle-Enhanced Ionic Liquids (NEILs) Heat-Transfer Fluids." Energy & Fuels 27(6): 3385-3393.

Fredlake, C. P., J. M. Crosthwaite, et al. (2004). "Thermophysical Properties of Imidazolium-Based Ionic Liquids." Journal of Chemical & Engineering Data 49(4): 954-964.

Frez, C., G. J. Diebold, et al. (2006). "Determination of Thermal Diffusivities, Thermal Conductivities, and Sound Speeds of Room-Temperature Ionic Liquids by the Transient Grating Technique." Journal of Chemical & Engineering Data 51(4): 1250-1255.

Fröba, A. P., M. H. Rausch, et al. (2010). "Thermal Conductivity of Ionic Liquids: Measurement and Prediction." International Journal of Thermophysics 31(11-12): 2059-2077.

Gambit (2007). "Gambit 2.4.6, User Guide, Fluent Inc., Lebanon, New Hampshire, USA,."

Gardas, R. L. and J. A. P. Coutinho (2008). "Applying a QSPR correlation to the prediction of surface tensions of ionic liquids." Fluid Phase Equilibria 265(1–2): 57-65.

Gardas, R. L. and J. A. P. Coutinho (2008). "A Group Contribution Method for Heat Capacity Estimation of Ionic Liquids." Industrial & Engineering Chemistry Research 47(15): 5751-5757.

Gardas, R. L. and J. A. P. Coutinho (2009). "Group contribution methods for the prediction of thermophysical and transport properties of ionic liquids." AIChE Journal 55(5): 1274-1290.

Ge, R., C. Hardacre, et al. (2008). "Heat Capacities of Ionic Liquids as a Function of Temperature at 0.1 MPa. Measurement and Prediction." Journal of Chemical & Engineering Data 53(9): 2148-2153.

Ge, R., C. Hardacre, et al. (2007). "Thermal Conductivities of Ionic Liquids over the Temperature Range from 293 K to 353 K." Journal of Chemical & Engineering Data 52(5): 1819-1823.

Globe, S. and D. Dropkin (1959). "Natural convection heat transfer in liquids confined by two horizontal plates and heated from below." J. Heat Transfer 81(1): 24-28.

Gnielinski, V. (1975). "New equations for heat and mass transfer in the turbulent flow in pipes and channels." NASA STI/Recon Technical Report A 75: 22028.

Harris, K. R., M. Kanakubo, et al. (2007). "Temperature and Pressure Dependence of the Viscosity of the Ionic Liquids 1-Hexyl-3-methylimidazolium Hexafluorophosphate and 1-Butyl-3-methylimidazolium Bis(trifluoromethylsulfonyl)imide." Journal of Chemical & Engineering Data 52(3): 1080-1085.

He, Y., Y. Jin, et al. (2007). "Heat transfer and flow behaviour of aqueous suspensions of TiO2 nanoparticles (nanofluids) flowing upward through a vertical pipe." International Journal of Heat and Mass Transfer 50(11–12): 2272-2281.

Herrmann, U. and D. W. Kearney (2002). "Survey of thermal energy storage for parabolic trough power plants." Journal of Solar Energy Engineering 124(2): 145-152.

Herzog, A. V., Lipman, T. E., Kammen, D. M. (2001). "Renewable Energy Sources, in Our Fragile World: Challenges and Opportunities for Sustainable Development, forerunner to the Encyclopedia of Life Support Systems (EOLSS)." UNESCO-EOLSS Secretariat, EOLSS Publishers Co. Ltd. 1(1).

Ho, C.-J., M. Chen, et al. (2008). "Numerical simulation of natural convection of nanofluid in a square enclosure: effects due to uncertainties of viscosity and thermal conductivity." International Journal of Heat and Mass Transfer 51(17): 4506-4516.

Ho, C., W. Liu, et al. (2010). "Natural convection heat transfer of alumina-water nanofluid in vertical square enclosures: an experimental study." International Journal of Thermal Sciences 49(8): 1345-1353.

Ho, C. J., W. K. Liu, et al. (2010). "Natural convection heat transfer of alumina-water nanofluid in vertical square enclosures: An experimental study." International Journal of Thermal Sciences 49(8): 1345-1353.

Holbrey, J., W. M. Reichert, et al. (2010). "Heat capacities of ionic liquids and their applications as thermal fluids."

Hwang, K. S., J.-H. Lee, et al. (2007). "Buoyancy-driven heat transfer of water-based Al2O3 nanofluids in a rectangular cavity." International Journal of Heat and Mass Transfer 50(19–20): 4003-4010.

Hwang, K. S., J.-H. Lee, et al. (2007). "Buoyancy-driven heat transfer of water-based Al< sub> 2</sub> O< sub> 3</sub> nanofluids in a rectangular cavity." International Journal of Heat and Mass Transfer 50(19): 4003-4010.

Incropera, F. P., A. S. Lavine, et al. (2011). Fundamentals of heat and mass transfer, John Wiley & Sons.

Jacquemin, J., P. Husson, et al. (2007). "High-Pressure Volumetric Properties of Imidazolium-Based Ionic Liquids: Effect of the Anion." Journal of Chemical & Engineering Data 52(6): 2204-2211.

Jacquemin, J., P. Husson, et al. (2006). "Density and viscosity of several pure and water-saturated ionic liquids." Green Chemistry 8(2): 172-180.

Jang, S. P. and S. U. Choi (2004). Free convection in a rectangular cavity (Benard convection) with nanofluids. ASME 2004 International Mechanical Engineering Congress and Exposition, American Society of Mechanical Engineers.

Jang, S. P. and S. U. S. Choi (2004). "Role of Brownian motion in the enhanced thermal conductivity of nanofluids." Applied Physics Letters 84(21): 4316-4318.

Ji, Y., C. Wilson, et al. (2011). "Particle shape effect on heat transfer performance in an oscillating heat pipe." Nanoscale Research Letters 6(1): 296.

Jiménez, A. and M.-D. Bermúdez (2009). "Ionic Liquids as Lubricants of Titanium–Steel Contact." Tribology Letters 33(2): 111-126.

Jo, B., S. Jung, et al. (2011). Anomalous Rheological Behavior of Complex Fluids (Nanofluids). ASME 2011 International Mechanical Engineering Congress and Exposition, American Society of Mechanical Engineers.

Joback, K. G. (1984). A unified approach to physical property estimation using multivariate statistical techniques, Massachusetts Institute of Technology.

Johnson, K. E. (2007). "What's an ionic liquid?" Interface-Electrochemical Society 16(1): 38-41.

Jou, R.-Y. and S.-C. Tzeng (2006). "Numerical research of nature convective heat transfer enhancement filled with nanofluids in rectangular enclosures." International Communications in Heat and Mass Transfer 33(6): 727-736.

Kalogirou, S. A. (2004). "Solar thermal collectors and applications." Progress in Energy and Combustion Science 30(3): 231-295.

Katsuta, S., Y. Shiozawa, et al. (2009). "Stability of Ion Pairs of Bis(trifluoromethanesulfonyl)amide-Based Ionic Liquids in Dichloromethane." Journal of Chemical & Engineering Data 55(4): 1588-1593.

Kearney, D., U. Herrmann, et al. (2003). "Assessment of a Molten Salt Heat Transfer Fluid in a Parabolic Trough Solar Field." Journal of Solar Energy Engineering 125(2): 170-176.

Keblinski, P., J. A. Eastman, et al. (2005). "Nanofluids for thermal transport." Materials Today 8(6): 36-44.

Keblinski, P., S. R. Phillpot, et al. (2002). "Mechanisms of heat flow in suspensions of nano-sized particles (nanofluids)." International Journal of Heat and Mass Transfer 45(4): 855-863.

Keskin, S., D. Kayrak-Talay, et al. (2007). "A review of ionic liquids towards supercritical fluid applications." The Journal of Supercritical Fluids 43(1): 150-180.

Khanafer, K., K. Vafai, et al. (2003). "Buoyancy-driven heat transfer enhancement in a two-dimensional enclosure utilizing nanofluids." International Journal of Heat and Mass Transfer 46(19): 3639-3653.

Khoo, H. H. and R. B. H. Tan (2006). "Environmental Impact Evaluation of Conventional Fossil Fuel Production (Oil and Natural Gas) and Enhanced Resource Recovery with Potential CO2 Sequestration." Energy & Fuels 20(5): 1914-1924.

Kilaru, P., G. A. Baker, et al. (2007). "Density and Surface Tension Measurements of Imidazolium-, Quaternary Phosphonium-, and Ammonium-Based Room-Temperature Ionic Liquids: Data and Correlations." Journal of Chemical & Engineering Data 52(6): 2306-2314.

Kline, S. J. and F. McClintock (1953). "Describing uncertainties in single-sample experiments." Mechanical engineering 75(1): 3-8.

Krieger, I. M. and T. J. Dougherty (1959). "A Mechanism for Non-Newtonian Flow in Suspensions of Rigid Spheres." Transactions of The Society of Rheology (1957-1977) 3(1): 137-152.

Krishnamurthy, S., P. Bhattacharya, et al. (2006). "Enhanced Mass Transport in Nanofluids." Nano Letters 6(3): 419-423.

Kumełan, J., D. Tuma, et al. (2009). "Solubility of the Single Gases Carbon Dioxide and Hydrogen in the Ionic Liquid [bmpy][Tf2N]." Journal of Chemical & Engineering Data 55(1): 165-172.

Lai, W., R. Prasher, et al. (2009). "Convective heat transfer for water-based alumina nanofluids in a single 1.02-mm tube." Journal of Heat Transfer 131(11): 112401.

Lai, W. Y., P. E. Phelan, et al. (2008). Convective heat transfer for water-based alumina nanofluids in a single 1.02-mm tube. Thermal and Thermomechanical Phenomena in Electronic Systems, 2008. ITHERM 2008. 11th Intersociety Conference on.

Lazzús, J. A. (2012). "A group contribution method to predict the melting point of ionic liquids." Fluid Phase Equilibria 313(0): 1-6.

Lee, J.-H., K. S. Hwang, et al. (2008). "Effective viscosities and thermal conductivities of aqueous nanofluids containing low volume concentrations of Al2O3 nanoparticles." International Journal of Heat and Mass Transfer 51(11–12): 2651-2656.

Lee, K. J., S.-H. Yoon, et al. (2007). "Carbon Nanofibers: A Novel Nanofiller for Nanofluid Applications." Small 3(7): 1209-1213.

Leong, K. C., C. Yang, et al. (2006). "A model for the thermal conductivity of nanofluids – the effect of interfacial layer." Journal of Nanoparticle Research 8(2): 245-254.

Lewandowski, A. and A. Świderska-Mocek (2009). "Ionic liquids as electrolytes for Li-ion batteries—An overview of electrochemical studies." Journal of Power Sources 194(2): 601-609.

Li, C. H. and G. P. Peterson (2010). "Experimental Studies of Natural Convection Heat Transfer of Al2O3/DI Water Nanoparticle Suspensions (Nanofluids)." Advances in Mechanical Engineering 2010: 10.

Liu, H., E. Maginn, et al. (2012). "Thermal and Transport Properties of Six Ionic Liquids: An Experimental and Molecular Dynamics Study." Industrial & Engineering Chemistry Research 51(21): 7242-7254.

Manca, O., Y. Jaluria, et al. (2014). "Heat Transfer in Nanofluids 2013." Advances in Mechanical Engineering 2014: 2.

Marsh, K. N. (2009). "Thermodynamic and Thermophysical Properties of the Reference Ionic Liquid: 1-hexyl-3-methylimidazolium bis [(trifluoromethyl) sulfonyl] amide (including mixtures) part 1. Experimental Methods and Results." Pure & Applied Chemistry 81(5).

Marsh, K. N., J. A. Boxall, et al. (2004). "Room temperature ionic liquids and their mixtures—a review." Fluid Phase Equilibria 219(1): 93-98.

Mason, J. E. (2007). "World energy analysis: H2 now or later?" Energy Policy 35(2): 1315-1329.

Maxwell, J. C. (1873). Electricity and Magnetism, Clarendon Press,Oxford, UK.

Mazumder, A., J. Davis, et al. (2013). "Synthesis, Characterization, and Applications of Dendrimer-Encapsulated Zero-Valent Ni Nanoparticles as Antimicrobial Agents." ISRN Nanomaterials 2013.

Moens, L., D. Blake, et al. (2003). "Advanced Thermal Storage Fluids for Solar Parabolic Trough Systems." Journal of Solar Energy Engineering 125(1): 112-116.

Moens, L. and D. M. Blake (2010). "Mechanism of hydrogen formation in solar parabolic trough receivers." Journal of Solar Energy Engineering 132(3): 031006.

Moens, L., D. M. Blake, et al. (2003). "Advanced thermal storage fluids for solar parabolic trough systems." Journal of Solar Energy Engineering 125(1): 112-116.

Murshed, S. M. S., K. C. Leong, et al. (2005). "Enhanced thermal conductivity of TiO2—water based nanofluids." International Journal of Thermal Sciences 44(4): 367-373.

Murshed, S. M. S., K. C. Leong, et al. (2008). "Investigations of thermal conductivity and viscosity of nanofluids." International Journal of Thermal Sciences 47(5): 560-568.

Murshed, S. S., C. N. de Castro, et al. (2011). "Ionanofluids as novel fluids for advanced heat transfer applications." World Academy of Science, Engineering and Technology 76: 795-798.

Nakata, T. (2004). "Energy-economic models and the environment." Progress in Energy and Combustion Science 30(4): 417-475.

Namburu, P. K., D. K. Das, et al. (2009). "Numerical study of turbulent flow and heat transfer characteristics of nanofluids considering variable properties." International Journal of Thermal Sciences 48(2): 290-302.

Ngo, H. L., K. LeCompte, et al. (2000). "Thermal properties of imidazolium ionic liquids." Thermochimica Acta 357–358(0): 97-102.

Nielsen, L. E. (1970). "Generalized Equation for the Elastic Moduli of Composite Materials." Journal of Applied Physics 41(11): 4626-4627.

Nieto de Castro, C. A., M. J. V. Lourenço, et al. (2009). "Thermal Properties of Ionic Liquids and IoNanofluids of Imidazolium and Pyrrolidinium Liquids†." Journal of Chemical & Engineering Data 55(2): 653-661.

Nieto de Castro, C. A., S. M. S. Murshed, et al. (2012). "Enhanced thermal conductivity and specific heat capacity of carbon nanotubes ionanofluids." International Journal of Thermal Sciences 62(0): 34-39.

Nnanna, A. (2007). "Experimental model of temperature-driven nanofluid." Journal of Heat Transfer 129(6): 697-704.

Oztop, H. F. and E. Abu-Nada (2008). "Numerical study of natural convection in partially heated rectangular enclosures filled with nanofluids." International Journal of Heat and Fluid Flow 29(5): 1326-1336.

PallarÈs, J., I. Cuesta, et al. (1996). "Natural convection in a cubical cavity heated from below at low rayleigh numbers." International Journal of Heat and Mass Transfer 39(15): 3233-3247.

Paul, T. C., A. Morshed, et al. (2011). Experimental investigation of natural convection heat transfer of an ionic liquid in a rectangular enclosure heated from below. ASME 2011 International Mechanical Engineering Congress and Exposition, American Society of Mechanical Engineers.

Paul, T. C., A. Morshed, et al. (2012). Heat Transfer and Flow Behavior of Nanoparticle Enhanced Ionic Liquids (NEILs). ASME 2012 Heat Transfer Summer Conference.

Paul, T. C., A. Morshed, et al. (2014). "Buoyancy driven heat transfer behavior of [C_4mim][]NTf_2] ionic liquid: An experimental study." Applied Thermal Engineering 66(1): 534-540.

Paul, T. C., A. Morshed, et al. (2013). "Nanoparticle Enhanced Ionic Liquids (NEILS) as Working Fluid for the Next Generation Solar Collector." Procedia Engineering 56: 631-636.

Paul, T. C., A. Morshed, et al. (2013). Buoyancy Driven Heat Transfer Behavior of Zinc Oxide (ZnO)–Water Nanofluids. ASME 2013 Heat Transfer Summer Conference.

Paulechka, Y. U., D. H. Zaitsau, et al. (2005). "Vapor pressure and thermal stability of ionic liquid 1-butyl-3-methylimidazolium Bis(trifluoromethylsulfonyl)amide." Thermochimica Acta 439(1–2): 158-160.

Pensado, A. S. and A. A. H. Pádua (2011). "Solvation and Stabilization of Metallic Nanoparticles in Ionic Liquids." Angewandte Chemie International Edition 50(37): 8683-8687.

Pereiro, A. B., H. I. M. Veiga, et al. (2009). "Effect of temperature on the physical properties of two ionic liquids." The Journal of Chemical Thermodynamics 41(12): 1419-1423.

Plechkova, N. V. and K. R. Seddon (2008). "Applications of ionic liquids in the chemical industry." Chemical Society Reviews 37(1): 123-150.

Podgoršek, A., A. S. Pensado, et al. (2013). "Interaction Energies of Ionic Liquids with Metallic Nanoparticles: Solvation and Stabilization Effects." The Journal of Physical Chemistry C 117(7): 3537-3547.

Putra, N., W. Roetzel, et al. (2003). "Natural convection of nano-fluids." Heat and Mass Transfer 39(8-9): 775-784.

Putra, N., W. Roetzel, et al. (2003). "Natural convection of nano-fluids." Heat and Mass Transfer 39(8-9): 775-784.

Rashmi, W., A. Ismail, et al. (2011). "CFD studies on natural convection heat transfer of Al2O3-water nanofluids." Heat and Mass Transfer 47(10): 1301-1310.

Rashmi, W., M. Khalid, et al. (2013). "Experimental and numerical investigation of heat transfer in CNT nanofluids." Journal of Experimental Nanoscience(ahead-of-print): 1-19.

Reddy, R. G. (2009). Novel applications of ionic liquids in materials processing. Journal of Physics: Conference Series, IOP Publishing.

Rogers, R. D. and K. R. Seddon (2003). "Ionic Liquids--Solvents of the Future?" Science 302(5646): 792-793.

Rogner, H.-H. (2012). "World energy demand and supply." URL: http://www. iaea. org/nuclearenergy/nuclearknowledge/schools/NEM-school/2012/AbuDhabi/PDFs/day1/04 Rogner World Energy D% 26S. pdf, Accessed 15: 2013.

Rooney, D., J. Jacquemin, et al. (2010). Thermophysical Properties of Ionic Liquids. Ionic Liquids. B. Kirchner, Springer Berlin Heidelberg. 290: 185-212.

Sánchez, L. G., J. R. Espel, et al. (2009). "Density, Viscosity, and Surface Tension of Synthesis Grade Imidazolium, Pyridinium, and Pyrrolidinium Based Room Temperature Ionic Liquids." Journal of Chemical & Engineering Data 54(10): 2803-2812.

Shah, R. (1975). Thermal entry length solutions for the circular tube and parallel plates. Proc. 3rd National Heat Mass Transfer Conference. Indian Institute of Technology, Bombay.

Shen, B., A. J. Shih, et al. (2008). "Application of Nanofluids in Minimum Quantity Lubrication Grinding." Tribology Transactions 51(6): 730-737.

Shiina, Y., K. Fujimura, et al. (1994). "Natural convection in a hemispherical enclosure heated from below." International Journal of Heat and Mass Transfer 37(11): 1605-1617.

Shin, D. and D. Banerjee (2010). "Enhanced Specific Heat of Silica Nanofluid." Journal of Heat Transfer 133(2): 024501-024501.

Shin, D. and D. Banerjee (2011). "Enhancement of specific heat capacity of high-temperature silica-nanofluids synthesized in alkali chloride salt eutectics for solar thermal-energy storage applications." International Journal of Heat and Mass Transfer 54(5–6): 1064-1070.

Shin, S. and S.-H. Lee (2000). "Thermal conductivity of suspensions in shear flow fields." International Journal of Heat and Mass Transfer 43(23): 4275-4284.

Singh, P., K. Kumari, et al. (2009). "Copper Nanoparticles in Ionic Liquid: An Easy and Efficient Catalyst for Selective Carba-Michael Addition Reaction." Catalysis Letters 127(1-2): 119-125.

Solutia. (2014). "Therminol VP-1, Technical Bulletin 7239115c." Retrieved May 29, 2014, from http://www.therminol.com/products/Therminol-VP1.

Srivastava, S. (2012). "Effect of aggregation on thermal conductivity and viscosity of nanofluids." Applied Nanoscience 2(3): 325-331.

Sugden, S. and H. Wilkins (1929). "CLXVII.-The parachor and chemical constitution. Part XII. Fused metals and salts." Journal of the Chemical Society (Resumed)(0): 1291-1298.

Timofeeva, E. V., J. L. Routbort, et al. (2009). "Particle shape effects on thermophysical properties of alumina nanofluids." Journal of Applied Physics 106(1): -.

Tiznobaik, H. and D. Shin (2013). "Enhanced specific heat capacity of high-temperature molten salt-based nanofluids." International Journal of Heat and Mass Transfer 57(2): 542-548.

Tokuda, H., K. Hayamizu, et al. (2005). "Physicochemical Properties and Structures of Room Temperature Ionic Liquids. 2. Variation of Alkyl Chain Length in Imidazolium Cation." The Journal of Physical Chemistry B 109(13): 6103-6110.

Tokuda, H., S. Tsuzuki, et al. (2006). "How Ionic Are Room-Temperature Ionic Liquids? An Indicator of the Physicochemical Properties." The Journal of Physical Chemistry B 110(39): 19593-19600.

Tomida, D., S. Kenmochi, et al. (2007). "Thermal Conductivities of [bmim][PF6], [hmim][PF6], and [omim][PF6] from 294 to 335 K at Pressures up to 20 MPa." International Journal of Thermophysics 28(4): 1147-1160.

Tomida, D., S. Kenmochi, et al. (2007). "Thermal conductivities of [bmim][PF6],[hmim][PF6], and [omim][PF6] from 294 to 335 K at pressures up to 20 MPa." International Journal of Thermophysics 28(4): 1147-1160.

Tomida, D., S. Kenmochi, et al. (2007). "Measurements of thermal conductivity of 1-butyl-3-methylimidazolium tetrafluoroborate at high pressure." Heat Transfer—Asian Research 36(6): 361-372.

Torii, S. (2010). "Turbulent Heat Transfer Behavior of Nanofluid in a Circular Tube Heated under Constant Heat Flux." Advances in Mechanical Engineering 2010.

Trohalaki, S. and R. Pachter (2005). "Prediction of Melting Points for Ionic Liquids." QSAR & Combinatorial Science 24(4): 485-490.

Troncoso, J., C. A. Cerdeiriña, et al. (2006). "Thermodynamic Properties of Imidazolium-Based Ionic Liquids: Densities, Heat Capacities, and Enthalpies of Fusion of [bmim][PF6] and [bmim][NTf2]." Journal of Chemical & Engineering Data 51(5): 1856-1859.

Ueno, K., K. Hata, et al. (2008). "Nanocomposite Ion Gels Based on Silica Nanoparticles and an Ionic Liquid: Ionic Transport, Viscoelastic Properties, and Microstructure." The Journal of Physical Chemistry B 112(30): 9013-9019.

Ueno, K., S. Imaizumi, et al. (2008). "Colloidal Interaction in Ionic Liquids: Effects of Ionic Structures and Surface Chemistry on Rheology of Silica Colloidal Dispersions." Langmuir 25(2): 825-831.

Ueno, K., A. Inaba, et al. (2008). "Colloidal Stability of Bare and Polymer-Grafted Silica Nanoparticles in Ionic Liquids." Langmuir 24(10): 5253-5259.

Valkenburg, M. E. V., R. L. Vaughn, et al. (2005). "Thermochemistry of ionic liquid heat-transfer fluids." Thermochimica Acta 425(1–2): 181-188.

Waliszewski, D., I. Stępniak, et al. (2005). "Heat capacities of ionic liquids and their heats of solution in molecular liquids." Thermochimica Acta 433(1–2): 149-152.

Wandschneider, A., J. K. Lehmann, et al. (2008). "Surface Tension and Density of Pure Ionic Liquids and Some Binary Mixtures with 1-Propanol and 1-Butanol." Journal of Chemical & Engineering Data 53(2): 596-599.

Wang, B., X. Wang, et al. (2010). "Rheological and Tribological Properties of Ionic Liquid-Based Nanofluids Containing Functionalized Multi-Walled Carbon Nanotubes." The Journal of Physical Chemistry C 114(19): 8749-8754.

Wang, B., X. Wang, et al. (2011). "Ionic liquid-based stable nanofluids containing gold nanoparticles." Journal of Colloid and Interface Science 362(1): 5-14.

Wang, X., X. Xu, et al. (1999). "Thermal Conductivity of Nanoparticle - Fluid Mixture." Journal of Thermophysics and Heat Transfer 13(4): 474-480.

Wei, X. and L. Wang (2010). "Synthesis and thermal conductivity of microfluidic copper nanofluids." Particuology 8(3): 262-271.

Wen, D. and Y. Ding (2004). "Experimental investigation into convective heat transfer of nanofluids at the entrance region under laminar flow conditions." International Journal of Heat and Mass Transfer 47(24): 5181-5188.

Wen, D. and Y. Ding (2005). "Effect of particle migration on heat transfer in suspensions of nanoparticles flowing through minichannels." Microfluidics and Nanofluidics 1(2): 183-189.

Wen, D. and Y. Ding (2005). "Formulation of nanofluids for natural convective heat transfer applications." International Journal of Heat and Fluid Flow 26(6): 855-864.

Wilkes, J. S., J. A. Levisky, et al. (1982). "Dialkylimidazolium chloroaluminate melts: a new class of room-temperature ionic liquids for electrochemistry, spectroscopy and synthesis." Inorganic Chemistry 21(3): 1263-1264.

Wishart, J. F. (2009). "Energy applications of ionic liquids." Energy & Environmental Science 2(9): 956-961.

Wittmar, A., D. Ruiz-Abad, et al. (2012). "Dispersions of silica nanoparticles in ionic liquids investigated with advanced rheology." Journal of Nanoparticle Research 14(2): 1-10.

Wu, B., R. Reddy, et al. (2001). "Novel ionic liquid thermal storage for solar thermal electric power systems." Solar Engineering: 445-452.

Wu, W., D. Ewing, et al. (2006). "The effect of the top and bottom wall temperatures on the laminar natural convection in an air-filled square cavity." International Journal of Heat and Mass Transfer 49(11–12): 1999-2008.

Xie, H., H. Lee, et al. (2003). "Nanofluids containing multiwalled carbon nanotubes and their enhanced thermal conductivities." Journal of Applied Physics 94(8): 4967-4971.

Yamanaka, N., R. Kawano, et al. (2007). "Dye-Sensitized TiO2 Solar Cells Using Imidazolium-Type Ionic Liquid Crystal Systems as Effective Electrolytes†." The Journal of Physical Chemistry B 111(18): 4763-4769.

Zeinali Heris, S., M. Nasr Esfahany, et al. (2007). "Experimental investigation of convective heat transfer of Al2O3/water nanofluid in circular tube." International Journal of Heat and Fluid Flow 28(2): 203-210.

Zhang, S., N. Sun, et al. (2006). "Physical Properties of Ionic Liquids: Database and Evaluation." Journal of Physical and Chemical Reference Data 35(4): 1475-1517.

Zhou, S.-Q. and R. Ni (2008). "Measurement of the specific heat capacity of water-based Al2O3 nanofluid." Applied Physics Letters 92(9): -.

Zhou, Y. (2005). "Recent advances in ionic liquids for synthesis of inorganic nanomaterials." Current Nanoscience 1(1): 35-42.